GEOPHYSICAL, GEOCHEMICAL AND ISOTOPE ANALYSIS OF THE FIGUEIRA BRANCA SUITE, MATO GROSSO, BRAZIL

Vinicius Hector Abud Louro

A Thesis Submitted for the Degree of PhD
at the
University of St Andrews

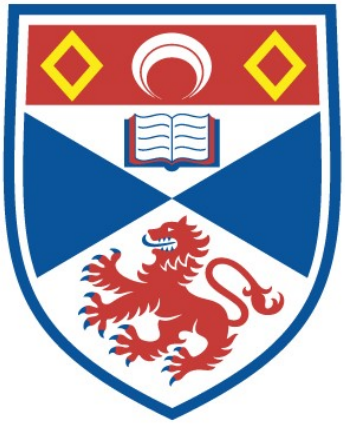

2017

Geophysical, Geochemical and Isotope Analysis of the Figueira Branca Suite, Mato Grosso, Brazil.

Vinicius Hector Abud Louro

University of
St Andrews

This thesis is submitted in partial fulfilment for the degree of PhD
at the
University of St Andrews

18 April 2017

Universidade de São Paulo
Instituto de Astronomia, Geofísica e Ciências Atmosféricas

University of St. Andrews
School of Earth and Environmental Sciences

Vinicius Hector Abud Louro

Geophysical, Geochemical and Isotopic Analysis of the Figueira Branca Suite, Mato Grosso, Brazil.

São Paulo
2017

Vinicius Hector Abud Louro

Geophysical, Geochemical and Isotopic Analysis of the Figueira Branca Suite, Mato Grosso, Brazil.

Tese apresentada ao Departamento de Geofísica do Instituto de Astronomia, Geofísica e Ciências Atmosféricas da Universidade de São Paulo e à School of Earth and Environmental Sciences da University of St. Andrews como requisito parcial para obtenção do título de Doutor em Ciências.

Área de Concentração: Ciências da Terra
Orientadores: Profa. Dra. Marta Silvia Maria Mantovani e Prof. Dr. Peter Anthony Cawood

São Paulo

2017

LOURO, V.H.A. Geophysical, Geochemical and Isotopic Analysis of the Figueira Branca Suite, Mato Grosso, Brazil.. 2017. 120 f. Tese (Doutorado em Ciências da Terra) – Instituto de Astronomia, Geofísica e Ciências Atmosféricas, Universidade de São Paulo, São Paulo, 2017.

Aprovado em:

Banca Examinadora / Examiners

Prof. Dr. _____

Instituição/Institution: _____

Julgamento/Decision: _____

Prof. Dr. _____

Instituição/Institution: _____

Julgamento/Decision: _____

Prof. Dr. _____

Instituição/Institution: _____

Julgamento/Decision: _____

Prof. Dr. _____

Instituição/Institution: _____

Julgamento/Decision: _____

Prof. Dr. _____

Instituição/Institution: _____

Julgamento/Decision: _____

"It ain't about how hard you can get hit,
It's about how hard you can get hit and keep moving forward.
How much you can take and keep moving forward.
That's how winning is done"

Rocky Balboa (2006)

ACKNOWLEDGEMENTS

I would like to thank my supervisors Marta Mantovani and Peter Cawood, my mentor Tony Prave (Oh Captain, my Captain), my partner and friend Vanessa B. Ribeiro, and my good friends in Brazil and in Scotland, who pushed me and kept me going. My big family, especially, for the love, support and care. Thank you to the several professors and professionals who contributed considerably not only to this research, but to teach me science, geology, humility and to never give up.

ABSTRACT

The Figueira Branca Suite is a layered mafic-ultramafic complex in the Jauru Terrane, southwest Amazon Craton. New lithological, geochemical, gamma-ray and potential field data, integrated with geological, isotope and paleomagnetic data are used to characterize this pulse of Mesoproterozoic extension-related magmatism. The Figueira Branca Suite formed through juvenile magma emplacement into the crust at 1425 Ma, coeval with the later stages of the Santa Helena Orogen. In three papers, this suite was studied from microscopic to continental scales. First, the Figueira Branca suite was analysed through thin sections to determine the influence of inaccurate constraints in magnetic and gravity field modelling. Then, the extent of magmatism within the suite was delimited to four bodies to the north of Indiavaí city, MT - Brazil, with potential fields and gamma-ray data. Modelling gravity and magnetic field data indicated that the anomalous sources are close to the surface or outcropping. These intrusions trend northwest over 8 km, with significant remanent magnetization that is consistent with published direction obtained through paleomagnetic data. The increasing enrichment of LREE in the gabbroic bodies of the suite was interpreted as evidence of progressive fractionation of the magma. The emplacement, mineralogy and geochemical signature point towards a back-arc extension tectonic framework in the later stages of the Santa Helena Orogen. The third part of the work consisted on evaluating reconstructions of the Paleo-Mesoproterozoic supercontinent Nuna with magnetic field data. The global magnetic anomaly map, EMAG2, allowed to observe continuity of magnetic lineaments and regimes in domains of similar ages in different cratons (Amazon, Baltica, West Africa and North China). These magnetic features indicated the theory which the magnetic field best supported, and suggested the regional environment where the Jauru Terrane was inserted by the time of the intrusion of the Figueira Branca Suite.

Keywords: Amazon Craton, Mafic Suite, Potential Fields, Geochemistry, Nuna

RESUMO

A Suíte Figueira Branca é um complexo máfico-ultramáfico no Terreno Jauru, sudoeste do Cráton Amazônico. Novos dados litológicos, geoquímicos, de raios gama e de campos potenciais, integrados com dados geológicos, isotópicos e paleomagnéticos, foram utilizados para caracterizar of pulso magmático Mesoproterozóico da suíte vinculado a um ambiente distensivo. A Suíte Figueira Branca foi formada pela intrusão na crosta de um magma juvenil em 1425 Ma, mesma idade dos estágios tardios da orogenia Santa Helena. Em três artigos, esta suíte foi estudada em escalas desde microscópicas a continentais. Primeiramente, a Suíte Figueira Branca foi analisada através de lâminas para determinar a influência da utilização de vínculos errados ou inadequados na modelagem de dados de campos magnéticos e gravimétricos. Em seguida, a extensão do magmatismo pertencente à suite foi delimitado, via campos potenciais e gamaespectrometria, a quatro corpos ao norte da cidade de Indiavaí, MT - Brasil. A modelagem dos dados de campos gravimétrico e magnético indicaram que as fontes dos sinais geofísicos se encontram em horizontes rasos ou aflorantes. Estas intrusões apresentam um alinhamento noroeste por mais de 8 Km, com magnetização remanente significativa consistentes direções publicadas em estudos paleomagnéticos. O crescente enriquecimento de Elementos de Terras-Raras leves em corpos gabróicos da suíte foi interpretado como evidência de fracionamento progressivo do magma. A instrusão, a mineralogia e a assinatura geoquímica indicaram um ambiente de extesão de retro-arco durante os estágios finais da orogenia Santa Helena. A terceira parte deste trabalho consistiu na avaliação de reconstruções através de dados de campo magnético do supercontinente paleo- a mesoproterozóico Nuna. O mapa global de anomalia magnética, EMAG2, permitiu observar continuidades de lineamentos e regimes magnéticos em domínios de idades similares em diferentes crátons (Amazônico, Báltico, Oeste Africano, do Norte da China). Estas propriedades magnéticas indicaram a teoria que melhor se adequava aos dados de campo magnético, e sugeriram o ambiente regional onde o Terreno Jauru se encontrava na época da intrusão da Suíte Figueira Branca.

Palavras-Chave: Cráton Amazônico, Suíte Máfica, Campos Potenciais, Geoquímica, Nuna

Summary

1. Introduction

How much a single and considerably small intrusive suite can tell with geology and geophysics? How much can it tell about common mistakes done even by specialists in geophysical modelling? What can it reveal about its own features and history? About the environment that hosts it and, ultimately, lead to better understand the Earth evolution? This thesis brings a set of three correlate studies seeking to answer these questions.

The studies that compose this thesis evaluate the Figueira Branca Mafic-Ultramafic Suite, from microscopic to continental scale. These studies were submitted to peer-reviewed journals, and are currently under review. The first manuscript discusses the influence of inaccurate constraints in magnetic and gravity field modelling, and why analysing samples microscopically is not only recommendable, but of major importance for a reliable geophysical modelling. The Figueira Branca Suite was used as background for this analysis, given the variable condition and petrophysical properties of its samples.

The Amazon Craton is divisible into six geochronological provinces: the Archean Central Amazon, and the Proterozoic provinces of Maroni-Itacaiúnas, Ventuari-Tapajós, Rio Negro-Juruena, Rondonian-San Ignácio and Sunsás-Aguapeí (Fig. 1.1a) (Tassinari & Macambira, 1999; Teixeira et al., 2010). The southern portion of the Rio Negro-Juruena (1.78 – 1.55 Ga) province includes the Jauru Terrane (1.78 – 1.40 Ga), which contains Paleoproterozoic basement rocks and the Mesoproterozoic Cachoeirinha and Santa Helena orogens (Fig. 1.1b) (Bettencourt et al., 2010). The Alto Jauru Group, part of the Paleoproterozoic basement of the Jauru Terrane, hosts the Figueira Branca Mafic-Ultramafic Intrusive Suite.

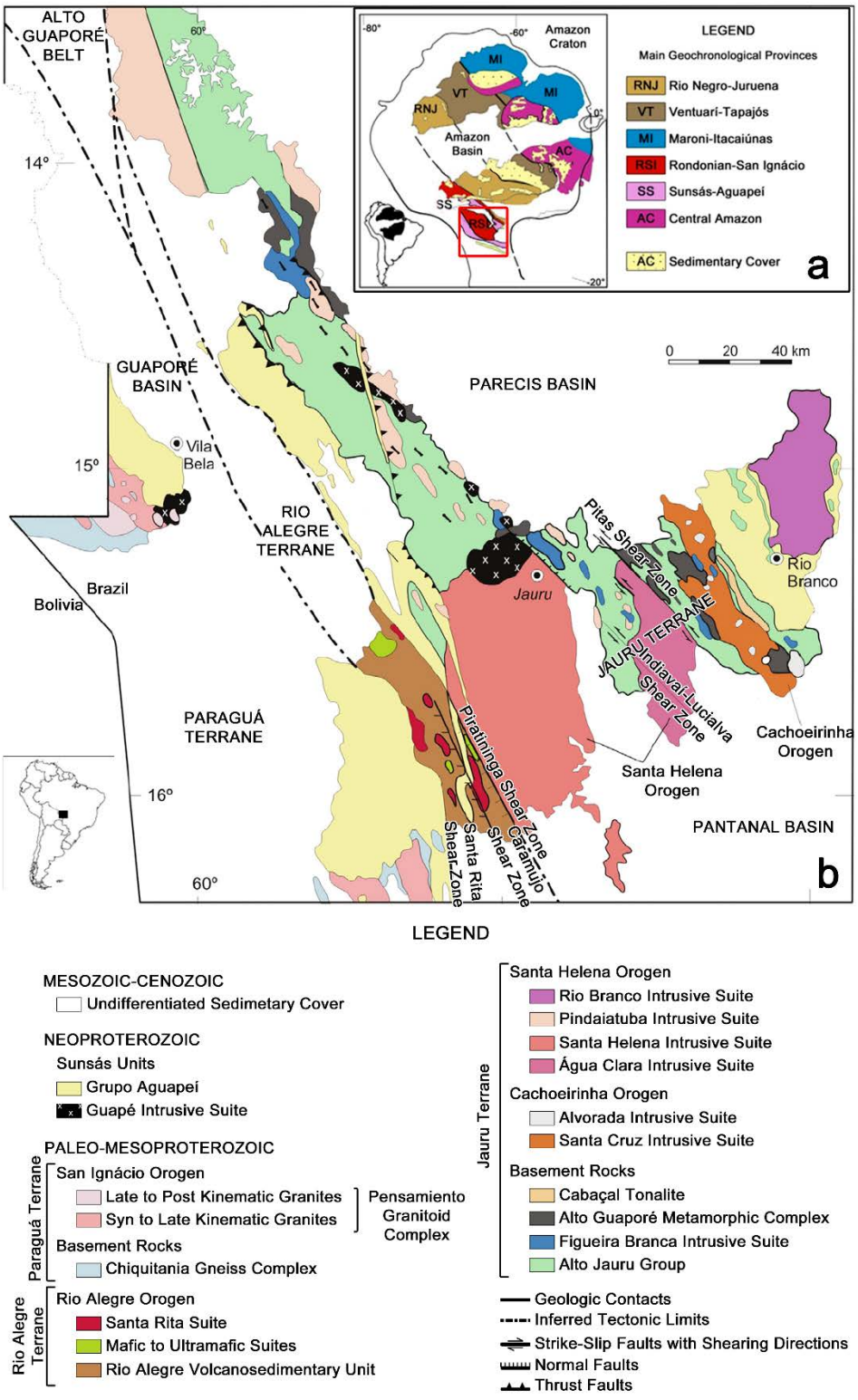

Fig. 1.1 - (a) Main geochronological provinces of Amazon Craton (Bettencourt et al., 2010). The red polygon delimits the area of Fig. 1b. (b) Southwest of the Rio Negro-Juruena and Rondonian-San Ignácio provinces of the Amazon Craton. The Figueira Branca Suite is represented in dark blue.

The Figueira Branca Intrusive Suite is a 1425 ± 8 Ma layered mafic-ultramafic complex composed from bottom to top of dunite, pyroxenite, gabbro-norite, anorthosite, thin layers of troctolite, and olivine-gabbro (Teixeira et al., 2011). Isotope data from its southern body indicate a juvenile source that crystallized during the later stages of the Santa Helena Orogeny (Tassinari, Bettencourt, Geraldes, Macambira, & Lafon, 2000; Teixeira et al., 2016; Teixeira et al., 2011).

The second work describes the Figueira Branca Intrusive Suite geophysical signature through potential field models, and geochemically with major, trace and Rare-Earth element analyses. It explores the magnitude of the magmatism that generated the suite, analysing the terrane that hosts it, the parental magma, and the tectonic framework involved. The potential field models displayed a northwest-southeast elongation in four bodies immediately to the north of Indiavaí city. Geochemical data confirmed the extensional setting proposed by Teixeira et al. (2011) through isotope data.

The third part of the thesis develop a continental scale analysis of the Amazon Craton by the time of the development of the Santa Helena Orogen and intrusion of the Figueira Branca Suite, from 1.6 to 1.4 Ga (Fig. 1.1b). The location of the Amazon Craton during the Paleo- to Mesoproterozoic supercontinent Nuna gave insights of the tectonic framework that the craton was subjected during the intrusion of the Figueira Branca Suite. This location is currently under debate, so as the configuration of the Nuna supercontinent. Three reconstructions of Nuna were chosen to evaluate the position of the Amazon Craton, of Mertanen and Pesonen (2012), which is based on paleomagnetic data; of Pisarevsky, Elming, Pesonen, and Li (2014), based on paleomagnetic and geological constraints; and of Pehrsson, Eglington, Evans, Huston, and Reddy (2015) who integrated paleomagnetic and geological data with ore deposit features (Fig. 1.2). Using magnetic field data, it was possible to recognize magnetic regimes and lineament patterns in the Amazon Craton, and nearby blocks according with the reconstructions. This

dataset was the basis to evaluate which theory was better supported by the magnetic field. The better supported theory, by consequence, proportionated evidences about what was occurring with the southwest of the Amazon Craton when the Figueira Branca Suite intruded the Jauru Terrane.

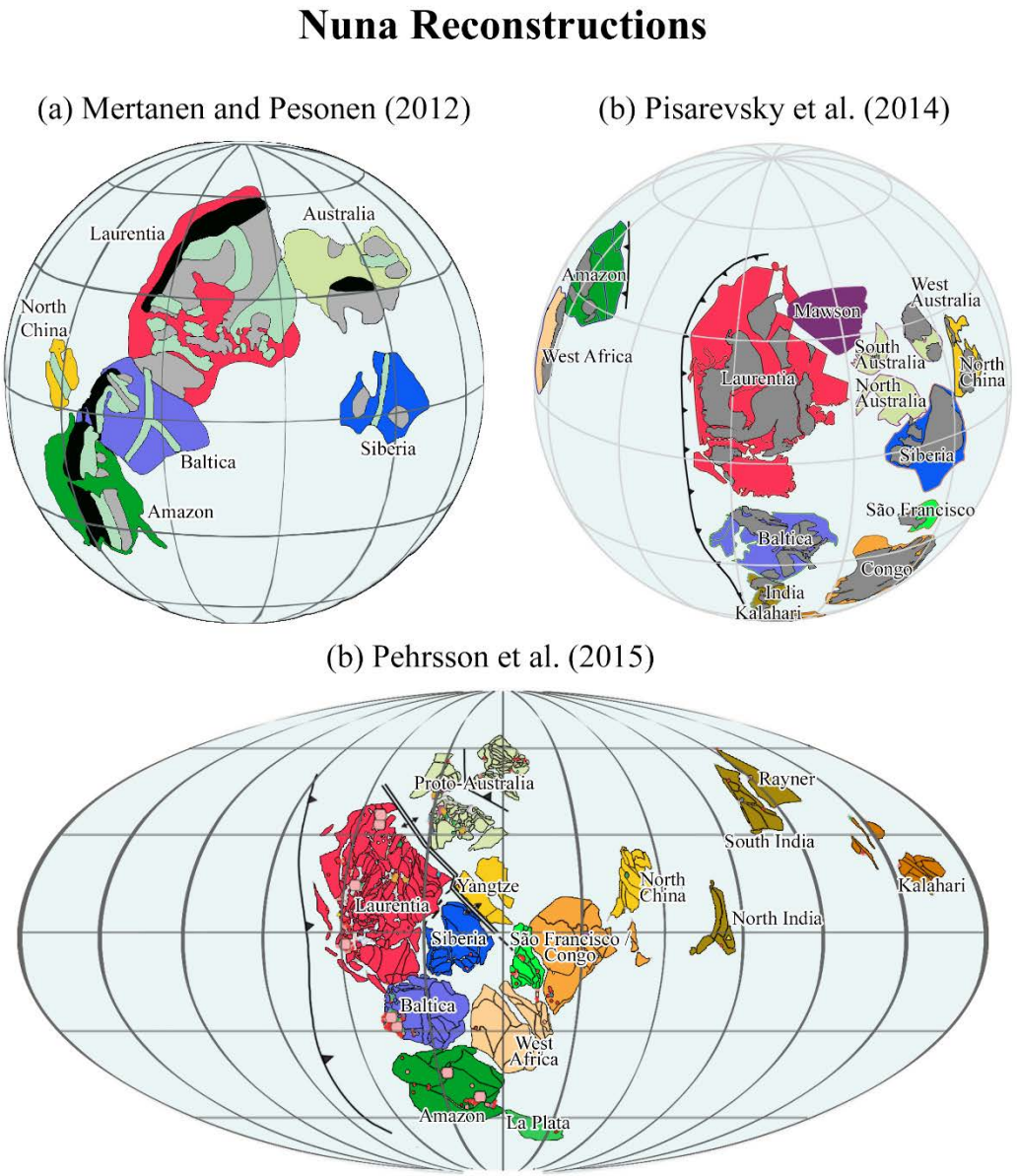

Fig. 1.2 - Reconstructions of Nuna proposed by (a) Mertanen and Pesonen (2012), (b) Pisarevsky et al. (2014), and (c) Pehrsson et al. (2015).

The scale of the problems and the proposed answers increase from the first to the third part of the thesis. The three manuscripts that compose this thesis were submitted to the journals Tectonophysics, Geophysical Journal International and Precambrian Research. The final chapter presents the major conclusions obtained through the results generated, arguing about the questions raised here.

In parallel to this project, the PhD student worked in different projects and published as author and co-author four papers. A fifth paper was submitted and is currently under review. The published and submitted papers are available in the Attachment 1 of this thesis.

2. Manuscript 1: Effects of inaccurate constraints in magnetic and gravity field modelling

Starting in small scales, this chapter presents the importance of not only having constraints for modelling, but having them accurate. Measuring the properties that are going to be modelled is the most common procedure to define constraints for modelling. However, simple measurements without a deeper mineralogical analysis can produce inaccurate constraints and compromise the modelling. This manuscript shows how inaccurate magnetic susceptibilities and densities influence in the result of a joint magnetic and gravity modelling using two datasets: one synthetic, to observe the effective difference between using the correct and the inaccurate constraints; and one real dataset, using the Indiavaí anomaly (the southern body of the Figueira Branca Suite) as background for the analysis.

Geophysical Journal International

Effects of inaccurate constraints in magnetic and gravity field modelling

Journal:	*Geophysical Journal International*
Manuscript ID	GJI-S-17-0112
Manuscript Type:	Research Paper
Date Submitted by the Author:	31-Jan-2017
Complete List of Authors:	Louro, Vinicius; Instituto de Astronomia, Geofísica e Ciências Atmosféricas da Universidade de São Paulo, Geophysics Department; University of St. Andrews, Department of Earth Sciences Cawood, Peter; University of St. Andrews, Department of Earth Sciences Mantovani, Marta; Instituto de Astronomia, Geofísica e Ciências Atmosféricas da Universidade de São Paulo, Geophysics Department
Keywords:	Gravity anomalies and Earth structure < GEODESY and GRAVITY, Magnetic anomalies: modelling and interpretation < GEOMAGNETISM and ELECTROMAGNETISM, Numerical modelling < GEOPHYSICAL METHODS, Magnetic mineralogy and petrology < GEOMAGNETISM and ELECTROMAGNETISM

Effects of inaccurate constraints in magnetic and gravity field modelling

Vinicius Hector Abud Louro[1,2], Peter Anthony Cawood[2], Marta Silvia Maria Mantovani[1]

[1] Instituto de Astronomia, Geofísica e Ciências Atmosféricas, Universidade de São Paulo, São Paulo, Brazil.

[2] Department of Earth and Environmental Sciences, University of St. Andrews, St. Andrews, KY16 9AL, UK.

E-mails: vilouro@usp.br, pac20@st-andrews.ac.uk, msmmanto@usp.br

Corresponding author: Vinicius Hector Abud Louro. **E-mail:** vilouro@usp.br

Date of Submission: 29 January 2017

ORCID: Louro, V. H. A.: 0000-0003-3430-4507

Cawood, P. A.: 0000-0003-2357-0068

Mantovani, M. S. M.: n/a

Summary

Modelling potential fields is a common procedure in geophysical exploration. The nature and type of data used to constrain the model determine the feasibility and viability of the output and hence the ability of the model to provide a valid representation of reality. This paper presents a set of models, from synthetic and real cases that were used to investigate how poorly defined or inaccurate constraints affect the results of potential field modelling. The staged-inversion methodology was used in the investigation, and four approaches were modelled for synthetic data and two approaches for the real data. The real data assessed a mafic-ultramafic intrusion in the southwest Amazon Craton. Unsurprisingly, the results indicate that the use of the correct magnetic susceptibility and density values, and keeping them fixed during staged inversion produces the best model. However, when only limited data are available to constrain the modelling, acceptable results can still be achieved if the process is rigorously executed.

1. Introduction

Modelling of data is a common component of most geophysical studies and facilitates the resolution of poorly, or non-, exposed geological bodies and structures. The quality of the geophysical model (i.e. its ability to accurately represent a body or structure) is highly dependent on the quality of data constraints. The constraints can be geological, geophysical, geochemical, or any kind of information that limits the possibilities and/or ambiguities in the geophysical methodology. Here we discuss the effects that inaccurate magnetic susceptibilities and densities can cause in gravity and magnetic field modelling, respectively.

To analyse the effects of inaccurate constraints, we have worked with synthetic and real data sets. The constraints used for the modelling were obtained from potential field data, hand samples and

thin-sections. For potential field models, the constraints were the lateral extent of a body, the depth to the top of the source of the signal and, in the magnetic field case, estimates of the total magnetization. For the real data sets, hand samples and thin-sections provided additional constraints.

For assessment of synthetic models using gravity and magnetic data we used two sets of parameters for each case. The differences between the sets were the initial magnetic susceptibility and density. In one set, we used the correct values, whereas in the second set, we used half the actual value for each property (e.g. correct density contrast: 0.24 g/cm^3, half the value: 0.12 g/cm^3). In the real world, smaller values for magnetic susceptibility and density can reflect weathering, a common effect on rock units, especially in tropical and equatorial areas, and alteration.

The real cases scenarios presented in this study are for the Indiavaí igneous body, from the Figueira Branca mafic-ultramafic suite, Mato Grosso, Brazil. The suite lies on the southwest of the Amazon Craton. Two situations were considered. In the first the available data included potential field information, hand samples, and magnetic susceptibility and density measurements, which is similar to parameters routinely available in the processing and modelling of potential fields. In a second situation, thin-section data were used to further constraint the input data.

2. Methodology

The magnetic modelling used a fixed direction of total magnetization, estimated through the MaxiMin method (Fedi *et al.* 1994). Cordani and Shukowsky (2009) implemented the MaxiMin technique in a MATLAB algorithm. This algorithm selects 30 pairs of inclination and declination angles and performs RTP filtering from the residual magnetic field with each pair. The resulting grid that presents the most negative values is discarded, and a new iteration is initiated. This process is repeated until the 30 pairs of values do not differ from each other by more than a predefined error (5° in this work) or the process reaches a predefined maximum number of iterations (4000). Lateral limits

of the body (real and synthetic) were defined by their gradient of horizontal derivatives of the magnetic field reduced to the pole. These fields were preferred over the gravity fields due the larger amount, and better spaced, magnetic data than the gravity fields. The depths to the top of the potential field anomaly sources, in the synthetic cases, were estimated using Euler Deconvolution (Reid *et al.* 1990). In the real case, the depth estimation was not necessary because the Indiavaí igneous body outcrops, therefore the depth to the top of the initial model was considered zero.

The modelling was performed using the staged-inversion methodology (Foss 2006). The modelling took two phases: one using a block body as the initial model, and one using prisms sliced from the body modelled in the first phase as the initial model. The prisms were parallel and centred on the north-south surveyed lines, with a fixed 500 m width in east-west direction. The steps of the first phase of staged-inversion consisted of: (1) varying the amplitude of the total magnetization and depth extent of the block model; (2) varying the amplitude of the total magnetization, depth extent and horizontal position; (3) varying the amplitude of the total magnetization, depth extent, horizontal position and vertex movements in the north-south direction; (4) varying the parameters of the previous stage plus the position of the vertices of the model in east-west direction; and (5) varying the previous parameters and the magnetic susceptibility (in the magnetic inversion), or the density (in the gravity inversion). In the second phase, the modelling using the prisms had two differences: instead of varying the depth extent in all stages, the vertices were allowed to vary their positions in vertical direction, and stage (4) was skipped.

The quality of the modelling was assessed by the "inversion confidence" (Pratt 2006), where the confidence that the modelled body exists in the studied area varies from 0 to 100%. This interval of confidence is expressed by the root mean square value (rms-error).

3. *Synthetic Model*

A synthetic block model was created and it's magnetic and gravity fields calculated (Fig. 1, Table 1). This model presents a significant remanent magnetization, and it is exposed to an environment of negligible magnetization (0.0001 S.I.) and density of 2.67 g/cm^3. The calculated fields were then the starting point for evaluating the effects of inaccurate constraints using the staged-inversion methodology.

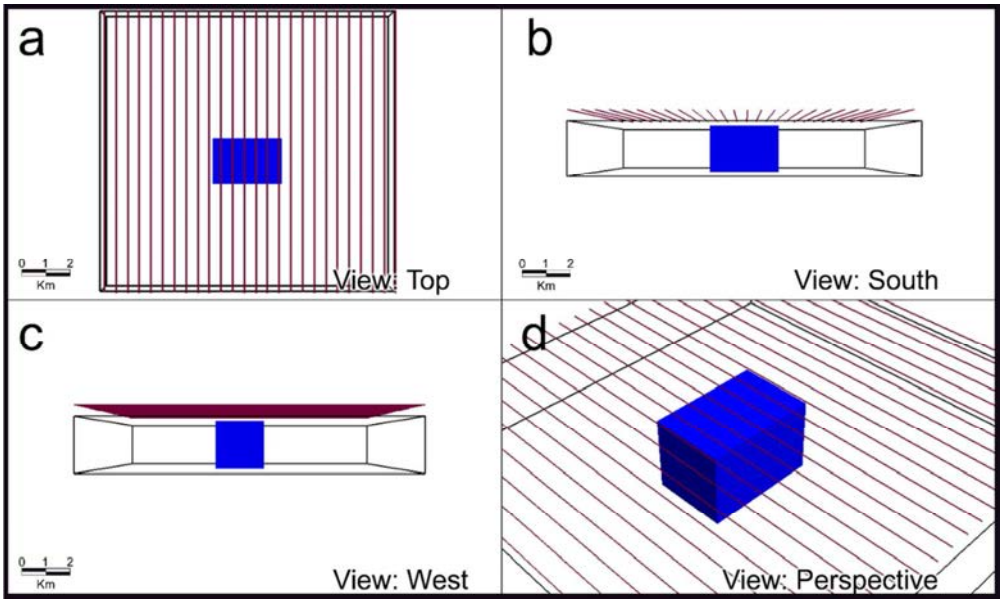

Fig. 1 – Synthetic model used in the experiments in the view: (a) top, (b) south, (c) west, and (d) perspective. The model parameters are described in Table 1.

Table 1 – Parameters of the synthetic model. In the magnetization fields, I refers to Inclination, D to Declination and J to the Intensity.

Shape	Block		
Size (E-W) (m)	3000		
Size (E-W) (m)	2000		
Depth Extent (m)	2000		
Depth (m)	200		
Density (g/cm^3)	2.94		
Magnetic Susceptibility (S.I.)	0.05		
Magnetization	Inclination	Declination	Intensity
Induced Magnetization	-11.3°	346.9°	0.95 A/m
Remanent Magnetization	49.6°	199.4°	4.39 A/m
Total Magnetization	56°	213°	3.8 A/m

Four experiments were undertaken to model the synthetic fields (Fig. 2). In two experiments the magnetic susceptibility and density were fixed, discarding step (5) of the staged-inversion, whereas for the other two experiments, these parameters were varied. In each of the two sets of experiments, one experiment started with the correct values of magnetic susceptibility and density, and the other started with half the actual contrast of both parameters with the background (Fig. 3).

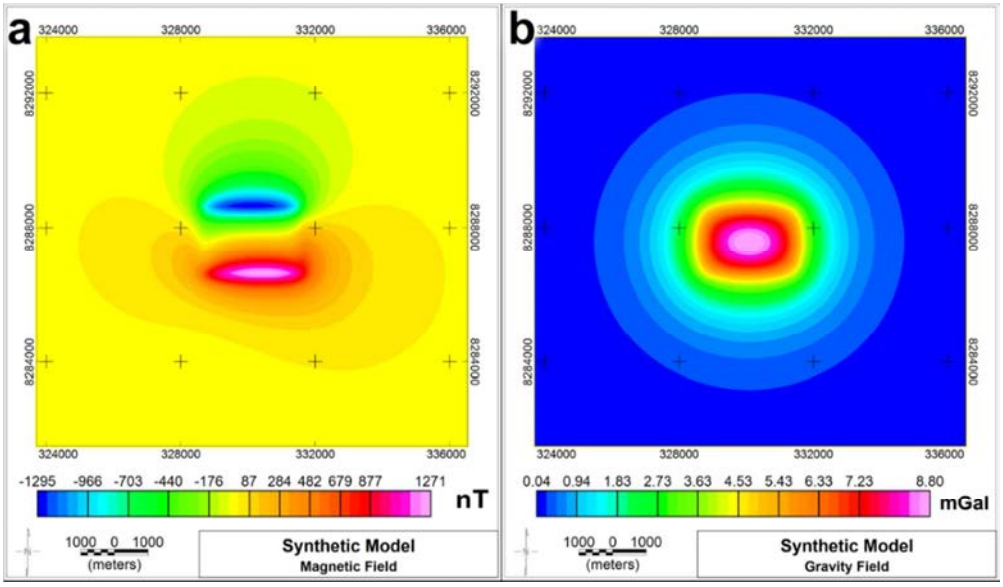

Fig. 2 – (a) Magnetic and (b) gravity fields of the synthetic body.

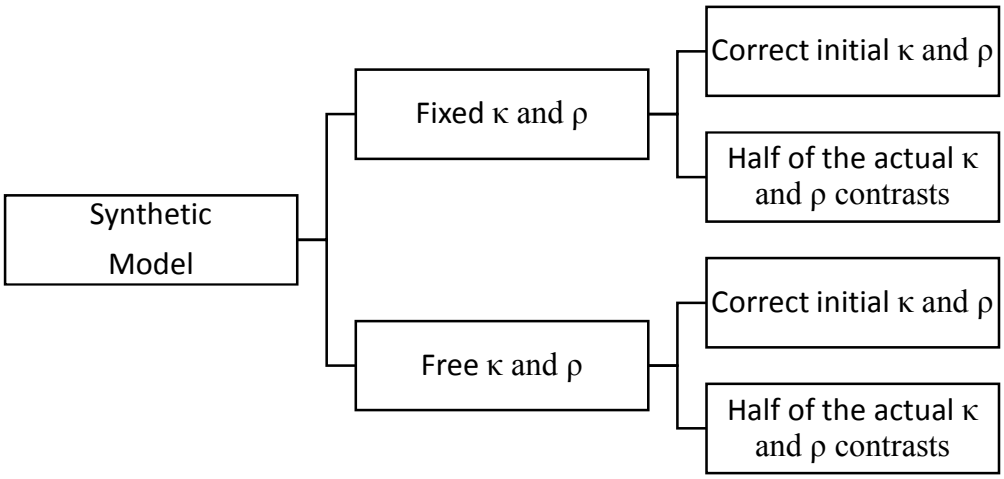

Fig. 3 – Scheme of the synthetic experiments treating the role of the magnetic susceptibility and densities in the staged-inversion. κ represents the magnetic susceptibility and ρ the density.

The MaxiMin method produced the inclination 55.6° and declination 201.9° ($\alpha_{95\%}$=5.0°), which are 0.22% and 3.25% different respectively, from the actual total magnetization direction. The field reduced to the magnetic pole showed good approximation to the shape of the body (Fig. 4a), and was positive and centered over the location of the anomaly. The lateral limits obtained with the horizontal gradient of the RTP-filtered field showed adequate compatibility with the model lateral limits (Fig. 4b). The depths obtained through Euler Deconvolution varied from 19 m to 362 m, but had the majority of solutions around 200 m (Fig. 4c and d) consistent with the depth to the top of the original model (Table 1). The structural index used was 0, with the window size of 375 m. Table 2 shows the initial model parameters used in the staged-inversion.

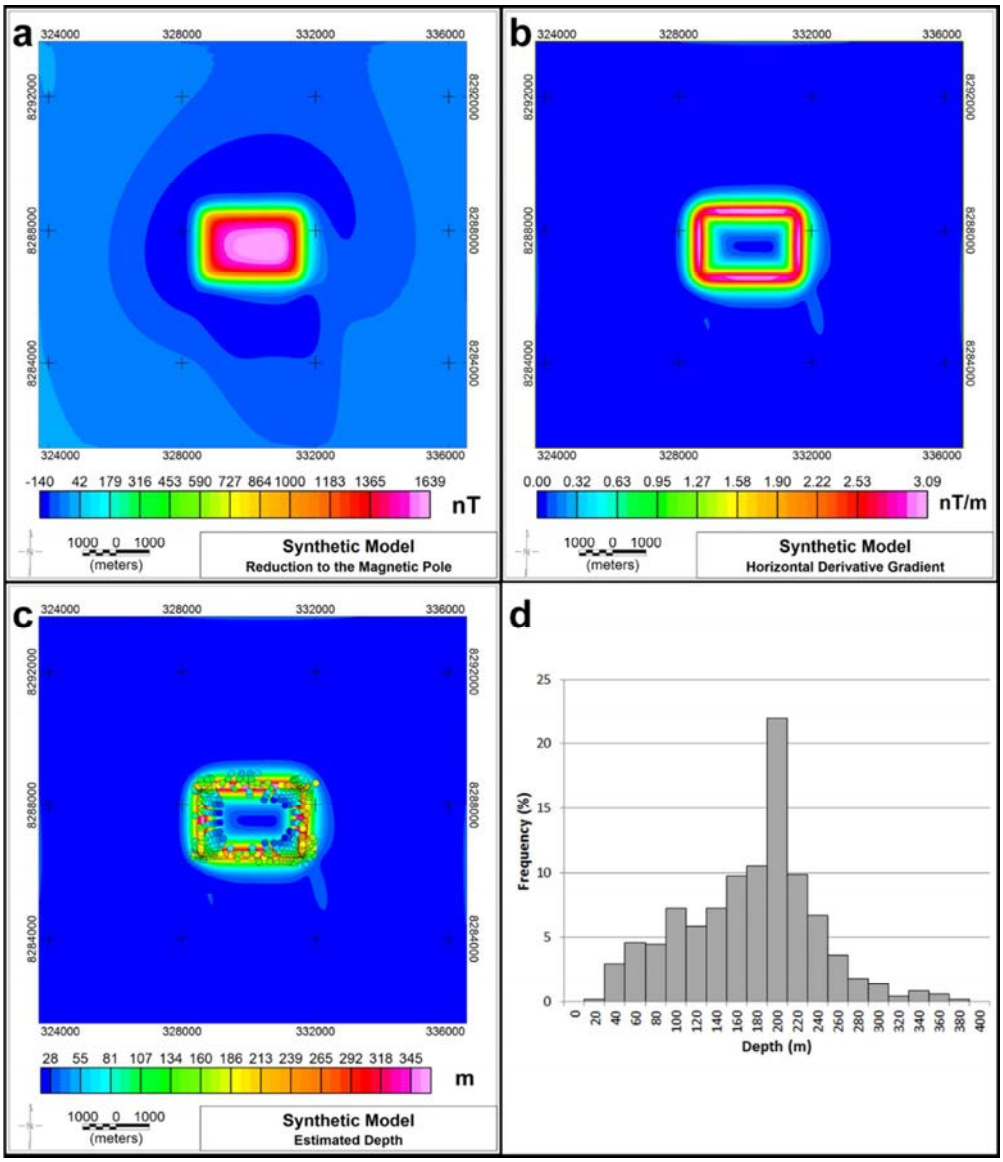

Fig. 4 – (a) RTP field, (b) horizontal derivative gradient, (c) depths estimated with the Euler Deconvolution, and (d) histogram of the solutions of the Euler Deconvolution.

Table 2 – Initial parameters used in the synthetic data modelling. In the magnetization fields, I refers to inclination, D to declination and J to the intensity.

Shape	Tabular		
Size (E-W) (m)	3000		
Size (E-W) (m)	2000		
Depth Extent (m)	1000		
Depth (m)	200		
Density (g/cm^3)	2.94	2.805 (half contrast)	
Magnetic Susceptibility (S.I.)	0.05	0.025 (half contrast)	
Magnetization	Inclination	Declination	Intensity
Induced	-11.3°	346.9°	0.5 A/m
Remanent	43.2°	186.2°	1.3 A/m
Total	55.6°	201.9°	1.0 A/m

The inversions showed low residuals: 4.0% in the worst case (Table 3). However, low residuals do not necessarily mean that an inversion was successful. The inverted models vary significantly in their physical properties (when allowed), shape and volume (Fig. 5). Model 1 (Fig. 5a and b), in which susceptibility and density were kept fixed with the correct values, reproduced the original model with reduced errors. The difference between the volume of Model 1 and the original model was 1.48 km³ (12.3%) and the top of the model was kept around 200 m below the surface. The magnetization vectors differed less than 8° in direction and 0.1 A/m in intensity from the original, with an $\alpha_{95\%}$ of 1.27° for the remanent magnetization vector.

Model 2 (Fig. 5c and d), with magnetic susceptibility of 0.025 and density of 2.81 g/cm^3 fixed, achieved directions of the magnetic vectors as close to the original model as Model 1 (Table 3, Fig 5a and b). Other features however, were not as well-resolved as in Model 1. The volume of Model 2 was 15.74 km³ larger than the actual volume, and the depth extent overestimated to compensate the reduced susceptibility and density (Fig. 5c and d). The block model had its vertex spread in the east-west direction to an area larger than the original model after the first inversion process. This spread resulted in the addition of two more sections than necessary to represent the original model, and resulted in the much larger volume.

Table 3 – Inversion results for the models 1 to 4. κ and ρ represent the magnetic susceptibility and the density, respectively.

Geophysical Models			
Background (Host-rock)			
Avg Mag Suscep		0.001 (SI)	
Avg Density		2.67 g/cm³	
Model 1: Fixed κ and ρ – Correct κ and ρ			
Avg Mag Suscep	0.05 (SI)	**Total Volume**	13.48 km³
Avg Density	2.94 g/cm³	**Difference of Volume**	1.48 km³
Magnetic and Gravity Fields Inversions			
Magnetization	**Induced**	**Total ($\alpha_{95\%}$ = 5.0°)**	**Remanent ($\alpha_{95\%}$ = 1.27°)**
Inclination (°)	-11.6	55.6	48.4
Declination (°)	346.9	201.9	191.5
Intensity (A/m)	0.9	3.8	4.4
RMS-Mag (%)	0.7	**# of Points**	78832
RMS-Grav (%)	0.5	**# of Points**	78832
Model 2: Fixed κ and ρ – Half of the correct κ and ρ			
Avg Mag Suscep	0.025 (SI)	**Total Volume**	27.74 km³
Avg Density	2.81 g/cm³	**Difference of Volume**	15.74 km³
Magnetic and Gravity Fields Inversions			
Magnetization	**Induced**	**Total ($\alpha_{95\%}$ = 5.0°)**	**Remanent ($\alpha_{95\%}$ = 9.4°)**
Inclination (°)	-11.6	55.6	49.1
Declination (°)	346.9	201.9	192.4
Intensity (A/m)	1.3	2.1	2.5
RMS-Mag (%)	1.6	**# of Points**	78832
RMS-Grav (%)	4.0	**# of Points**	78832
Model 3: Free κ and ρ – Correct κ and ρ			
Avg Mag Suscep	0.13 (SI)	**Total Volume**	12.98 km³
Avg Density	2.92 g/cm³	**Difference of Volume**	1.98 km³
Magnetic and Gravity Fields Inversions			
Magnetization	**Induced**	**Total ($\alpha_{95\%}$ = 5.0°)**	**Remanent ($\alpha_{95\%}$ = 13.9°)**
Inclination (°)	-11.6	55.6	38.9
Declination (°)	346.9	201.9	182.7
Intensity (A/m)	2.5	3.5	5.4
RMS-Mag (%)	1.5	**# of Points**	78832
RMS-Grav (%)	2.1	**# of Points**	78832
Model 4: Free κ and ρ – Half of the correct κ and ρ			
Avg Mag Suscep	0.09 (SI)	**Total Volume**	19.45 km³
Avg Density	2.81 g/cm³	**Difference of Volume**	7.45 km³
Magnetic and Gravity Fields Inversions			
Magnetization	**Induced**	**Total ($\alpha_{95\%}$ = 5.0°)**	**Remanent ($\alpha_{95\%}$ = 12.2°)**
Inclination (°)	-11.6	55.6	40.3
Declination (°)	346.9	201.9	183.7
Intensity (A/m)	3.1	2.7	3.9
RMS-Mag (%)	1.0	**# of Points**	78832
RMS-Grav (%)	1.1	**# of Points**	78832

The intensities of the magnetization vectors of Model 2 (Fig. 5c and d) were affected by the change in the magnetic susceptibility, from 0.9 A/m to 1.3 A/m in the induced magnetization and from 4.4 A/m to 2.5 A/m in the remanent magnetization. Changing the induced and remanent magnetizations caused the decrease in the total magnetization intensity from 3.8 A/m to 2.1 A/m.

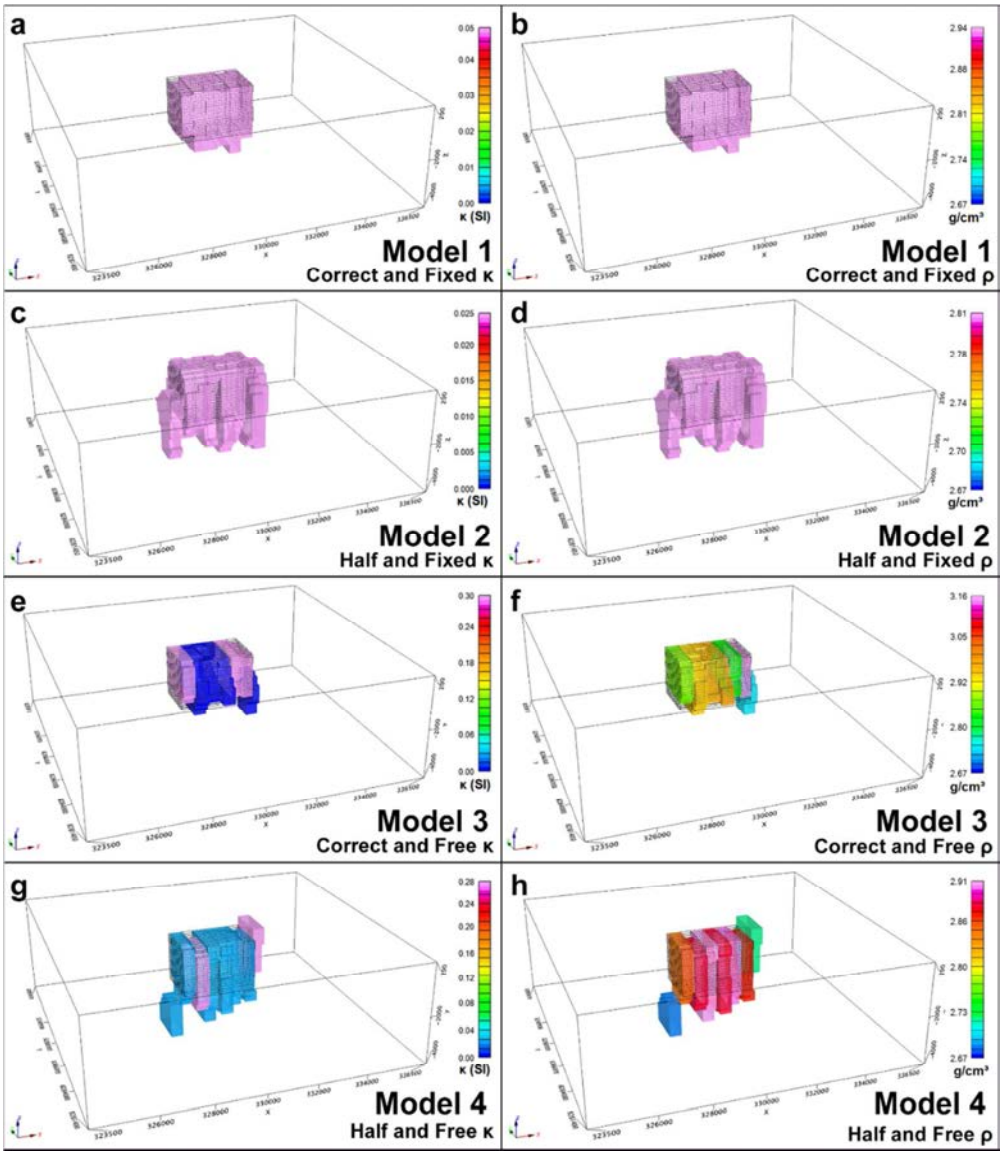

Fig. 5 – Perspective views of the modelled bodies, where (a), (c), (e) and (g) shows the magnetic susceptibility models, and (b), (d), (f) and (h) the density models. The black wireframe model in each of the models represents the original model (Fig. 1).

The inversion of Model 3 (Fig. 5e and f) started with the correct properties (magnetic susceptibility and density), and the inversion of Model 4 (Fig. 5g and h) with magnetic susceptibility of 0.025 (S.I.) and density of 2.81 g/cm^3. These features were allowed to vary during the inversion. The result for Model 3 was a body with volume and shape close to the original model (1.98 km³ larger, Fig. 5e and f). In the Model 4 inversion (Fig. 5g and h), a 7.45 km³ higher disparity to the original model was found. As in Model 2, the lateral spread of the block model after the first inversion process took to the creation of more north-south sections than necessary in models 3 (1 section) and 4 (2 sections). In both cases, the additional sections were displaced to shallower or much deeper positions than the remaining sections (Fig. 5e to h). The additional section in Model 3, displaced to a deeper horizon, had significantly reduced magnetic susceptibility and density, making its contribution to the gravity and magnetic fields insignificant (Figs. 6 and 7).

In Model 4 (Fig. 5g and h), the western additional section had the same behaviour as the additional section of Model 3 (Fig. 5e and f), whereas the eastern additional section was displaced to shallower depth. The easternmost additional section, and the second westernmost section, of Model 4 had increased magnetic susceptibility to 0.30 (S.I.), which caused the decrease of magnetic susceptibility in the remaining sections to compensate the field. The additional eastern section had a decrease in density, diminishing its contribution to the gravity field, whereas the rest of the sections showed minimal variation near the density value of the original model.

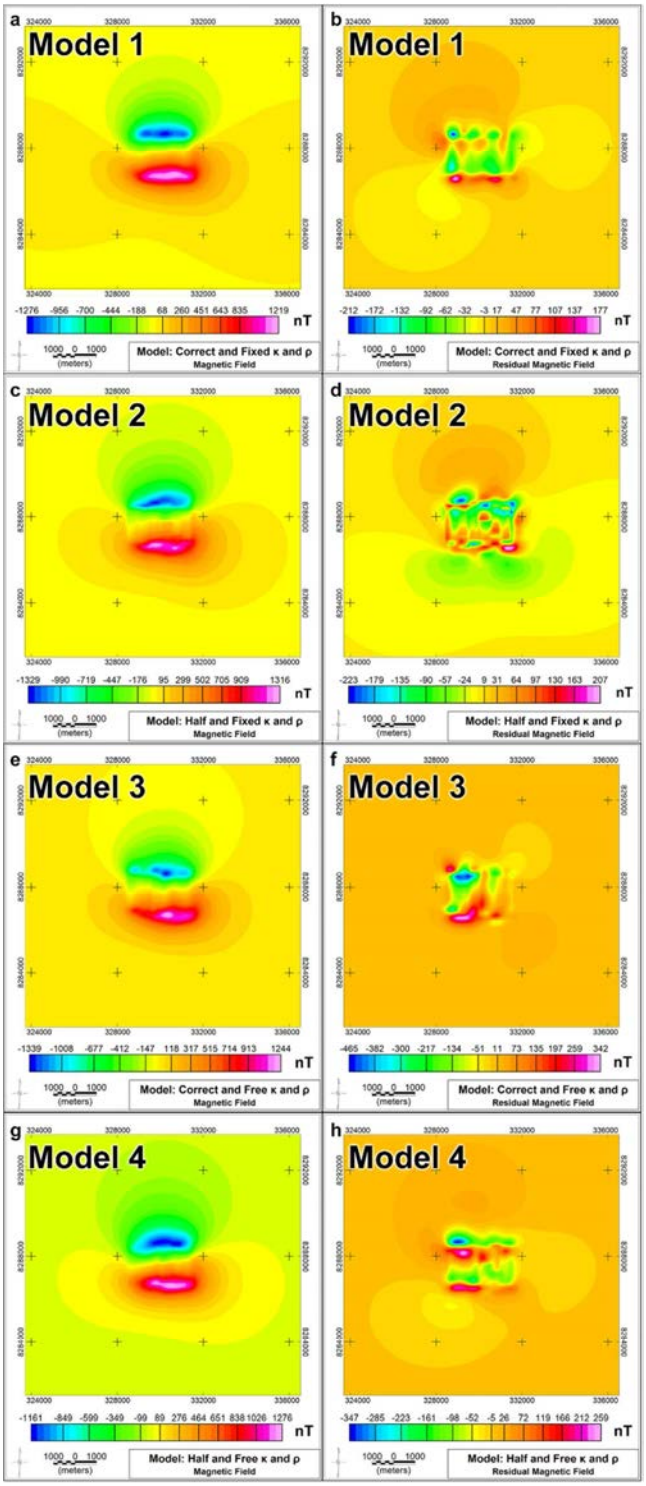

Fig. 6 – Magnetic and residual magnetic fields, respectively, of Model 1 (a and b), Model 2 (c and d), Model 3 (e and f), and Model 4 (g and h).

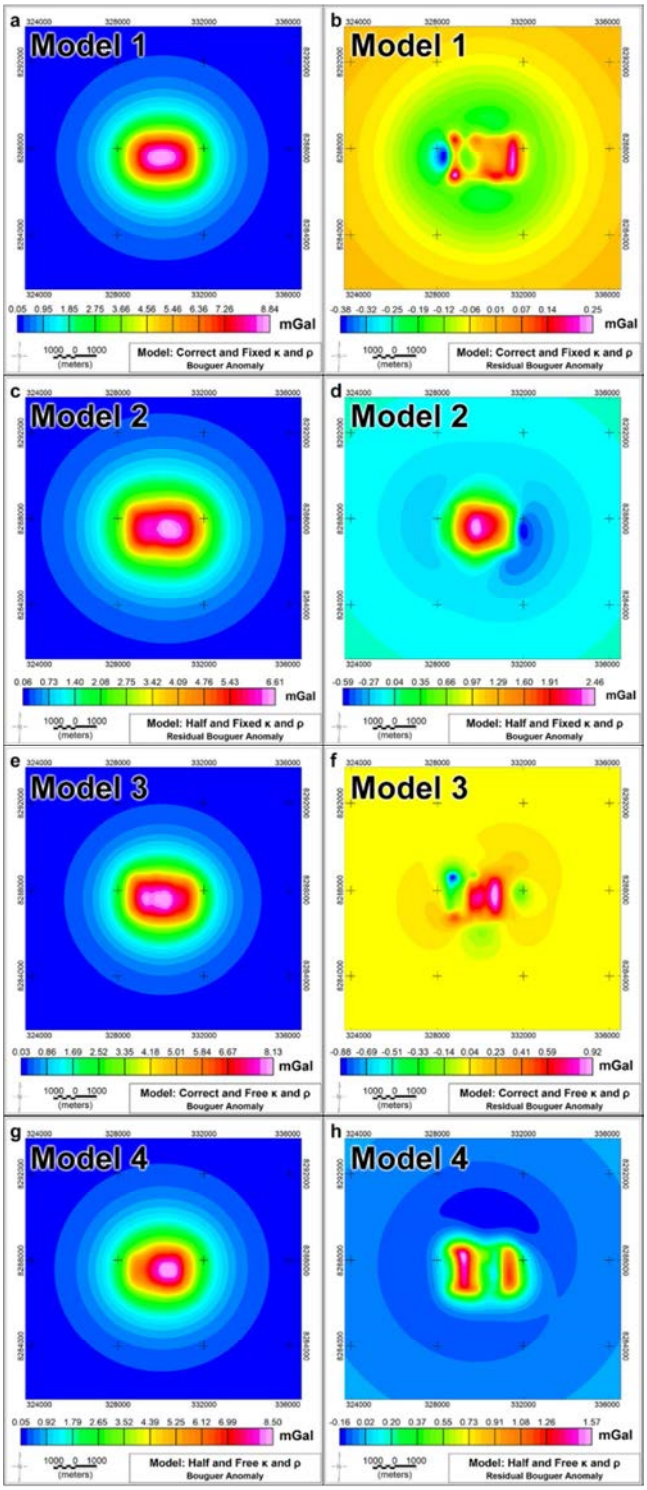

199

200 Fig. 7 – Gravity and residual gravity fields, respectively, of Model 1 (a and b), Model 2 (c and d),

201 Model 3 (e and f), and Model 4 (g and h).

The distribution of magnetic susceptibilities, and as a consequence magnetization, were severely affected in both models 3 and 4 (Fig. 5e to h). Higher magnetic susceptibilities and magnetizations were concentrated in three (Model 3, Fig. 5e) and two (Model 4, Fig. 5g) north-south sections. This concentration caused significant decrease in physical properties in the other sections of both models. The highest values of magnetic susceptibility were up to 0.28 and 0.30 (S.I.), six times higher than the original model (Table 2). The densities had less drastic lateral change, with values that approximated to the original model (Table 2 and 3).

The residual fields (Figs. 6 and 7) indicated low values, with local significant anomalies that usually represented the compensation of volume in Model 2 and the additional sections in models 3 and 4. The residuals of the magnetic and gravity fields of Model 1 were considerably low, indicating good solutions for the modelled field.

4. Real Case

4.1. Geological Context

Lying in the southwest of Mato Grosso State, Brazil, the Jauru Terrane contains the Alto Jauru Group and the Alto Guaporé Metamorphic Complex (Souza *et al.* 2009; Matos *et al.* 2009). The Alto Jauru Group (1760 to 1720 Ma) (Monteiro *et al.* 1985; Bettencourt *et al.* 2010) comprises gneiss, migmatites and the Cabaçal, Araputanga and Jauru meta-volcanosedimentary sequences. The Alto Guaporé Metamorphic Complex (1790 to 1740 Ma) (Menezes 1993) is characterized by orthogneiss intruded into supracrustal volcanosedimentary sequences, both metamorphosed to greenschist or amphibolite facies (Bettencourt *et al.* 2010).

The Figueira Branca Suite (Fig. 8) is a layered mafic-ultramafic complex composed of dunite, pyroxenite, gabbro-norite, anorthosite, troctolite, and olivine-gabbro (Teixeira *et al.* 2011). The

crystallization age of the Indiavaí gabbro, the southernmost intrusion of the Figueira Branca Suite, was dated by SHRIMP U-Pb zircon at 1425 ± 8 Ma. Ar-Ar dating on biotites yielded plateau ages of 1275 ± 4 Ma and 1268 ± 4 Ma, which were evaluated as minimum ages for regional cooling (Teixeira *et al.* 2011).

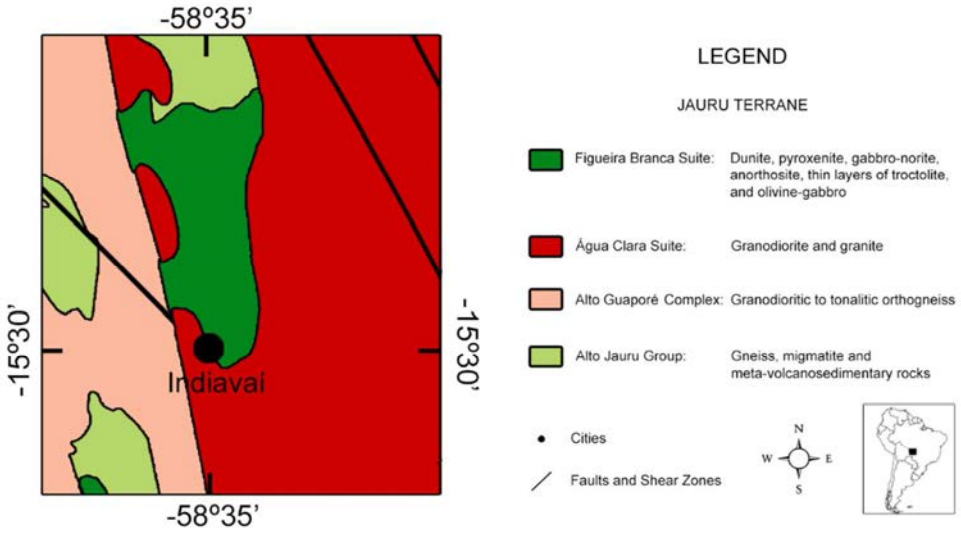

Fig. 8 – Local geological map (Saes *et al.* 1984; Nunes 2000; Teixeira *et al.* 2011).

In 2006, the Brazilian Geological Service (CPRM) undertook the magnetic field airborne survey "Projeto 1080 – Área 2 Mato Grosso". This survey covers the region occupied by the Figueira Branca Suite. The collected magnetic field data revealed a magnetic anomaly coherent with the Indiavaí body outcrops. The magnetic anomaly showed a complex signature (Fig. 9), which is different from that expected for purely induced magnetic anomalies in the south hemisphere, where the positive area is to the north and the negative to the south of the centre of the magnetic source. The magnetization contrast supported a gravity ground survey and the collection of samples for geophysical and mineralogical analyses over the suite. 50 samples were collected, 15 in the Indiavaí area, of mafic-ultramafic rocks of the Figueira Branca Suite, of granitic suites adjacent to the Figueira Branca, and of the meta-volcanosedimentary Alto Jauru Group (Fig. 8).

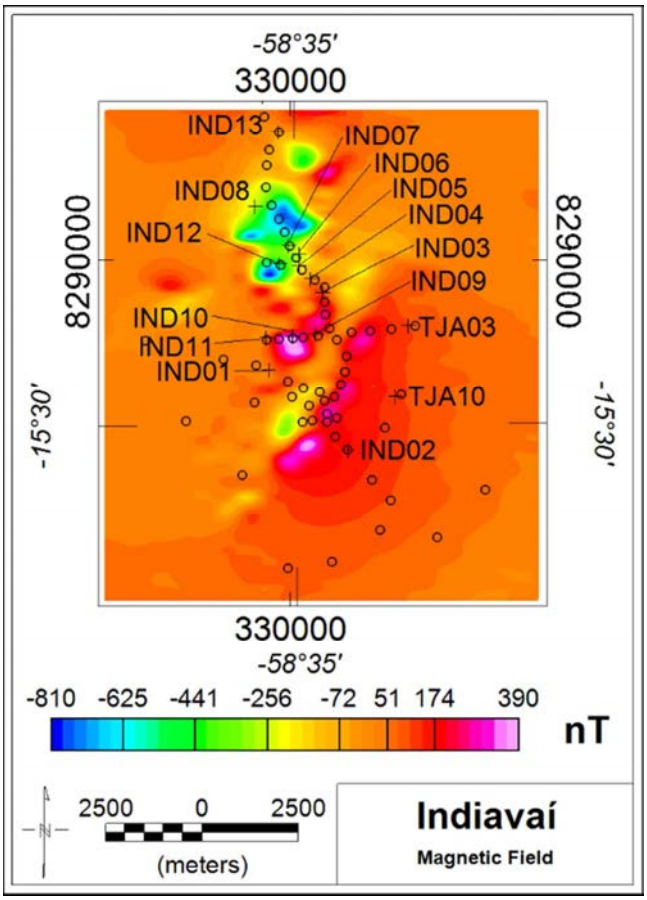

Fig. 9 – Magnetic anomaly of Indiavaí. The black circles indicate the location of the gravity stations.

4.2. Data

The magnetic field survey used Geometrics G-822A Cesium magnetometers with a resolution of 0.001 nT. The sampling interval of 0.1 s resulted in an approximate sample spacing of 7.8 m. The magnetic noise level is 0.5 nT after the industry standard corrections were applied. The average International Geomagnetic Reference Field (IGRF) ambient field for this period had inclination -11.6°, declination 234.9°, and intensity 23749 nT.

Density measurements were made on the collected samples using the "Archimedes method". These measurements were performed with distilled water and a high-precision analytic balance. Magnetic susceptibility measures were taken using a Kappameter KT-9 magnetic susceptibility meter (Table 4). Thin sections of the samples from the intrusion and from the host-rock were prepared and analysed.

Table 4 – Densities and magnetic susceptibilities of the samples from Figueira Branca Suite area.

Sample	Lithology	Suite/Group	Density (g/cm^3)	Error (g/cm^3)	Magnetic Susceptibility (SI)	Error (SI)
IND01	Granite	Água Clara	2.63	$4.31 \cdot 10^{-7}$	0.010	0.001
IND02	Gneiss	Alto Guaporé	2.96	$3.50 \cdot 10^{-5}$	0.011	0.001
IND03	Gabbro	Figueira Branca	2.96	$2.59 \cdot 10^{-5}$	0.073	0.005
IND04	Gabbro	Figueira Branca	2.89	$2.64 \cdot 10^{-7}$	0.028	0.002
IND05	Gabbro	Figueira Branca	2.99	$2.30 \cdot 10^{-7}$	0.038	0.003
IND06	Gabbro	Figueira Branca	2.87	$3.28 \cdot 10^{-5}$	0.024	0.002
IND07	Diorite	Água Clara	2.91	$2.51 \cdot 10^{-5}$	0.002	0.000
IND08	Granite	Alto Jauru	2.66	$1.85 \cdot 10^{-5}$	0.000	0.000
IND09	Gabbro	Figueira Branca	2.92	$3.52 \cdot 10^{-5}$	0.039	0.003
IND10	Gabbro	Figueira Branca	2.93	$1.74 \cdot 10^{-5}$	0.057	0.004
IND11	Gabbro	Figueira Branca	2.76	$2.03 \cdot 10^{-7}$	0.000	0.000
IND12	Granite	Água Clara	2.76	$2.57 \cdot 10^{-7}$	0.001	0.000
IND13	Granite	Água Clara	2.69	$1.33 \cdot 10^{-5}$	0.031	0.004
TJA03	Gneiss	Alto Jauru	2.89	$2.59 \cdot 10^{-7}$	0.000	0.000
TJA10	Gneiss	Alto Jauru	2.82	$2.17 \cdot 10^{-7}$	0.010	0.000

The samples were divided in two groups: one comprising specimens from the Figueira Branca Suite, and one from the adjacent lithologies that host the suite. The limits of Figueira Branca Suite have been defined since the 1980's. Rocks assigned to the suite and to the country rock were based on field and thin-section analysis. The density and magnetic susceptibility measurements for the samples collected in the suite domain showed a large variation. The densities varied from 2.63 g/cm^3 to 2.99 g/cm^3, whereas the magnetic susceptibility ranged from 0 to 0.073 (S.I.). Averages for the density and magnetic susceptibility of the mafic rock samples were, 2.89 g/cm^3 and 0.027 (S.I.) respectively. The

average values are low for a mafic-ultramafic suite, so thin section analyses were taken to evaluate the cause.

4.3. Samples and Thin Sections

Despite the apparent freshness of the hand samples, the thin sections showed variable degrees of alteration and weathering. Seven thin sections of samples collected from the Indiavaí body (Fig. 10) revealed plagioclase to be the dominant mineral phase (c.a. 70%), followed by olivine (c.a. 20%) and pyroxene (c.a. 10%). The samples IND01, IND08 and IND13 were recognized as granitic rocks and considered as part of the host-rock. The samples IND03 and IND10 were the least affected by weathering or alteration, and maintained higher values of density and magnetic susceptibility. These two samples were coarse grained, with plagioclase crystals reaching 5 mm and olivine crystals of 2 mm. Samples IND04, IND05, IND06 and IND09 showed signs of weathering along fractures of olivine grains, and more significantly in plagioclase grains in sample IND06, which displayed both weathering and alteration. The weathering was present on a smaller scale than in IND05, but it is possible to observe serpentinization along olivine fractures. IND07 displayed intense weathering, and it was impossible to identify primary igneous crystals.

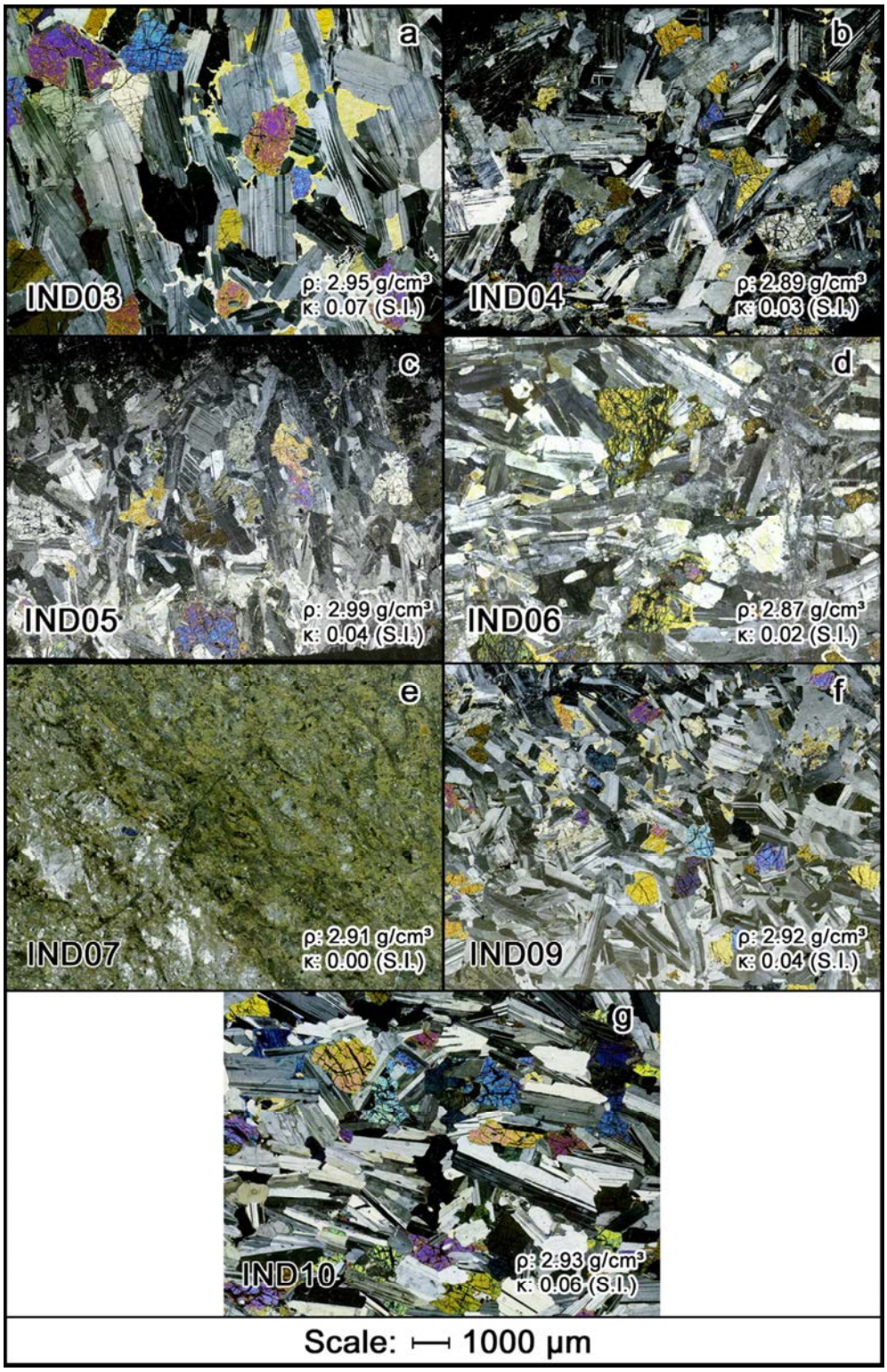

Fig. 10 – Thin sections from the Indiavaí body (a) IND03, (b) IND04, (c) IND05, (d) IND06, (e) IND07, (f) IND09 and (g) IND10. ρ indicates the measured density, whereas κ represents the magnetic susceptibility. The images were produced with cross-polarized light.

The presence of opaque oxide crystals occurs in a number of samples (e.g., IND03 and IND10). D'Agrella-Filho et al. (2012) identified euhedral magnetite crystals (Fig. 11) up to approximately 0.5 mm in samples from the same outcrop as sample IND03. The higher content of opaque crystals in IND03 and IND10 can be associated with the considerably higher magnetic susceptibility, when compared with other Indiavaí samples.

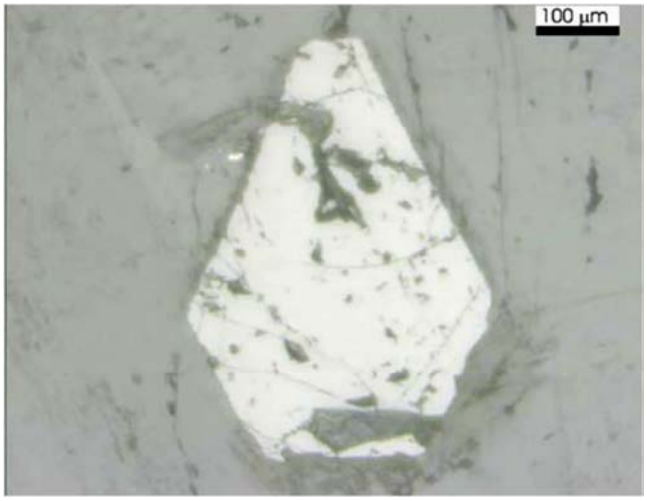

Fig. 11 – Euhedral magnetite crystal from the Indiavaí body (D'Agrella-Filho *et al.* 2012).

4.4. Potential Fields Modelling

The outcrops of the Indiavaí body indicate the body extends to the surface. The complex magnetic anomaly pattern of the body, likely reflecting different sources, impeded the MaxiMin method to reduce the field to the pole with minimum negative values (Fig. 12a). The best approximation was an inclination of 56° and declination of 213° ($\alpha_{95\%}$=5°, 386 iterations). The inclination 56° and the declination 213° were used as fixed total magnetization directions during the

whole staged-inversion. The lateral limits were assessed through horizontal gradient derivatives of the field reduced to the pole (Fig. 12b).

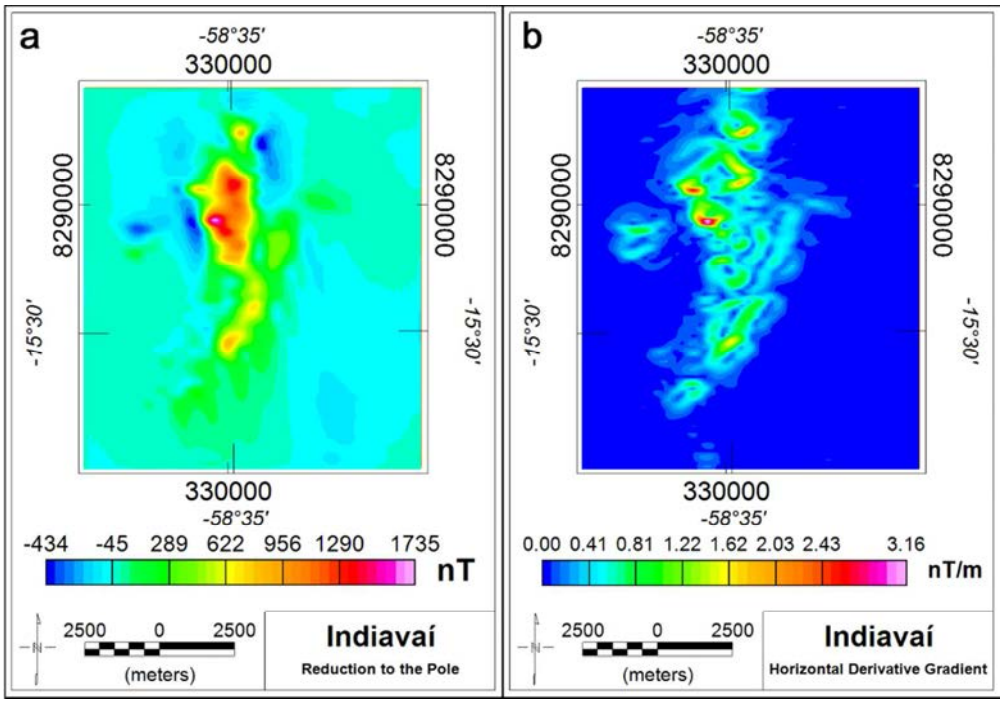

Fig. 12 – (a) Reduction to the pole and (b) horizontal derivative gradient of the Indiavaí magnetic anomaly.

Two inversions were performed following the same principles as applied to the synthetic models. Model R1 (Fig. 14a to c) used only measurements from samples considered fresh on the basis of the thin section analysis, and kept them fixed during the inversion; the best case scenario. Model R2 (Fig. 14d to f) used all density and magnetic susceptibility measurements and let them vary during the inversion, as is generally used in exploration projects. Table 5 shows the characteristics and rms-errors for the two real-case models. The inversion of the magnetic field happened in the two phases described in the methodology section, whereas the gravity field inversion occurred only in profiles (second phase of the staged-inversion) due to the reduced number and restricted spread of gravity stations.

Table 5 - Inversion results for the model considering all the magnetic susceptibilities and density measurements, and for the model with the magnetic susceptibilities and densities from samples considered fresh after the thin sections analyses. κ and ρ represent the magnetic susceptibility and the density, respectively.

Geophysical Models			
Background (Host-rock)			
Average Magnetic Susceptibility		0.007 (SI)	
Average Density		2.70 g/cm³	
Model R1: Fixed κ and ρ – IND03, IND05, IND09 and IND10			
Average Magnetic Susceptibility		0.05 (SI)	
Average Density		2.94 g/cm³	
Total Volume		9.35 km³	
Magnetic and Gravity Fields Inversions			
Magnetization	**Induced**	**Total ($\alpha_{95\%}$ = 5.0°)**	**Remanent ($\alpha_{95\%}$ = 8.9°)**
Inclination (°)	-11.6	56	49.6
Declination (°)	346.9	213	199.5
Intensity (A/m)	0.9	3.8	4.4
RMS-Mag (%)	4.9	**# of Points**	29003
Average RMS-Grav (%)	8.6	**# of Points**	60
Model R1: Free κ and ρ – Samples IND02 to IND07 and IND09 to IND12			
Average Magnetic Susceptibility		0.29 (SI)	
Average Density		2.83 g/cm³	
Total Volume		22.23 km³	
Magnetic and Gravity Fields Inversions			
Magnetization	**Induced**	**Total ($\alpha_{95\%}$ = 5.0°)**	**Remanent ($\alpha_{95\%}$ = 13.6°)**
Inclination (°)	-11.6	56	27.7
Declination (°)	346.9	213	207.7
Intensity (A/m)	4.2	1.4	4.7
RMS-Mag (%)	7.4	**# of Points**	29003
Average RMS-Grav (%)	11.0	**# of Points**	60

The inversion using magnetic susceptibility and density measurements on samples IND03, IND05, IND09 and IND10 (Model R1) achieved a rms-error of 4.9% in the magnetic case and 8.6%, on average for the Bouguer anomaly profiles (Table 5). The maximum absolute residuals were 450 nT (Fig. 13a to c) and 0.6 mGal (Fig. 14a). The highest residual amplitudes are concentred in two spikes. The modelled body had 10500 m in north-south direction and 4000 m in the east-west. The maximum vertical extension achieved was 1000 m (Fig. 15). The remanent magnetization obtained for this model had an inclination 49.6°, declination 199.5° and intensity 4.4 A/m ($\alpha_{95\%}$ = 8.9°).

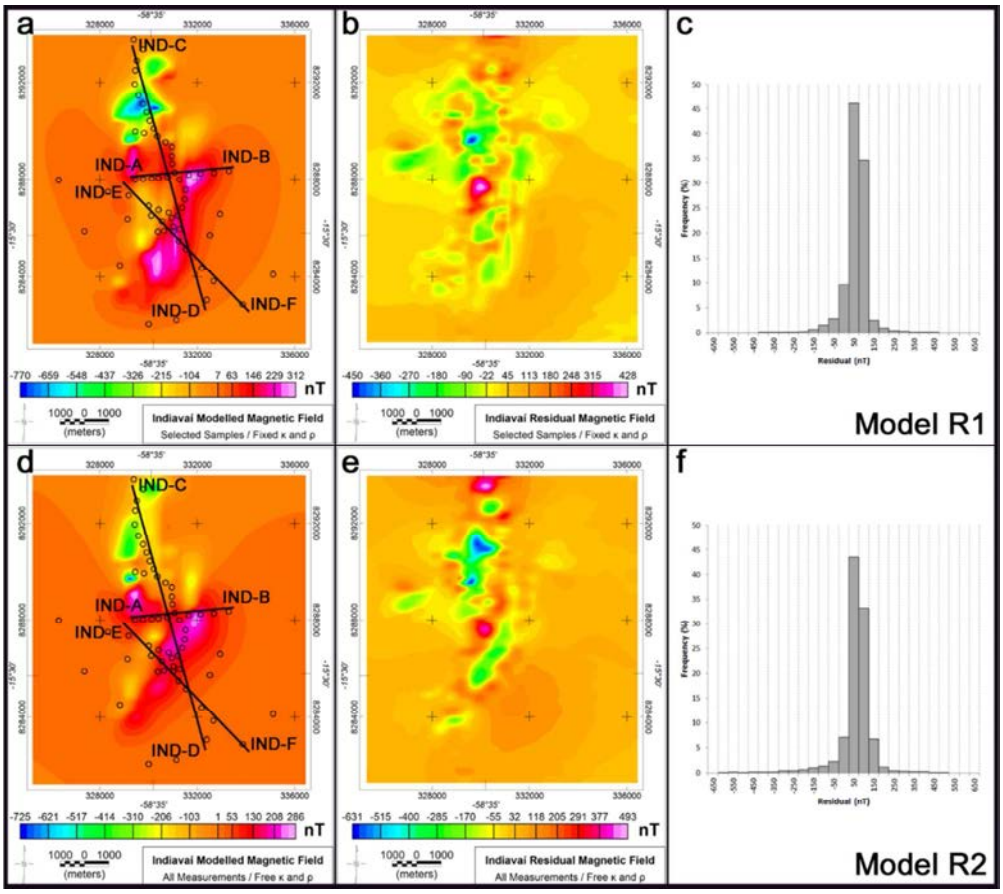

Fig. 13 – Model R1 (a) modelled and (b) residual magnetic fields, (c) histogram of residual values. Model R2 (d) modelled and (e) residual magnetic fields, (f) histogram of residual values. The black circles indicate the location of the gravity stations and the black lines the profiles used for gravity modelling.

Model R2 (Fig. 14d to f) used all the available measurements (samples IND02 to IND07 and IND09 to IND12), and let them vary during the staged-inversion. The modelled magnetic field had rms-error of 7.4%, and the average rms-error of 11% in the Bouguer anomaly profiles (Table 5). The absolute residuals were 631 nT and 0.8 mGal (Fig. 14). The more significant values are distributed along four regions in the centre and at the north of the magnetic and Bouguer anomaly fields (Figs. 14 and 15). The lateral extension of the modelled body was 10700 m in north-south direction and 4000 m in the east-west, and it had maximum vertical extension of 2500 m (Fig. 14). The remanent magnetization obtained in this case was defined by inclination 27.7°, declination 207.7° and intensity 4.7 A/m ($\alpha_{95\%}$ = 13.6°).

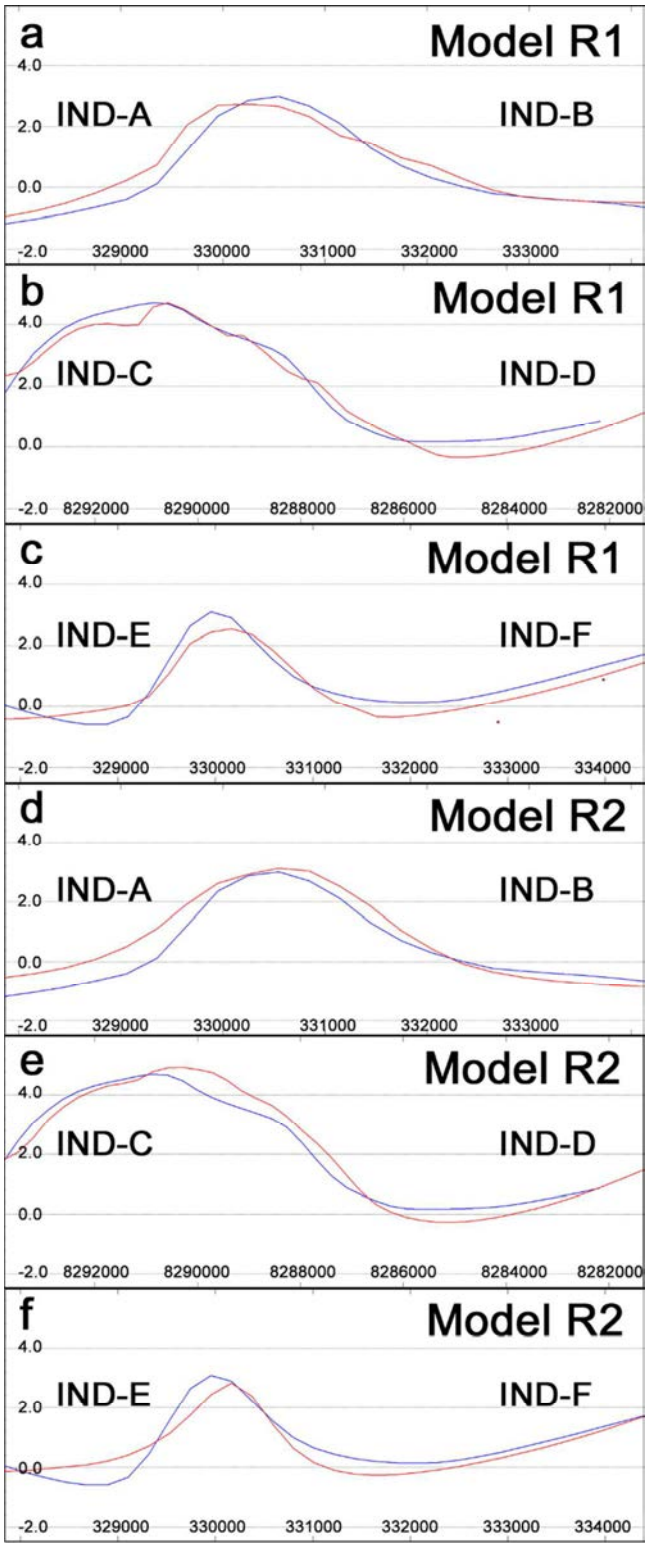

Fig. 14 – Bouguer anomaly profiles (blue) and modelled Bouguer anomaly (red) for models R1 and R2. (a) and (d) shows the profile from IND-A to IND-B (Fig. 13), (b) and (e) the profile from IND-C to IND-D, and (f) and (g) present the profile from IND-E to IND-F.

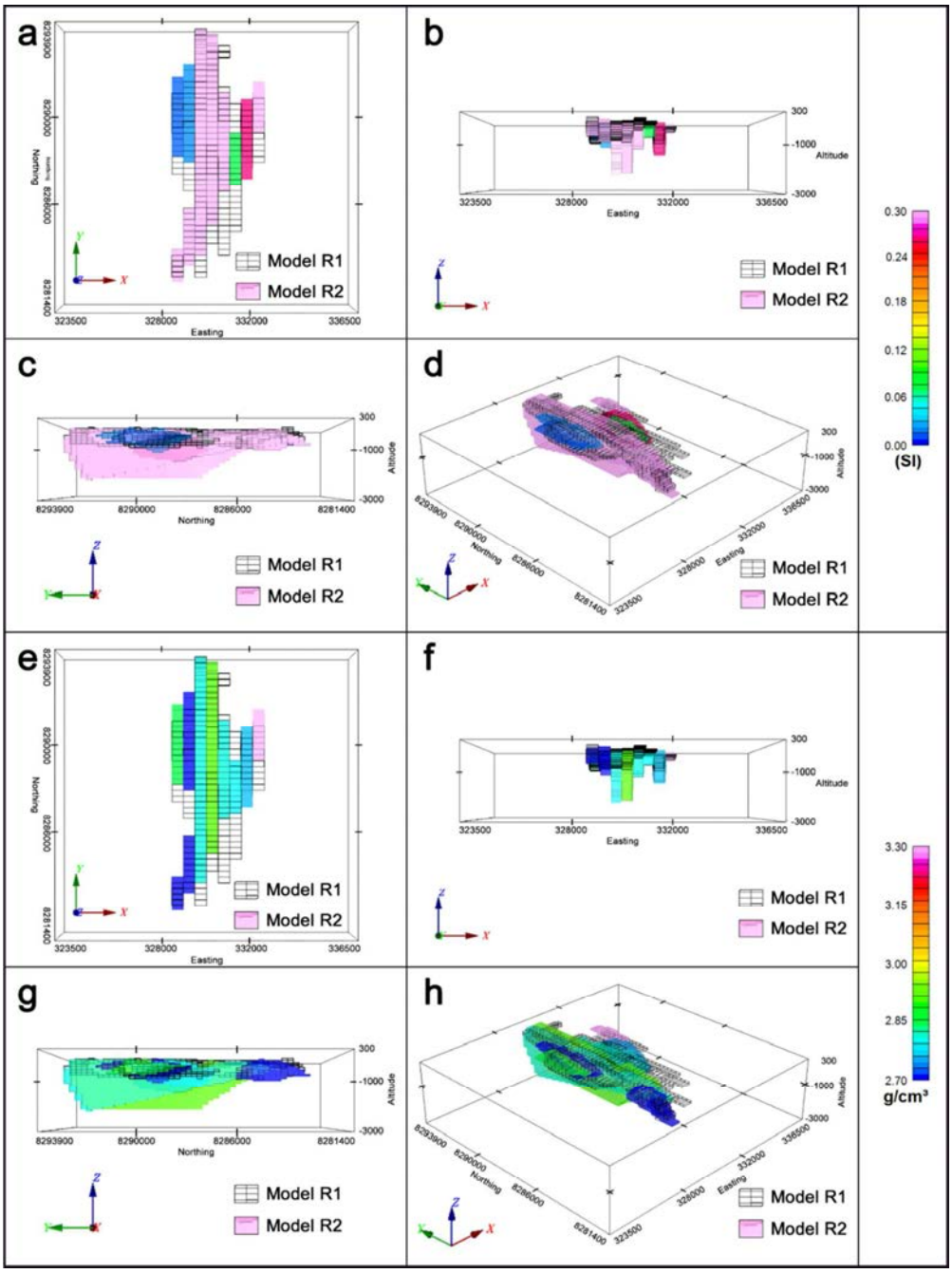

Fig. 15 – Magnetic susceptibility and density distribution for models R1 and R2 in the views: (a) and (e) top, (b) and (f) south, (c) and (g) west, and (d) and (h) perspective (inclination 30°, azimuth 45°). Model R1 is represented by a black grid and represents the magnetic susceptibility 0.05 and density 2.94 g/cm^3.

5. Discussion

Modelling the magnetic and gravity field of the synthetic body using both the same parameters as the original synthetic body and using inaccurate constraints, and keeping them fixed or allowing them to vary in the staged inversion, indicated that the rms-error can be reduced to acceptable values in all cases. However, the shape of the modelled body and the distribution of magnetic susceptibilities and densities were severely affected. The modelled fields had rms-errors smaller than 4.0%, a good value considering that it is a synthetic model without noise or interfering anomalies. The apparent remanent magnetization in all cases differed from the original model by less than 10°, both in inclination and declination, whereas the intensities have not exceeded more than 2 A/m of difference.

The lateral distribution of the modelled bodies kept the overall shape of the original model. Model 1 (Fig. 5a and b) had the best distribution as would be expected for a model using all the correct constraints. Models 2 to 4 (Fig. 5c to h) presented one to two sections more than the original model, and their depths and depth extents were overestimated during the inversion. Model 2, which kept fixed the magnetic susceptibility and density, extended to depths almost twice the size of the original model. Models 3 and 4 (Fig. 5e to h) showed smaller variations in depth, except for the sections that lay beyond the original model limits, which were displaced to considerably shallower or deeper depths (Fig. 6).

Models 3 and 4 (Fig. 5e to h), in which magnetic susceptibilities and densities were allowed to vary during the staged inversion, displayed variation in these features along the north-south oriented sections. Both cases showed much higher properties in two or three sections, whereas the remaining sections had values next to zero. This behavior was reflected in the residual fields, indicating exactly the sections with higher proprieties, and what increased the rms-error.

The four synthetic cases showed that inaccurate constraints can interfere with the final result of the modelling. Unsurprisingly, the best solution for the synthetic gravity and magnetic fields was achieved by modelling with the right constraints fixed (Model 1, Fig. 5a and b), which resulted in a

low rms-error (Table 2) and a model with the closest shape, volume and physical properties to the original body. In real cases, having all the correct constraints is not trivial or even possible in some situations. The next best result was achieved by modelling with the correct initial constraints and then allowing the magnetic susceptibility and density to change during the inversion (Model 3). Model 4, which used inaccurate parameters that were allowed to change during the modelling, had the third best result on the basis of the model and the rms-errors. The least reliable model used inaccurate magnetic susceptibility and density values that were keep fixed during the inversion.

The magnetic and gravity anomalies associated with the Indiavaí body of the Figueira Branca Suite were modelled using two of the cases shown with the synthetic models. One case (R1) used only magnetic susceptibilities and densities from samples selected after mineralogical analyses, and kept these features fixed during the staged inversion, similarly to Model 1. The second case, Model R2, used all the measurements available and let magnetic susceptibility and density change during the staged inversion, like Model 4. The two methodologies were chosen to apply the best case scenario indicated by the synthetic model inversion, and the most common situation in geophysical exploration, with limited data available.

The two inversions obtained low rms-errors for real data. Low rms-errors do not necessarily reflect an adequate and geologically feasible result. Both models were elongated in north-south direction and presented the same 4000 m extension in east-west direction. The major differences between the two models were in the vertical extension, the volume, and the distribution of magnetic susceptibility and density (Table 5 and Fig. 15). The maximum vertical extension of Model R2 was 2.5 times larger than in Model R1. This difference reflected directly in the volume, which showed similar proportion (2.37 times).

Model R1 kept the magnetic susceptibility and density fixed, but varied the amplitude of total magnetization, depth and the position of the vertices of the model. This staged-inversion proved to be more time-consuming, especially on areas where the gravity profiles crossed the magnetic lines and each other. The results showed a more compact body, and smaller errors than the inversions of Model R2. The staged-inversion of Model R2 reduced the error considerably faster than in Model R1

process. Model 2, however, presented a large variation in the depth of the base of the model and in the magnetic susceptibility and density. These last two features, similarly to the synthetic cases 3 and 4 (Fig. 5e to h), presented the concentration of higher values in some north-south sections, whereas the remaining sections ended up with values near zero (Fig. 15).

The apparent remanent magnetization obtained in both real data cases were similar to the paleomagnetic data obtained by D'Agrella-Filho *et al.* (2012). The natural remanence magnetization (NRM) for the Indiavaí body has inclination 50.7° and declination 209.8° ($\alpha_{95\%}$ = 8.0°). The apparent remanent magnetization for Model R1 had inclination 63.0° and declination 187.3° ($\alpha_{95\%}$=8.9°), and for Model R2, inclination 27.7° and declination 207.7° ($\alpha_{95\%}$=13.6°). The proximity of the indirectly estimated apparent magnetic remanence with the calculated NRM is remarkable, considering the complexity and degree of interference of smaller anomalies over the main Indiavaí magnetic anomaly.

6. Conclusions

Measurements of densities and magnetic susceptibilities of samples from the Indiavaí body from the Figueira Branca suite were abnormally low. Modelling potential fields with inaccurate constraints can produce results significantly different than the actual source of the geophysical signals.

A synthetic model was composed and used to test four different approaches for the staged-inversion: two keeping the magnetic susceptibility and density fixed, and two setting them free during the inversion. Correct and inaccurate properties were used in both cases. The model keeping the correct properties fixed was the one that best reduced the residuals between observed and modelled magnetic and gravity fields, and resulted in the shape and volume that best approached the original model. The other models approximated to the original synthetic model, minimizing the rms-errors and

quantitatively followed the sequence, from best to worst: correct properties set free (Model 3), inaccurate properties set free (Model 4), and inaccurate fixed properties (Model2).

Based on the results from the synthetic models, the magnetic and gravity field anomalies associated with the Indiavaí body of the Figueira Branca Suite were modelled. Values of density and magnetic susceptibilities were averaged from measurements obtained from hand-samples. Some of the values obtained on these measurements were relatively low for the mafic-ultramafic rocks that constitute the Figueira Branca Suite and corresponded with thin-section observations indicating varying degrees of alteration and weathering.

Based on the variation in the condition of the samples, two approaches were used to evaluate the effects of inaccurate constraints in the modelling of real potential fields. One model (R1) used measurements made only on fresh samples, indicated by thin-sections, and kept these values fixed during inversion. The second model (R2) used all the measurements, emulating a case where thin-section analyses would not be available. Although both inversions presented rms-errors below 13% for a considerably complex anomaly, Model R1 still had an rms-error of almost half of Model R2. The shape of R1 was more regular and compact, with a single magnetic susceptibility and density for all sections. Model R2 had 2.5 times the volume and vertical extension of Model R1. However, it took much less time to achieve the rms-error than in Model R1. Distributions of magnetic susceptibility and density as seen in Model R2 (north-south-oriented sections of fixed physical properties) are geologically feasible, but less plausible for potential field modelling than assuming a homogeneous distribution, as in Model R1.

Exploration projects frequently do not have the necessary time to spend on long and complex modelling procedures, which makes the approach used in Model R2 appealing. Nevertheless, the magnetic susceptibility and the density evidenced the importance of using correct constraints. The results obtained in this paper showed that geological observation, thin-sections, and any other direct, and/or indirect, constraints are valuable assets for a proper and reliable modelling.

7. Acknowledgements

The authors would like to thank Sebastian Fischer, Stuart Allison and Donald Herd for the help with the thin sections, Vanessa B. Ribeiro for comments, and the Brazilian Geological Service for the data. This work was done with the support of the CNPq, National Council for Technological and Scientific Development – Brazil.

8. References

Bettencourt, J.S., Leite Jr, W.B., Ruiz, A.S., Matos, R., Payolla, B.L. & Tosdal, R.M., 2010. The Rondonian-San Ignacio Province in the SW Amazonian Craton: An overview, *Journal of South American Earth Sciences,* 29**,** 28-46.

Cordani, R. & Shukowsky, W., 2009. Virtual Pole from Magnetic Anomaly (VPMA): A procedure to estimate the age of a rock from its magnetic anomaly only, *J Appl Geophys,* 69**,** 96-102.

D'Agrella-Filho, M.S., Trindade, R.I.F., Elming, S.A., Teixeira, W., Yokoyama, E., Tohver, E., Geraldes, M.C., Pacca, I.I.G., Barros, M.A.S. & Ruiz, A.S., 2012. The 1420 Ma Indiavai Mafic Intrusion (SW Amazonian Craton): Paleomagnetic results and implications for the Columbia supercontinent, *Gondwana Res,* 22**,** 956-973.

Fedi, M., Florio, G. & Rapolla, A., 1994. A Method to Estimate the Total Magnetization Direction from a Distortion Analysis of Magnetic-Anomalies, *Geophys Prospect,* 42**,** 261-274.

Foss, C., 2006. Evaluation of strategies to manage remanent magnetization effects in magnetic field inversion. *in 76th Annual SEG International Meeting*, pp. 4SEG, New Orleans.

Matos, J.B.d., Silva, C.H.d., Costa, A.C.D.d., Ruiz, A.S., Souza, M.Z.A.d., Batata, M.E.F., Corrêa da Costa, P.C. & Paz, J.D.d.S., 2009. Geologia e Recursos Minerais da Folha Jauru (SD.21-Y-C-III). *in Programa Geologia do Brasil*, pp. 134, Cuiabá.

Menezes, R.G., 1993. Pontes e Lacerda. Folha SD. 21-Y-c-n. *in Programa Levantamentos Geológicos Básicos do Brasil - PLGB*CPRM - Serviço Geológico do Brasil.

Monteiro, H., Macedo, P.M.d., Silva, M.D.d., Moraes, A.A.d. & Marcheto, C.M.L., 1985. O 'Greenstone Belt' do Alto Jauru. *in XXXIV Congresso Brasileiro de Geologia*Sociedade Brasileira de Geologia, Goiânia.

Nunes, N.S.d.V., 2000. Geologia e resultados prospectivos da área de Figueira Branca/Indiavaí, Mato Grosso. *in Série Metais do Grupo da Platina e Associados*CPRM - Serviço Geológico do Brasil.

Pratt, D.A.F., C. A.; Roberts, S., 2006. User Guided Inversion & Visualisation of Interpretation Confidence. *in AESC Conference*, pp. 1-7AESC, Melbourne, Australia.

Reid, A.B., Allsop, J.M., Granser, H., Millett, A.J. & Somerton, I.W., 1990. Magnetic interpretation in three dimensions using Euler deconvolution, *Geophysics,* 55**,** 80.

Saes, G.S., Leite, J.A.S. & Weska, R.K., 1984. Geologia da Folha Jauru (SD.21.Y.C.III): uma síntese de conhecimentos. *in 33rd Congresso Brasileiro de Geologia*Sociedade Brasileira de Geologia, Rio de Janeiro.

Souza, M.Z.A.d., Batata, M.E.F., Ruiz, A.S., Lima, G.A.d., Matos, J.B.d., Paz, J.D.d.S., Costa, A.C.D.d., Silva, C.H.d. & Corrêa da Costa, P.C., 2009. Geologia e Recursos Minerais da Folha Rio Branco (SD-21-Y-D-1). *in Programa Geologia do Brasil*, pp. 178, Cuiabá.

Teixeira, W., Geraldes, M.C., D'Agrella, M.S., Santos, J.O.S., Barros, M.A.S., Ruiz, A.S. & da Costa, P.C.C., 2011. Mesoproterozoic juvenile mafic-ultramafic magmatism in the SW Amazonian Craton (Rio Negro-Juruena province): SHRIMP U-Pb geochronology and Nd-Sr constraints of the Figueira Branca Suite, *Journal of South American Earth Sciences,* 32**,** 309-323.

3. Manuscript 2:Tectonic insights of the Southwest Amazon Craton from geophysical, geochemical and mineralogical data of Figueira Branca Mafic-Ultramafic Suite, Brazil

Once defined the mineralogy and lithology of the samples, and ultimately, the proper constraints to be used in a potential field inversion, the following stage was to analyse the Figueira Branca Suite. This chapter develops geophysical models of the bodies that compose the suite, investigates the extent of the magmatism that generated it, the geochemical features of the parental magma and the local tectonic framework by the time of the intrusion.

Magnetic and gravity field data were modelled to evaluate the geometry and an approximation of the volume of the bodies from the Figueira Branca Suite. Gamma-ray spectrometry revealed areas where the intrusions outcropped or were very shallow. Major and trace elements geochemistry identified the samples as gabbros and peridotite-gabbros, whereas light-Rare-Earth element trends suggest a progressive fractionation of the magma. Trace element plots, allied with the observed and previously published geology of the region, indicated a back-arc extension framework in the later stages of the Santa Helena Orogen.

Elsevier Editorial System(tm) for Tectonophysics

Manuscript Draft

Manuscript Number: TECTO11736

Title: Tectonic insights of the Southwest Amazon Craton from geophysical, geochemical and mineralogical data of Figueira Branca Mafic-Ultramafic Suite, Brazil

Article Type: Research Paper

Keywords: Potential Fields; Geochemistry; Mineralogy; Radiometrics; Amazon Craton

Corresponding Author: Mr. Vinicius Hector Louro, MSc.

Corresponding Author's Institution: Instituto de Astronomia, Geofísica e Ciências Atmosféricas da Universidade de São Paulo

First Author: Vinicius Hector Louro, MSc.

Order of Authors: Vinicius Hector Louro, MSc.; Peter A Cawood, PhD; Marta S Mantovani, PhD

Abstract: The Figueira Branca Suite is a layered mafic-ultramafic complex in the Jauru Terrane, southwest Amazon Craton. New lithological, geochemical, gamma-ray and potential field data, integrated with geological, isotope and paleomagnetic data are used to characterize this pulse of Mesoproterozoic extension-related magmatism. The Figueira Branca Suite formed through juvenile magma emplacement into the crust at 1425 Ma, coeval with the later stages of the Santa Helena Orogen. Gabbros and peridotite-gabbros display increasing enrichment of LREE, interpreted as evidence of progressive fractionation of the magma. Magnetic and gamma-ray data delimit the extent of magmatism within the suite to four bodies to the north of Indiavaí city. Modelling gravity and magnetic field data indicate that the anomalous sources are close to the surface or outcropping. These intrusions trend northwest over 8 km, with significant remanent magnetization that is consistent with published direction obtained through paleomagnetic data. The emplacement, mineralogy and geochemical signature point towards a back-arc extension tectonic framework in the later stages of the Santa Helena Orogen.

Suggested Reviewers: Clive Foss
CSIRO
clive.foss@csiro.au
His research on potential field methods, developing modelling methodologies and applying in mining and tectonics.

Amarildo S Ruiz
Universidade Federal do Mato Grosso
asruiz@gmail.com
Researcher specialist in the Jauru Terrane, southwest Amazon Craton

Mauro C Geraldes
Universidade Estadual do Rio de Janeiro
geraldes@uerj.br

Researcher specialist in geochronology and geochemistry of the Amazon Craton

Fabio C Tontini
GNS Science
f.caratori.tontini@gns.cri.nz
Researcher specialist in potential fields modelling and tectonics

Tectonic insights of the Southwest Amazon Craton from geophysical, geochemical and mineralogical data of Figueira Branca Mafic-Ultramafic Suite, Brazil

Vinicius Hector Abud Louro, Peter Anthony Cawood, Marta Silvia Maria Mantovani

Abstract

The Figueira Branca Suite is a layered mafic-ultramafic complex in the Jauru Terrane, southwest Amazon Craton. New lithological, geochemical, gamma-ray and potential field data, integrated with geological, isotope and paleomagnetic data are used to characterize this pulse of Mesoproterozoic extension-related magmatism. The Figueira Branca Suite formed through juvenile magma emplacement into the crust at 1425 Ma, coeval with the later stages of the Santa Helena Orogen. Gabbros and peridotite-gabbros display increasing enrichment of LREE, interpreted as evidence of progressive fractionation of the magma. Magnetic and gamma-ray data delimit the extent of magmatism within the suite to four bodies to the north of Indiavaí city. Modelling gravity and magnetic field data indicate that the anomalous sources are close to the surface or outcropping. These intrusions trend northwest over 8 km, with significant remanent magnetization that is consistent with published direction obtained through paleomagnetic data. The emplacement, mineralogy and geochemical signature point towards a back-arc extension tectonic framework in the later stages of the Santa Helena Orogen.

Tectonic insights of the Southwest Amazon Craton from geophysical, geochemical and mineralogical data of Figueira Branca Mafic-Ultramafic Suite, Brazil

Vinicius Hector Abud Louro, Peter Anthony Cawood, Marta Silvia Maria Mantovani

Graphical Abstract

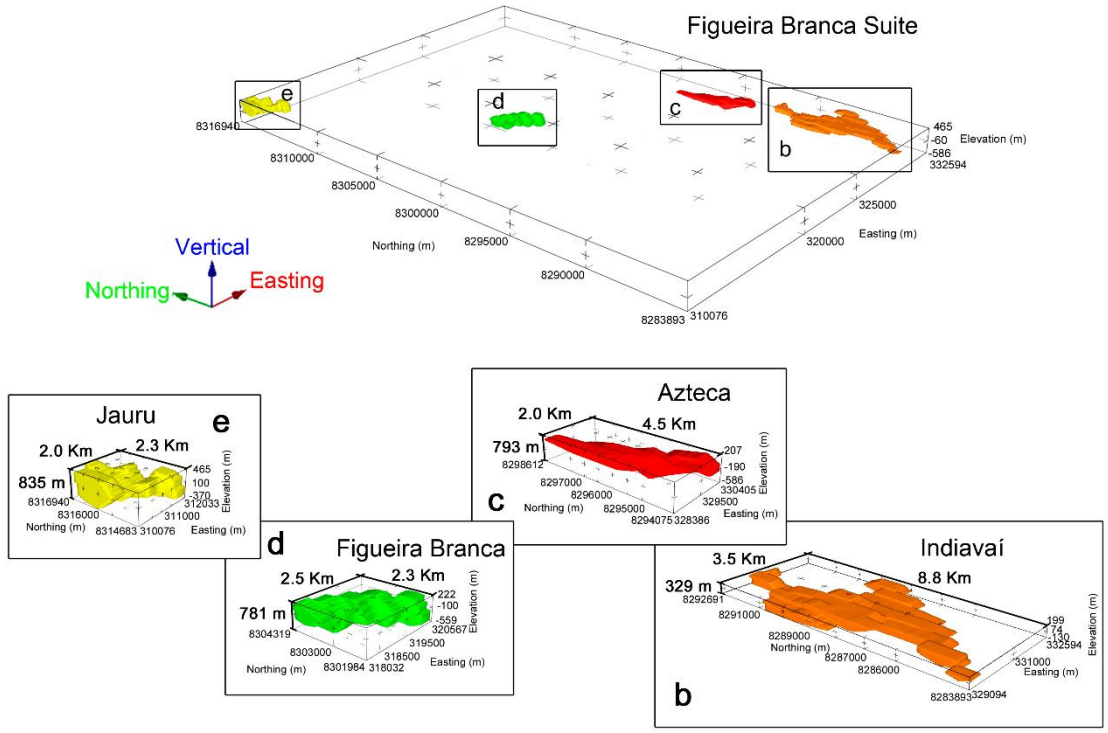

Joint magnetic and gravity models of the Figueira Branca Suite constrained by petrophysical, geochemical and mineralogical analysis. In detail, (a) Indiavaí, (b) Azteca, (c) Figueira Branca and (d) Jauru models.

Tectonic insights of the Southwest Amazon Craton from geophysical, geochemical and mineralogical data of Figueira Branca Mafic-Ultramafic Suite, Brazil

Vinicius Hector Abud Louro, Peter Anthony Cawood, Marta Silvia Maria Mantovani

Highlights

- A model for the tectonic framework of the Jauru Terrane at 1.42 Ga is proposed.
- Gravity and magnetic field models constrained by geochemistry and mineralogy.
- The multi-method data showed indicated mafic intrusions in a back-arc setting.

Tectonic insights of the Southwest Amazon Craton from geophysical, geochemical and mineralogical data of Figueira Branca Mafic-Ultramafic Suite, Brazil

Vinicius Hector Abud Louro[1,2], Peter Anthony Cawood[2], Marta Silvia Maria Mantovani[1]

[1] Instituto de Astronomia, Geofísica e Ciências Atmosféricas, Universidade de São Paulo, São Paulo, Brazil.

[2] Department of Earth and Environmental Sciences, University of St. Andrews, St. Andrews, KY16 9AL, UK.

E-mails: vilouro@usp.br, pac20@st-andrews.ac.uk, msmmanto@usp.br

Corresponding author: Vinicius Hector Abud Louro.

E-mail: vilouro@usp.br

Phone: +55 (11) 99985 1501

Date of Submission: 28 January 2017

Abstract

The Figueira Branca Suite is a layered mafic-ultramafic complex in the Jauru Terrane, southwest Amazon Craton. New lithological, geochemical, gamma-ray and potential field data, integrated with geological, isotope and paleomagnetic data are used to characterize this pulse of Mesoproterozoic extension-related magmatism. The Figueira Branca Suite formed through juvenile magma emplacement into the crust at 1425 Ma, coeval with the later stages of the Santa Helena Orogen. Gabbros and peridotite-gabbros display increasing enrichment of LREE, interpreted as evidence of progressive fractionation of the magma. Magnetic and gamma-ray data delimit the extent of magmatism within the suite to four bodies to the north of Indiavaí city. Modelling gravity and magnetic field data indicate that the anomalous sources are close to the surface or outcropping. These intrusions trend northwest over 8 km, with significant remanent magnetization that is consistent with published direction obtained through paleomagnetic data. The emplacement, mineralogy and geochemical signature point towards a back-arc extension tectonic framework in the later stages of the Santa Helena Orogen.

Keywords

Potential Fields; Geochemistry; Mineralogy; Radiometrics; Amazon Craton

1. *Introduction*

The Amazon Craton is divisible into six geochronological provinces: Central Amazon, including the stable Archean nuclei of the craton, and the Proterozoic provinces of Maroni-Itacaiúnas, Ventuari-Tapajós, Rio Negro-Juruena, Rondonian-San Ignácio and Sunsás-Aguapeí (Fig. 1a) (Tassinari and Macambira, 1999; Teixeira et al., 2010). The southern portion of the Rio Negro-Juruena (1.78 – 1.55 Ga) province includes the Jauru Terrane (1.78 – 1.40 Ga), which contains Paleoproterozoic basement rocks and the Mesoproterozoic Cachoeirinha and Santa Helena orogens (Fig. 1b) (Bettencourt et al., 2010). The Alto Jauru Group, part of the Paleoproterozoic basement, hosts the Figueira Branca Mafic-Ultramafic Suite, the focus of this paper.

The Figueira Branca Suite occurs in the southwest of the Mato Grosso State, Brazil, and to the southwest of the Parecis Basin (Fig. 1b). Our aim is to integrate new lithological, geochemical, gamma-ray and potential field data with available geological, isotope and paleomagnetic data to characterize the Figueira Branca Suite and delimit the extent of this Mesoproterozoic magmatic pulse.

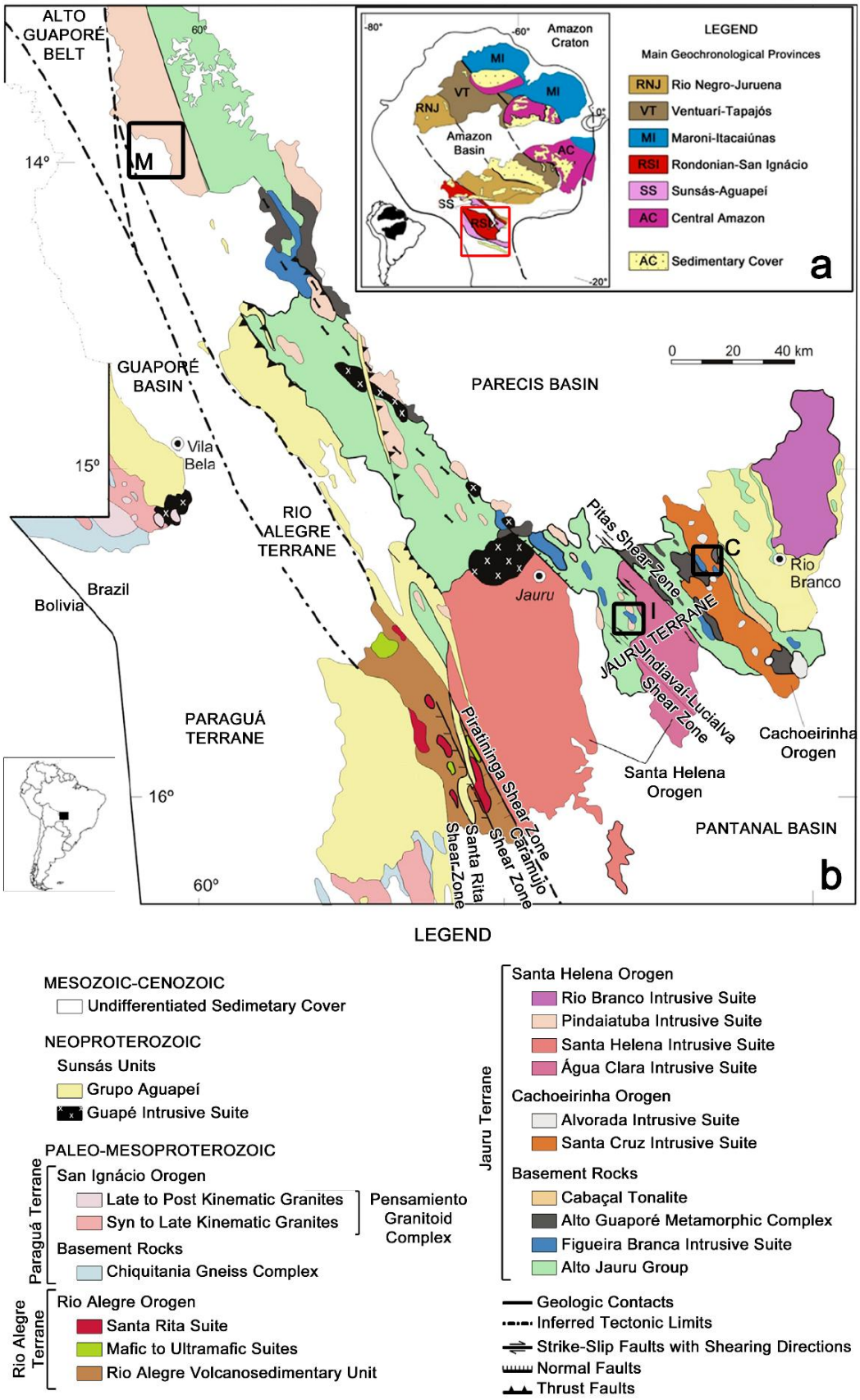

Fig. 1 – (a) Main geochronological provinces of Amazon Craton (Bettencourt et al., 2010). The red polygon delimits the area of Fig. 1b. (b) Southwest of the Rio Negro-Juruena and Rondonian-San

Ignácio provinces of the Amazon Craton. The Figueira Branca Suite is represented in dark blue. The black boxes indicate the bodies near the city of Indiavaí (I) and Cachoeirinha (C) (Bettencourt et al., 2010), and the Morro do Leme and Morro do Sem-Boné mafic-ultramafic suites (M).

2. Geologic and Tectonic Framework

Cordani et al. (2010) use regional geochronological and tectonic patterns to propose that the development of the southwest Amazon Craton occurred within a series of accretionary orogens. This regime was responsible for the production of numerous magmatic arcs and related magmatism until the late Mesoproterozoic (Teixeira et al., 2016). The Alto Jauru Group and the Alto Guaporé Metamorphic Complex (Fig. 1b) compose the Jauru Terrane, Rio Negro-Juruena Province (Matos et al., 2009; Souza et al., 2009). The Alto Jauru Group (1760 to 1720 Ma) (Monteiro et al., 1986; (Bettencourt et al., 2010) comprises gneiss, migmatites and three meta-volcanosedimentary sequences: Cabaçal, Araputanga and Jauru. The Alto Guaporé Metamorphic Complex (1790 to 1740 Ma) (Menezes, 1993) is characterized by granodioritic to tonalitic orthogneiss intruded into supracrustal volcanosedimentary sequences, with all metamorphosed to greenschist or amphibolite facies (Bettencourt et al., 2010).

During the evolution of the Rondonian-San Ignácio Province, the Jauru Terrane underwent compressional deformation related to ocean closure, marked by the Guaporé suture and collision of the Paraguá terrane (Rizzotto et al., 2013) (Fig. 01). Subduction associated with ocean closure resulted in magmatic activity preserved in the Cachoeirinha (1587 to 1522 Ma) and Santa Helena (1485 to 1425 Ma) orogens (Geraldes et al., 2001) and was intruded into the Alto Jauru Group.

The Cachoeirinha orogen consists of the Alvorada (1.53 to 1.44 Ga) and Santa Cruz (1.56 to 1.52 Ga) intrusive suites. These suites are represented by granite, tonalite, granodiorite and gneissic migmatite (Geraldes et al., 2001), and show an Andean-type arc signature with $\varepsilon_{Nd(t)}$ values varying from -1.3 to +2.0 and T_{DM} ages of 1.9 to 1.7 Ga (Bettencourt et al., 2010; Geraldes et al., 2001). The Santa Helena orogen comprises the Santa Helena (1.44 to 1.42 Ga), the Pindaituba (1.46 to 1.42 Ga) and the Água Clara (1.44 to 1.42 Ga) intrusive suites (Ruiz, 2005). The intrusive suites of the Santa Helena Orogen consist of monzonites,

granodiorites and tonalites in an oceanic-continental arc setting evidenced by $\varepsilon_{Nd(t)}$ values varying from +1.0 to +4.0 and T_{DM} ages of 1.8 to 1.5 Ga (Geraldes et al., 2001; Ruiz, 2005).

The Figueira Branca Suite is a layered mafic-ultramafic complex composed from bottom to top of dunite, pyroxenite, gabbro-norite, anorthosite, thin layers of troctolite, and olivine-gabbro (Teixeira et al., 2011). The Indiavaí gabbro from the suite yielded a U-Pb SHRIMP zircon age of 1425 ± 8 Ma (Fig. 1b, box I), and a second intrusion near Cachoeirinha city (Fig. 1b, box C) was dated at 1541 ± 23 Ma (Teixeira et al., 2011). Ar-Ar dating of biotites yielded plateau ages of 1275 ± 4 Ma and 1268 ± 4 Ma for the Indiavaí gabbro, which were evaluated as minimum ages for regional cooling. $\varepsilon_{Nd(1.42\ Ga)}$ values vary from +3.0 to +4.7, and $\varepsilon_{Sr(1.42\ Ga)}$ values from -39.1 to -8.1 indicating a predominantly juvenile source (Fig. 2). The crystallization age of the Indiavaí gabbro is coeval with the later stages of evolution of the Santa Helena Orogen (Fig. 1b) (Tassinari et al., 2000).

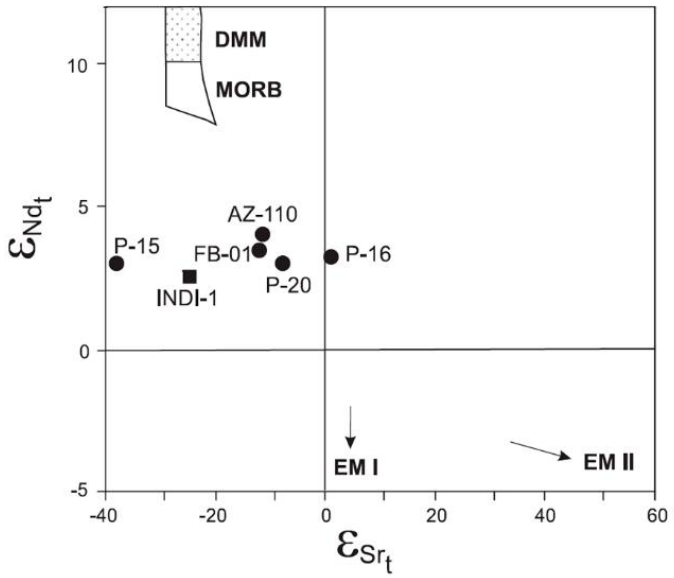

Fig. 2 - ε_{Nd} (1.42 Ma) vs. ε_{Sr}(1.42 Ga) diagram of the Figueira Branca Suite (Teixeira et al., 2011).

Our study is focused on the geological, geophysical, isotope and geochemical character of four northwest aligned intrusions of the Figueira Branca Suite between the towns of Indiavaí and Lucialva (Fig. 3). This data set provided a basis for evaluating other bodies with similar features usually associated with this suite (Fig. 1). By associating different bodies of similar geophysical signature with the Figueira Branca Suite, we were able to estimate the extent of the magmatism that generated the suite during the Mesoproterozoic and its role for the tectonic framework of the area.

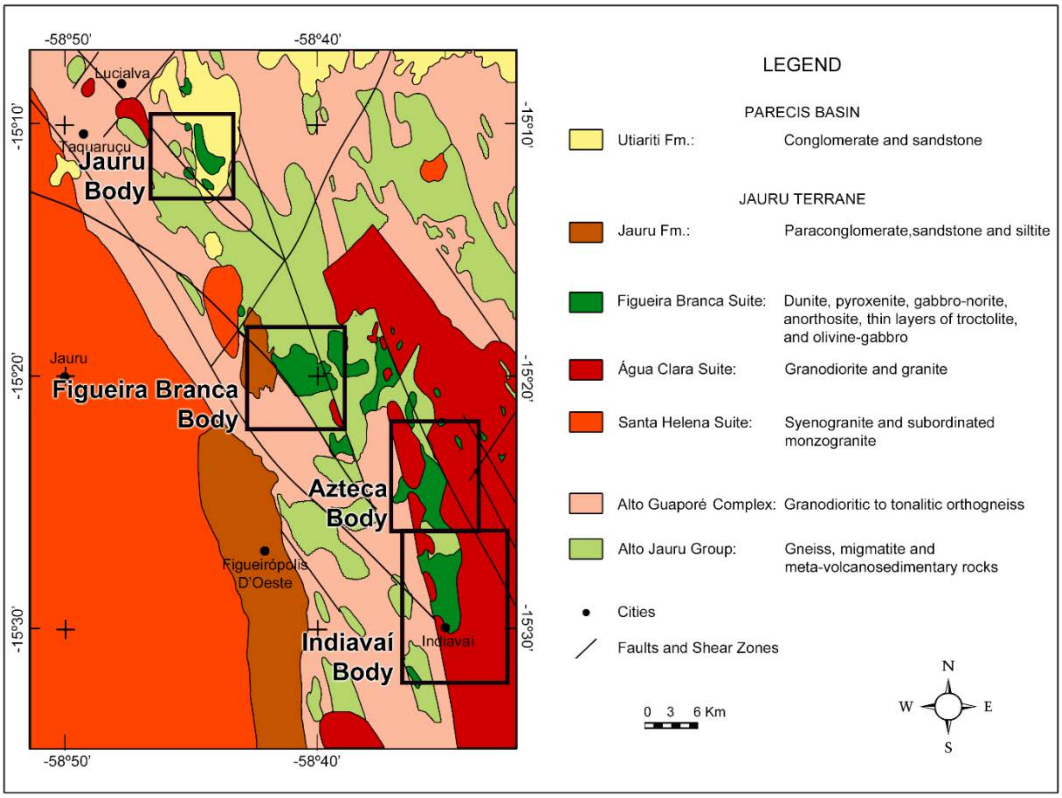

Fig. 3 – Local geological map (Nunes, 2000a; Saes et al., 1984; Teixeira et al., 2011).

Bettencourt et al. (2010) suggested rocks of the Figueira Branca Suite mafic-ultramafic suite extend north of the Santa Helena batholith. In more detailed studies, Ruiz (2005), Corrêa da Costa et al. (2009) and Girardi et al. (2012) associate the mafic-ultramafic plutons to the north of the Santa Helena batholith to the Córrego Dourado Suite (Fig. 1). This suite is made of foliated metagabbro, metatroctolite, tremolite, pyroxenite and serpentinite (Corrêa da Costa et al., 2009; Ruiz, 2005). Although there is no direct dating of the Córrego Dourado Suite, Ruiz (2005) associate the rock type and deformation of this suite to the 1439 ± 4 Ma Salto do Céu gabbroic sill (Teixeira et al., 2016).

Northwest of the Jauru Terrane, a set of mafic-ultramafic intrusions crops out in the Alto Guaporé Metamorphic Complex. (Nunes, 2000b) associated these bodies, the Morro do Leme and the Morro do Sem-Boné suites, to the Cacoal Suite (not mapped in Fig. 01, more outcrops are found to the north of Fig. 1). These suites are basic-ultrabasic intrusions, made up of dunites and peridotites of 1349 ± 14 Ma (Rb-Sr, whole rock) (Quadros and Rizzotto, 2007).

3. *Data*

In 2006, the Brazilian Geological Service undertook a gamma-ray and magnetic field airborne survey named "Projeto 1080 – Área 2 Mato Grosso" that covers the region occupied by the Figueira Branca Suite. The nominal terrain clearance was 100 m at an airspeed of approximately 280 Km/h. The north-south line spacing was 500 m, whereas the east-west tie lines were spaced at 10000 m. The airborne survey was processed by LASA Prospecções S/A and Prospectors Aerolevantamentos e Sistemas LTDA.

The gamma-ray data were measured with an Exploranium GR-820 Spectrometer of 256 channels. This spectrometer uses 5 sets of NaI (Tl) crystals, three of them downward-oriented, and two upward. The downward-oriented sets are composed by two sets crystal of 16.8 L and one set of 8.4 L. The two upward-oriented sets contain 4.2 L crystals. The sampling interval was 1 s, resulting in an observation spacing of approximately 78 m.

The acquisition of the magnetic field data used Geometrics G-822A Cesium magnetometers of resolution of 0.001 nT. The sampling interval of 0.1 s resulted in an approximate sample spacing of 7.8 m. The magnetic noise level is 0.5 nT after the industry standard corrections were applied. The average International Geomagnetic Reference Field (IGRF) ambient field for this period, which had an inclination -11.6°, declination 234.9°, and intensity 23749 nT.

195 ground gravity stations were installed in the region where the suite is emplaced. 50 samples of different rock types were collected for petrophysical and geochemical measurements. Density data were collected by the "Archimedes method" with distilled water and a high-precision analytic balance, whereas magnetic susceptibility measures were taken using a Kappameter KT-9 magnetic susceptibility meter. Thin sections were prepared and analysed to select samples for geochemical measurements and for constraining the geophysical models. 30 samples were selected for whole-rock major elements analyses through XRF, from which 20 were designed for trace and rare-earth elements analyses by ICP-MS, containing specimens of the Figueira Branca Suite, Alto Jauru Group and adjacent granitic suites.

The selected samples were powdered and homogenized as bulk material. The XRF analyses were made in a Philips PW2400 XRF instrument at the Geoanalítica laboratory of the Instituto de Geociências of the Universidade de São Paulo, Brazil. The trace and REE analyses were made at the Laboratório de Geoquímica Analítica of the Universidade Estadual

de Campinas, Brazil. The samples were digested in Parr-type bombs with HF and HNO_3 mix. All solutions were prepared with ultra-pure water through the Milli-Q system. The HNO_3 was purified by sub-ebulition. The containers used on the dilutions were previously cleaned with HNO_3 (5%) and washed with ultra-pure water. The trace elements measurements used an ICP-MS XseriesII (Thermo) equipped with CCT (Collision Cell Technology). The calibration of the equipment was made using multielementary solutions gravity-prepared by monoelementary standard solutions of 100 mg/L (AccuStandards). The detection limit (DL = $x + 3\sigma$) was determined as the average (x) plus three standard deviations (σ) of ten measurements of the laboratory blanks and the instrument background. The quality control used the reference materials BRP-1 (basalt) and GS-N (granite) from the Laboratório de Geoquímica Analítica. The results and their respective uncertainties for the eleven samples from the Figueira Branca Suite rocks are available in Table 1.

Table 1 – XRF and ICP-MS results for the Figueira Branca Suite.

XRF Results (%)													
Sample	IND03	IND06	IND09	IND10	AZT05	AZT10	FIG01	FIG02	FIG03	JAU01	JAU02	DL	Error (±)
SiO2	47.09	46.96	47.79	47.04	50.97	48.39	48.89	39.64	40.74	49.48	50.18	0.03	0.48
TiO2	0.41	0.35	0.26	0.28	0.57	0.42	0.22	0.06	0.08	0.28	0.55	0.003	0.009
Al2O3	20.48	23.95	21.72	20.7	18.37	18.1	6.15	9.39	18.13	21.18	17.62	0.02	0.09
Fe2O3	9.89	6.52	8.04	9.08	8.25	8.45	9.31	11.3	6.64	7.7	9.36	0.01	0.09
MnO	0.14	0.09	0.11	0.12	0.14	0.13	0.17	0.15	0.09	0.1	0.14	0.002	0.003
MgO	9.01	7.09	8.79	9.83	7.27	5.67	22.96	26.97	16.26	7.66	10.56	0.01	0.06
CaO	10.27	12.35	11.02	10.3	9.43	10.5	7.89	4.92	9.4	10.02	8.73	0.01	0.02
Na2O	2.38	2.13	2.46	2.36	2.75	2.22	0.32	0.33	1.13	2.76	2.37	0.02	0.12
K2O	0.12	0.11	0.11	0.12	0.38	0.81	0.21	0.03	0.03	0.19	0.24	0.01	0.01
P2O5	0.03	0.03	0.01	0.02	0.04	0.02	0.12	0.01	0.01	0.01	0.11	0.003	0.003
LOI	<0.01	0.86	0.1	0.16	1.48	5.72	5.28	7.98	6.98	0.16	0.2	0.01	---
Total	99.81	100.44	100.41	100.02	99.65	100.43	101.52	100.78	99.49	99.54	100.06	---	---
ICP-MS Results ($mg.g^{-1}$)													
Sample	IND03	IND06	IND09	IND10	AZT05	AZT10	FIG01	FIG02	FIG03	JAU01	JAU02	DL	Error (±)
Cu	89.1	---	32.5	---	74.3	35.3	4.89	32.0	12.9	46.6	42.6	3	0.2
Nb	0.52	---	0.37	---	1.53	0.75	0.61	0.32	1.33	0.20	1.38	0.9	0.05
Rb	4.31	---	3.58	---	11.4	13.8	0.93	0.94	0.81	3.55	3.41	1	0.2
Sr	238	---	236	---	218	218	178	137	225	522	458	6	0.07
Zn	55.9	---	46.1	---	59.2	45.9	58.7	63.1	41.4	52.3	71.5	2	3.4
Zr	17.4	---	13.4	---	42.8	22.6	13.0	3.30	5.13	4.74	32.9	5	0.04
Cr	17.2	---	32.5	---	390	103	1703	136	1184	137	609	1	0.4
Ba	41.7	---	39.0	---	85.5	71.6	8.47	24.9	28.0	112	154	7	0.08
Ni	202	---	160	---	40.7	49.6	1054	1112	720	168	175	0.9	0.2
Be	0.15	---	0.09	---	0.35	0.23	0.39	0.06	0.04	0.16	0.32	0.1	0.04

V	100	---	65.6	---	139	134	110	19.8	26.9	69.7	112	7	0.1
Co	56.8	---	52.9	---	40.3	39.3	82.9	125	70.7	50.7	54.1	1.4	0.02
Ga	16.3	---	15.9	---	19.0	17.1	5.65	5.99	10.6	16.3	15.3	0.6	0.009
Y	8.87	---	6.19	---	14.7	10.6	5.43	1.56	1.77	3.12	8.85	1	0.02
Mo	0.10	---	0.08	---	0.28	0.14	0.13	0.08	0.08	0.06	0.15	0.1	0.02
Sn	0.14	---	0.06	---	0.32	0.19	0.06	<DL	<DL	<DL	0.14	0.4	0.08
Sb	0.03	---	0.02	---	0.14	0.10	0.39	0.01	0.01	0.01	0.01	0.01	0.01
Cs	0.06	---	0.05	---	0.83	0.40	0.02	0.14	0.15	0.11	0.19	0.02	0.004
Hf	0.53	---	0.42	---	1.20	0.69	0.35	0.09	0.13	0.16	0.81	0.2	0.005
Ta	0.05	---	0.09	---	0.12	0.05	0.05	0.09	0.40	0.03	0.08	0.08	0.003
Pb	0.57	---	0.51	---	1.78	1.47	1.09	0.28	0.25	0.67	1.04	0.3	0.05
Bi	0.03	---	0.03	---	0.04	0.08	0.06	0.02	0.02	0.02	0.02		0.006
Th	0.28	---	0.22	---	0.85	0.33	0.46	0.14	0.05	0.05	0.14	0.1	0.003
U	0.08	---	0.05	---	0.39	0.12	0.33	0.19	0.06	0.01	0.08	0.03	0.03
La	1.82	---	1.47	---	5.31	2.70	4.02	0.96	0.90	1.57	5.08	1	0.01
Ce	4.13	---	3.28	---	11.5	6.16	8.37	1.75	1.99	3.02	11.7	1.2	0.02
Pr	0.60	---	0.46	---	1.51	0.87	1.15	0.24	0.27	0.37	1.60	0.2	0.006
Nd	2.95	---	2.20	---	6.77	3.97	4.85	0.93	1.10	1.66	6.98	0.9	0.009
Sm	0.98	---	0.69	---	1.78	1.17	1.08	0.21	0.27	0.45	1.61	0.2	0.007
Eu	0.49	---	0.46	---	0.63	0.60	0.28	0.14	0.19	0.47	0.71	0.08	0.003
Gd	1.13	---	0.80	---	1.96	1.36	1.03	0.21	0.27	0.44	1.57	0.3	0.006
Tb	0.22	---	0.16	---	0.36	0.26	0.16	0.03	0.05	0.07	0.26	0.05	0.003
Dy	1.57	---	1.10	---	2.56	1.88	0.98	0.26	0.31	0.53	1.61	0.3	0.003
Ho	0.36	---	0.24	---	0.54	0.40	0.20	0.05	0.07	0.11	0.34	0.06	0.003
Er	0.96	---	0.67	---	1.56	1.17	0.53	0.14	0.18	0.31	0.94	0.1	0.004
Tm	0.14	---	0.10	---	0.22	0.17	0.08	0.02	0.03	0.05	0.13	0.02	0.02
Yb	0.91	---	0.60	---	1.44	1.05	0.51	0.17	0.18	0.34	0.86	0.09	0.005
Lu	0.14	---	0.10	---	0.22	0.17	0.08	0.03	0.03	0.05	0.14	0.02	0.002
Sc	14.7	---	13.5	---	27.2	29.2	21.3	5.95	4.74	12.2	20.3	0.8	1.4
Li	4.20	---	7.44	---	8.97	5.31	1.39	3.72	2.68	5.68	5.76	0.3	0.03
Cd	0.07	---	0.05	---	0.09	0.07	0.05	0.01	0.01	0.07	0.07	0.1	0.02

4. Results & Discussion

4.1. Typical Magnetic Field Signature and Bodies Associated with the Suite

Initial data analysis used magnetic field method and the gamma-ray spectrometry to establish the geophysical signature of the Figueira Branca Suite and delineate analogue anomalies within the Jauru Terrane. The "Projeto 1080 – Área 2 Mato Grosso" provided a regional data set of magnetization contrasts and gamma-ray emissions (Fig. 4). The four recognized bodies

of the Figueira Branca Suite display significant contrasts of magnetization with their respective host-rocks, generating magnetic anomalies in the total magnetic field map (Fig. 4a). The intrusions were named, from the south to north, Indiavaí, Azteca, Figueira Branca and Jauru. These anomalies show a specific pattern with negative values to the north and positive to the south, indicating the presence of a significant remanent magnetization in their sources. The gamma-ray emission for the areas of the four bodies indicated discrete low counts (dark to black areas in Fig. 4b), typically associated with mafic rocks (Dickson and Scott, 1997). The Indiavaí and Azteca bodies show the general low counts pattern, but have higher concentrations of eTh and eU than their northern counterparts. The higher concentration of both elements produces a cyan coloration in the area of the bodies.

A group of small occurrences associated to the Figueira Branca Suite is found to the east of the Figueira Branca anomaly and to the north of Azteca (Fig. 4a). This anomaly shows a low trend of gamma-ray counts (Fig. 4b) as expected for mafic rocks, however the magnetic signature differs grandly from the other anomalies linked with the suite.

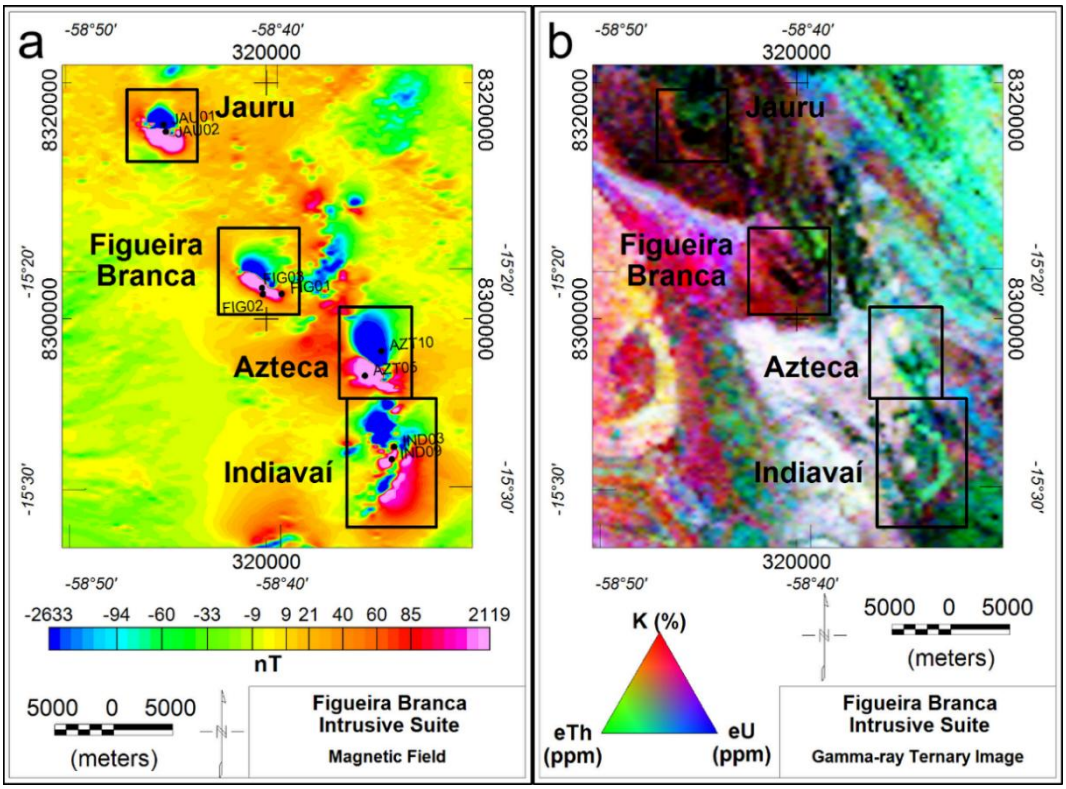

Fig. 4 - (a) Total magnetic field of the area of the Figueira Branca Suite, including the location of the samples associated to the intrusive suite. (b) Gamma-ray emission of the area.

The magnetic field and gamma-ray emissions were used as proxies to investigate for additional mapped and unmapped intrusions related with the Figueira Branca Suite. To use the magnetic field as a proxy, we applied the Reduction to the Magnetic Pole (RTP) operator to estimate the direction of total magnetization of the anomalies. A successful RTP filtering results in a magnetic field where the anomalies present positive contrasts centred over the limits of the bodies, as the negative values on the map are close to zero. The RTP filtering requires knowledge of the direction of total magnetization of the field. Hence, it is recommended to use of this filtering in areas with magnetic anomalies predominantly generated by the induced magnetization, where its direction is known by the geomagnetic field in the area during the survey. Fedi et al. (1994) and Cordani and Shukowsky (2009) proposed and implemented, respectively, a technique called MaxiMin, which does an inversion of the inclination and declination to estimate the values that better minimize the negative values of the field and maximize the positive values. The MaxiMin optimal results were inclination of 56º and declination of 213º, with an α_{95}º of 5º after 386 iterations. Figure 5a shows the RTP field of the Jauru Terrane with the targets found with the analogue characteristics of gamma-ray emission and/or magnetization. In order to define the lateral limits of the bodies and evaluate qualitatively the MaxiMin results, we used the 3-D Amplitude of the Analytic Signal (Fig. 5b and d) (Roest et al., 1992).

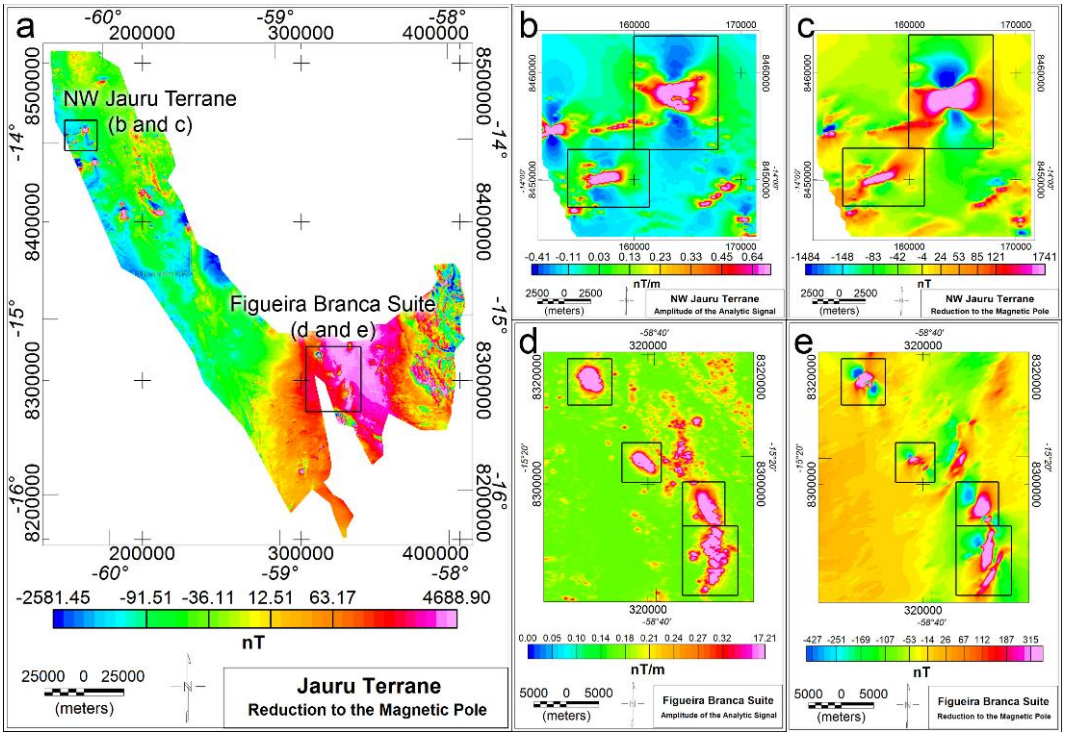

Fig. 5 – (a) RTP of the Jauru Terrane identifying bodies with similar features as those already recognized as part of the Figueira Branca Suite. (b) and (c) are the Amplitude of the Analytic Signal and the RTP, respectively, of the anomalies in the northwest of the Jauru Terrane, while (d) and (e) are the same maps, respectively, for the Figueira Branca Suite.

In the northwest of the Jauru Terrane, a set of other gamma-ray and/or magnetic anomalies presented similar geophysical signature inside the Jauru Terrane. The only two anomalies in the northwest that were properly reduced to the pole were spatially associated with the Morro do Leme and the Morro do Sem-Boné complexes (Fig. 1, 5b and c). These intrusive complexes are associated to Cacoal basic-ultrabasic intrusive suite and hosted by the Alto Guaporé Belt (Nunes, 2000b). The RTP of both complexes present similar shapes, indicating analogue direction of total magnetization. Louro et al. (2014) suggest a remanent magnetization with inclination of 41.8º and declination of 193º for the Morro do Leme. Therefore, in the absence of analogue geophysical signatures unrelated with known suites in the Jauru Terrane, we focused on characterizing the Figueira Branca Suite using the only the four recognized bodies that maintained the same signature on different and independent geological and geophysical data.

4.2. Gravity Field

The gravity field of the region showed three of the four gravity anomalies (Fig. 6). The Figueira Branca anomaly could not be properly surveyed due to flooding over the northern part of the body due to construction of a dam. The irregular distribution of gravity stations allied with a regional trend of the gravity field requiring regional-residual separation. We isolated the gravity anomaly signatures using a high-pass filter to remove wavelengths larger than 24400 Km. The cut-off wavelength was defined based on the first inclination change of the energy spectrum. The anomalies showed good spatial correlation with the magnetic field data and their maximum amplitudes varied from 1.6 (in the Figueira Branca magnetic anomaly area) to 7.6 mGal.

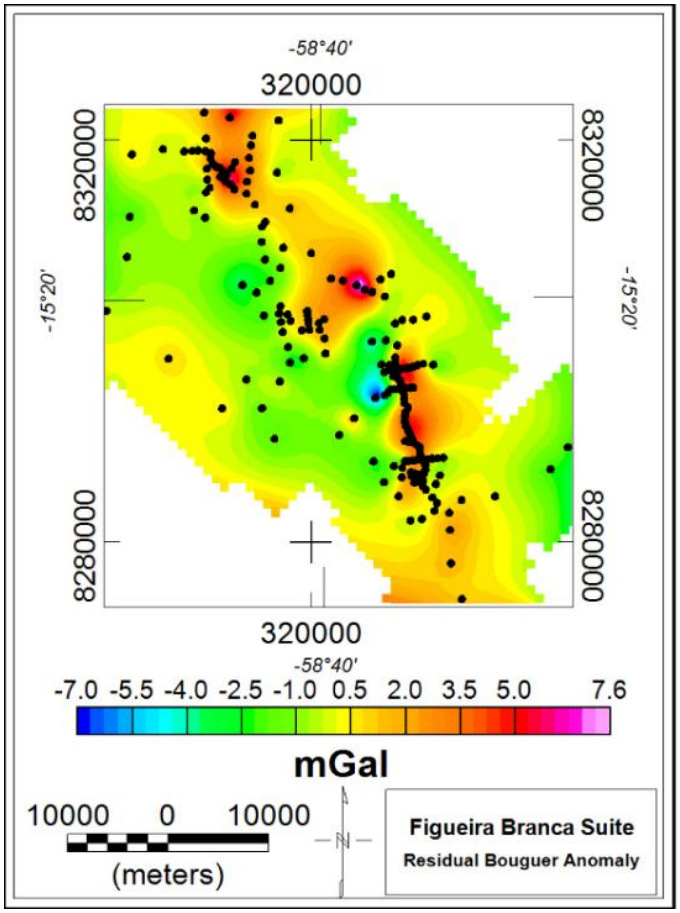

Fig. 6 – Residual Bouguer anomaly map of the Figueira Branca Suite. The black circles represent the location of the gravity stations.

4.3. *Mineralogy and Geochemical Signature*

Mineralogy of the Indiavaí, Azteca and Jauru bodies is dominated by plagioclase (ca. 60% to 70%) with fractured and serpentinized olivine (ca. 20% to 25%) and intergrown pyroxene (ca. 10% to 15%) (Fig. 7a, 7b and 7c). The Figueira Branca intrusion shows variable grain size with parts relatively fined grained and displaying significant serpentinization and weathering (Fig. 7d), whereas other sections are coarse grained and contain a higher proportion of olivine (ca. 60% olivine and ca. 40% plagioclase; Fig 7e and 7f). Opaque oxide minerals are present in all thin sections. D'Agrella-Filho et al. (2012) determined the opaque oxide phase as magnetite in the Indiavaí gabbro.

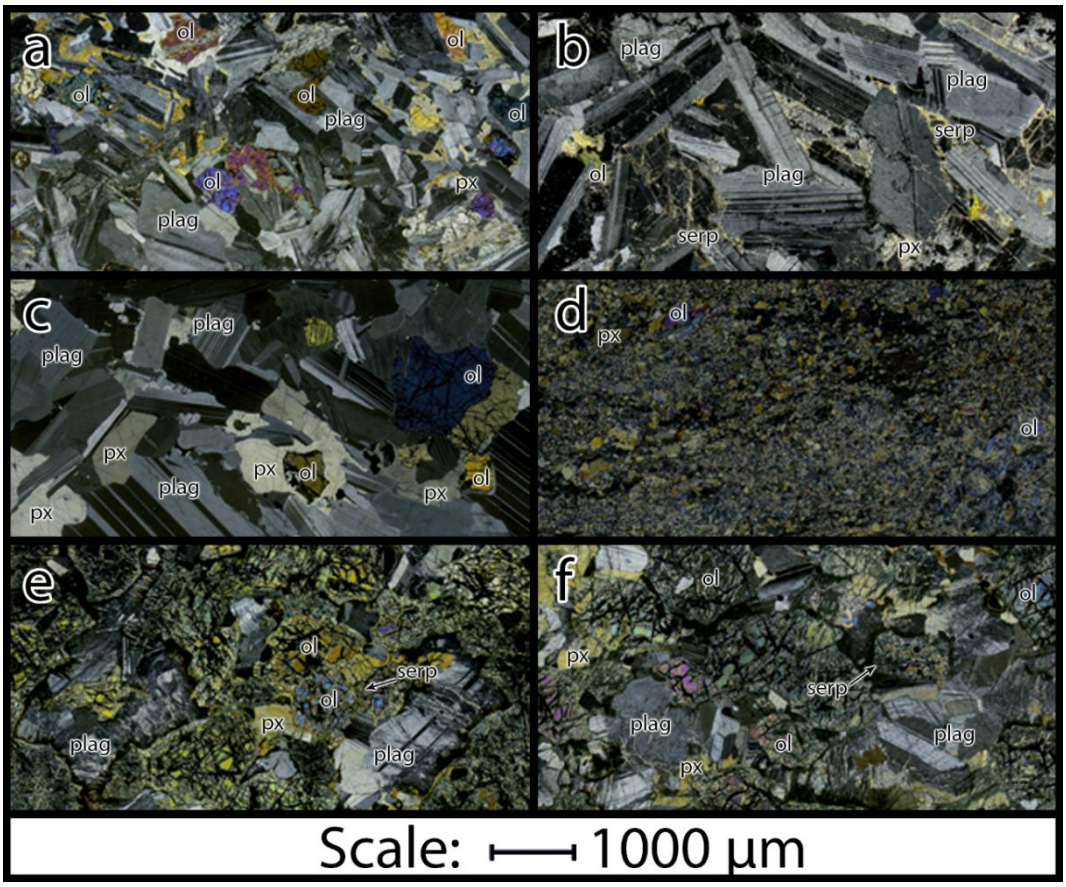

Fig. 7 – Thin sections of the samples (a) IND09, (b) AZT05, (c) JAU01, (d) FIG01, (e) FIG02 and (f) FIG03. The crystals are indicated by their abbreviations: ol – olivine, plag – plagioclase, px – pyroxene, and serp – serpentine. All photos were taken with cross-polarized light.

Geochemical data were collected on 11 samples (Table 1). On a TAS (SiO_2 vs. $NaO_2 + K_2O$) plot (Fig. 8a) (Middlemost, 1994), these samples were located inside the gabbro field, with

293 the exception of two out of three olivine-rich samples from the Figueira Branca intrusion
294 (FIG01 and FIG02) that showed significantly lower values of SiO_2 and Na_2O+K_2O and were
295 located in the peridotite-gabbro field (Fig. 8a).

296 The REE normalized to chondrites (Mcdonough and Sun, 1995) shows the increase in the
297 slopes among the intrusions, from lower to higher: Indiavaí, Figueira Branca, Azteca and
298 Jauru (Fig. 8b). The increase in the slopes indicate the evolution of the magma of the Figueira
299 Branca Suite, with the Jauru body representing the most, and the Indiavaí intrusion the least,
300 evolved. The majority of the samples display Eu anomalies consistent with the presence of
301 plagioclase (Fig. 7).

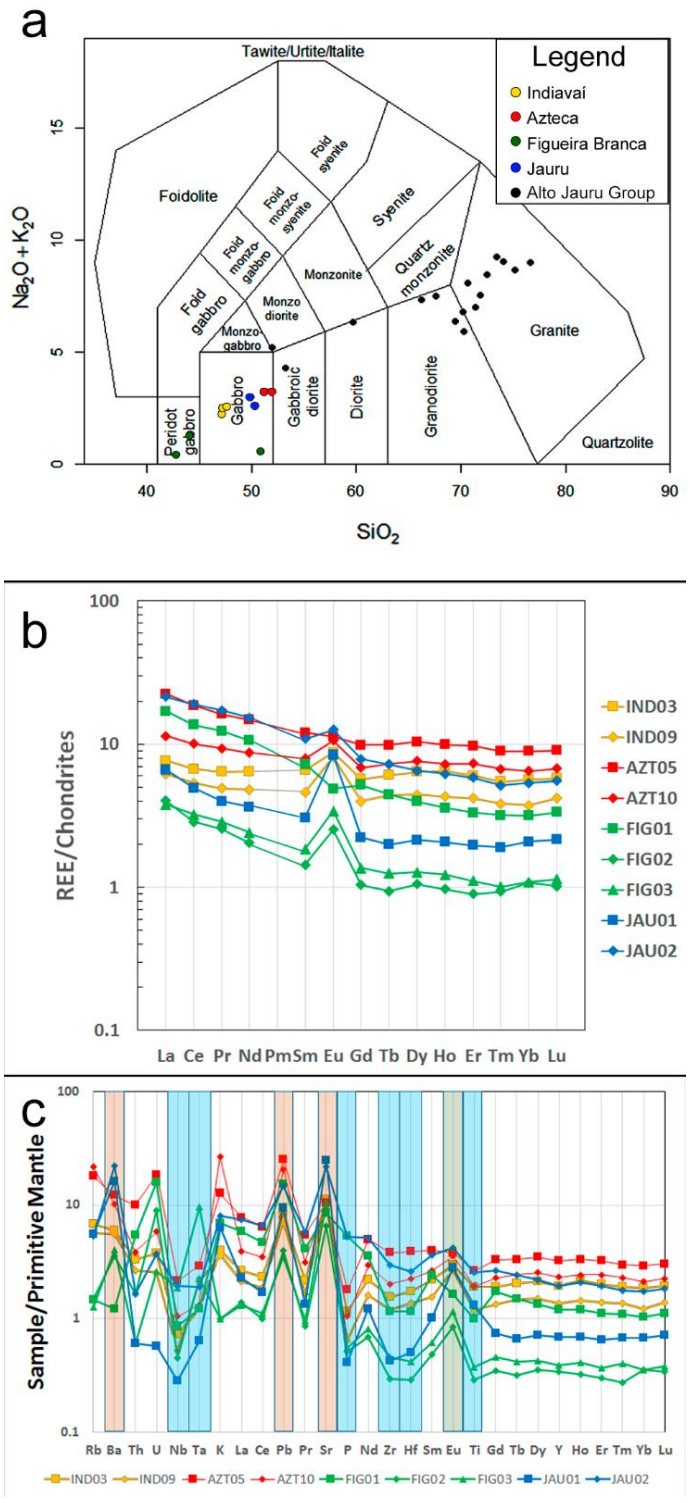

302

303 Fig. 8 – (a) TAS (SiO_2 vs. $NaO_2 + K_2O$) plot (Middlemost, 1994), (b) REE normalized to the
304 chondrite values (Mcdonough and Sun, 1995) and trace elements normalized to Primitive Mantle (Sun
305 and McDonough, 1989) of the Figueira Branca Suite.

306

307 According with Zheng (2012), Pb and Sr positive anomalies on a Primitive Mantle
308 normalized spidergram (Sun and McDonough, 1989) are associated to metasomatism in
309 subduction zones before the melting of the parental magma (Fig 8c). Two types of
310 metasomatized media are possible in these zones: a media characterized by slab-derived
311 fluids and one by hydrous melt. The first has high capacity to transport water-soluble
312 elements, but not water-insoluble. Hydrous melts, however, can transport both water-soluble
313 and insoluble elements. Rb/Y, Nb/Y, Nb/Zr and Th/Zr ratios can be used as proxies to
314 suggest the type of metasomatized media (Kepezhinskas et al., 1997). The mafic samples of
315 the Figueira Branca Suite indicated high values of Rb/Y and Th/Zr, and lower values of Nb/Y
316 and Nb/Zr (Fig. 9a and 9b), indicating a hydrous melt predominance in the parental magma.
317 The samples of the Figueira Branca intrusion showed significantly different Th/Zr and Nb/Zr
318 ratios than the remaining samples from the suite. This behaviour follows the contrast
319 observed on the mineralogy (Fig. 7c) and REE slopes (Fig. 8b) of these samples.

320

321

322

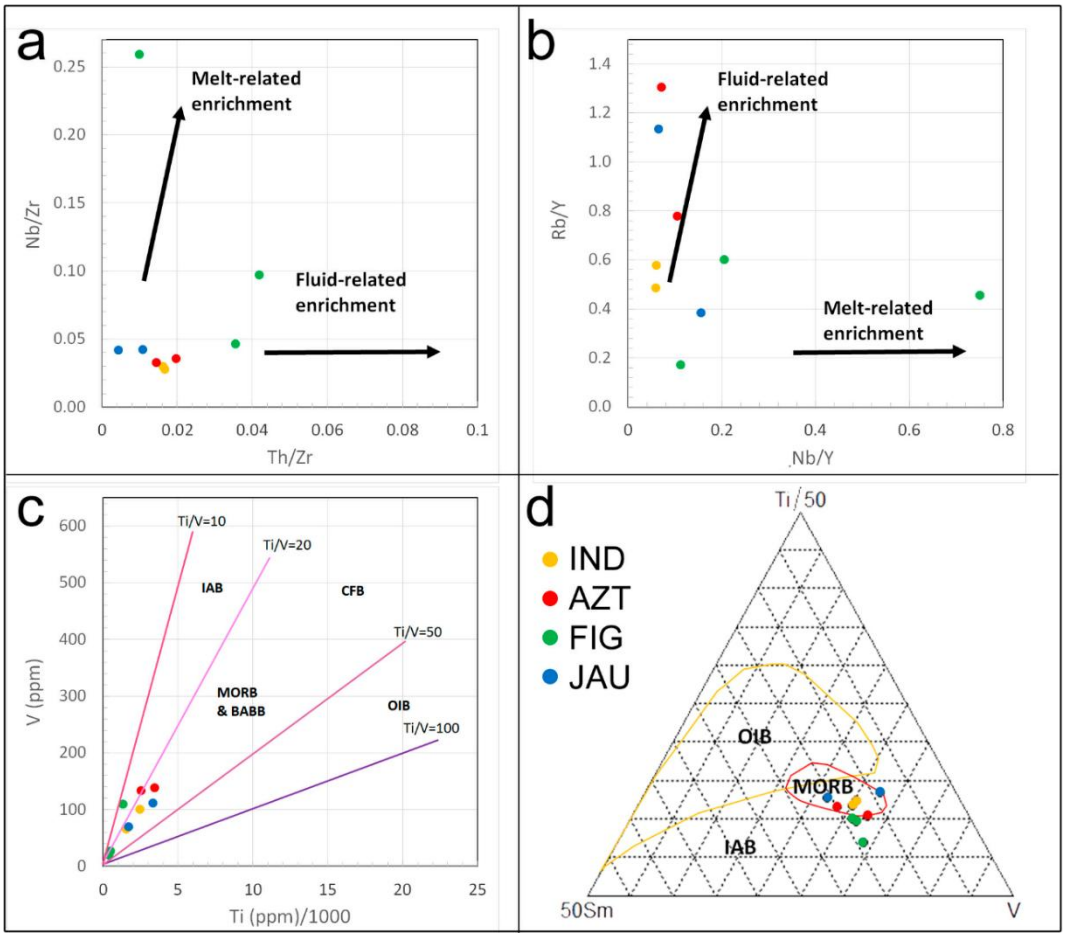

Fig. 9 – Petrogenetic diagrams (a) Nb/Zr vs. Th/Zr, and (b) Rb/Y vs. Nb/Y (Kepezhinskas et al., 1997), and tectonic discriminant (c) V vs. Ti/1000 (Shervais, 1982), and (d) ternary Ti/50 vs. Sm*50 vs. V (Vermeesch, 2006) of the Figueira Branca Suite.

Pronounced Zr and Hf negative anomalies for the Figueira Branca Suite samples (Fig. 8c) is indicative of a supra-subduction setting (Wang et al., 2013) and consistent with the Rb/Y, Nb/Y, Nb/Zr and Th/Zr ratios (Fig. 9a and b). The samples show Ti/V ratios (10>Ti/V>30) (Fig. 9c) related with MORB and Back-Arc Basin Basalts (BABB) (Shervais, 1982), whereas in the ternary Ti-Sm-V diagram (Vermeesch, 2006) (Fig. 9d), they fall in the transitional field between MORB and IAB. Vermeesch (2006) explains that the multiplying factors in the Ti-V and Ti-Sm-V diagrams are used because geochemical data is expressed as parts of a whole, so the concentration of some elements are not entirely independent to vary without interfering in the concentration of others in the same system.

The Figueira Branca Suite lies to the east of the Santa Helena orogen and to the west of the Água Clara orogen (Fig. 1), two structures originated by the subduction of oceanic crust

to the west of the Santa Helena orogen. These features, along with the ε_{Nd}(1.42 Ma) vs. ε_{Sr}(1.42 Ga) signature (Fig. 3), suggest that the Figueira Branca parental magma, originally depleted, metasomatized during and/or after the subduction of the same ocean crust that resulted in the Santa Helena and Água Clara orogens. Furthermore, the location of the suite between orogens and the parallel alignment of the geophysical anomalies with the extinct subduction zone, in an extensive environment (Teixeira et al., 2011), suggests a tectonic framework of back-arc magmatism.

4.4. Magnetic and Gravity Modelling

Density and magnetic susceptibility were measured on samples of the Figueira Branca Suite and adjacent rocks (Table 2). These values, along with the total field direction estimated by the MaxiMin technique (inclination 56º and declination of 213º), were used as constraints to develop magnetic and gravity models for the four anomalies of the Figueira Branca Suite. We adapted the methodology of staged inversion of Foss (2006) for the available dataset. First, we created outcropping block models with lateral limits based on the amplitude of the analytic signal over the magnetic field data. To each of these models were attributed the total magnetization direction, the average magnetic susceptibility and density (Table 2). The ambient magnetic field was defined by the IGRF by the time of the survey (inclination -11.6°, declination 234.9°, and intensity 23749 nT). The significantly smaller number and mostly irregularly distributed gravity data, was modelled as a secondary parameter which we allowed larger root mean square (RMS) errors (less than 20%) than to the magnetic field (less than 10%).

Table 2 - Measured average density and magnetic susceptibility of the four bodies of the Figueira Branca Suite.

Body	**Average Density (g/cm^3)**	**Average Magnetic Susceptibility (SI)**
Indiavaí	2.93888 ± 0.0001	0.043 ± 0.003
Azteca	2.91945 ± 0.0001	0.065 ± 0.004
Figueira Branca	2.84133 ± 0.0001	0.054 ± 0.004
Jauru	3.02962 ± 0.0001	0.066 ± 0.005

366 The staged inversion varied the following parameters at each stage: (1) the amplitude of the
367 total magnetization, and depth extent of the block model; (2) the amplitude of the total
368 magnetization, depth extent and horizontal position; (3) the amplitude of the total
369 magnetization, depth extent, horizontal position and vertices movements in north-south
370 direction; (4) the parameters of the previous stage plus the vertices movements in east-west
371 direction; and (5) all the previous parameters plus the magnetic susceptibility. By the end of
372 the first staged inversion, the body was subdivided in 500 m north-south oriented polygonal
373 prisms centred over the surveyed flight lines and the process was reinitiated to optimize the
374 results, with two differences: instead varying the depth extent in all stages, the vertices were
375 allowed to vary their positions on vertical direction, and the stage (4) was skipped. The third
376 and last pass of inversion permitted the variation of the density of the models, with the
377 modelling based on profiles of the Bouguer anomalies of the Figueira Branca Suite bodies
378 (Figs. 10 and 11).

379 The models achieved low RMS errors both for the magnetic and gravity data (Table 2). The
380 maps comparing the observed, modelled and residual fields are shown in Figure 10. The
381 modelled Azteca magnetic anomaly (Fig. 10b) showed higher amplitudes in the south of the
382 map unrelated to any model. We attributed the higher amplitude to border effects due to
383 interpolation of the modelled data. The observed Bouguer anomaly profiles are compared
384 with the modelled profiles in figure 11. The residual fields presented low amplitudes when
385 compared with the amplitude of the anomalies in the observed fields (see the RMS in Table
386 3). Although the average magnetic susceptibility and average density were used as constraints
387 for the modelling, we allowed their variation during the last stages of the inversion due the
388 small number of fresh samples available. The measured and the modelled values remained
389 the same after the inversion (Tables 2 and 3). The modelled amplitude of the total
390 magnetization varied from 2.8 to 8.6 A/m². These amplitudes, attributed to their respective
391 directions obtained through the MaxiMin RTP, enabled the determination of the total
392 magnetization vectors for the sources of the anomalies. The measured and modelled magnetic
393 susceptibilities, with the characteristics of the ambient field given by the IGRF, permitted the
394 estimation of the induced magnetization vectors on the Figueira Branca Suite modelled
395 bodies. Subtracting the total by the induced magnetization vector of each model, we
396 estimated their remanent magnetization vectors. The calculated remanent magnetization for
397 the four anomalies were quite similar as seen in Table 2. Their directions approximate the

398 average remanent magnetization direction of the Indiavaí gabbro reported by D'Agrella-Filho
399 et al. (2012) with inclination 50.7º, declination 209.8º, and α_{95}º 8.0.

400

401 Table 3 - Features and RMS values of the models of the Figueira Branca Suite.

Geophysical Models			
Alto Jauru Group (Host-rock)			
Samples			
Avg. Mag. Suscep.	0.007 (SI)	**# of Samples**	36
Avg. Density	2.70 g/cm³		
Indiavaí			
Samples			
Avg. Mag. Suscep.	0.05 (SI)	**# of Samples**	6
Avg. Density	2.94 g/cm³		
Magnetic and Gravity Fields Inversions			
Magnetization	**Induced**	**Total**	**Remanent**
Inclination (º)	-11.6	56	49.6
Declination (º)	346.9	213	199.5
Intensity (A/m)	0.9	3.8	4.4
RMS-Mag (%)	5.8	**# of Points**	29003
RMS-Grav (%)	18.9	**# of Points**	89
Azteca			
Samples			
Avg. Mag. Suscep.	0.07 (SI)	**# of Samples:**	2
Avg. Density	2.91 g/cm³		
Magnetic and Gravity Fields Inversions			
Magnetization	**Induced**	**Total**	**Remanent**
Inclination (º)	-11.6	56	51.2
Declination (º)	346.9	213	191.8
Intensity (A/m)	1.3	8.6	9.5
RMS-Mag (%)	6.4	**# of Points**	9251
RMS-Grav (%)	12.1	**# of Points**	37
Figueira Branca			
Samples			
Avg. Mag. Suscep.	0.06 (SI)	**# of Samples:**	3
Avg. Density	2.84 g/cm³		
Magnetic and Gravity Fields Inversions			
Magnetization	**Induced**	**Total**	**Remanent**
Inclination (º)	-11.6	56	45.9
Declination (º)	346.9	213	194
Intensity (A/m)	1.1	2.8	3.6
RMS-Mag (%)	3.7	**# of Points**	19206
RMS-Grav (%)	10.8	**# of Points**	17
Jauru			
Samples			
Avg. Mag. Suscep.	0.07 (SI)	**# of Samples:**	3
Avg. Density	3.02 g/cm³		
Magnetic and Gravity Fields Inversions			
Magnetization	**Induced**	**Total**	**Remanent**
Inclination (º)	-11.6	56	51.6
Declination (º)	346.9	213	202.9
Intensity (A/m)	1.3	7.8	8.6
RMS-Mag (%)	3.3	**# of Points**	9893
RMS-Grav (%)	13.8	**# of Points**	28

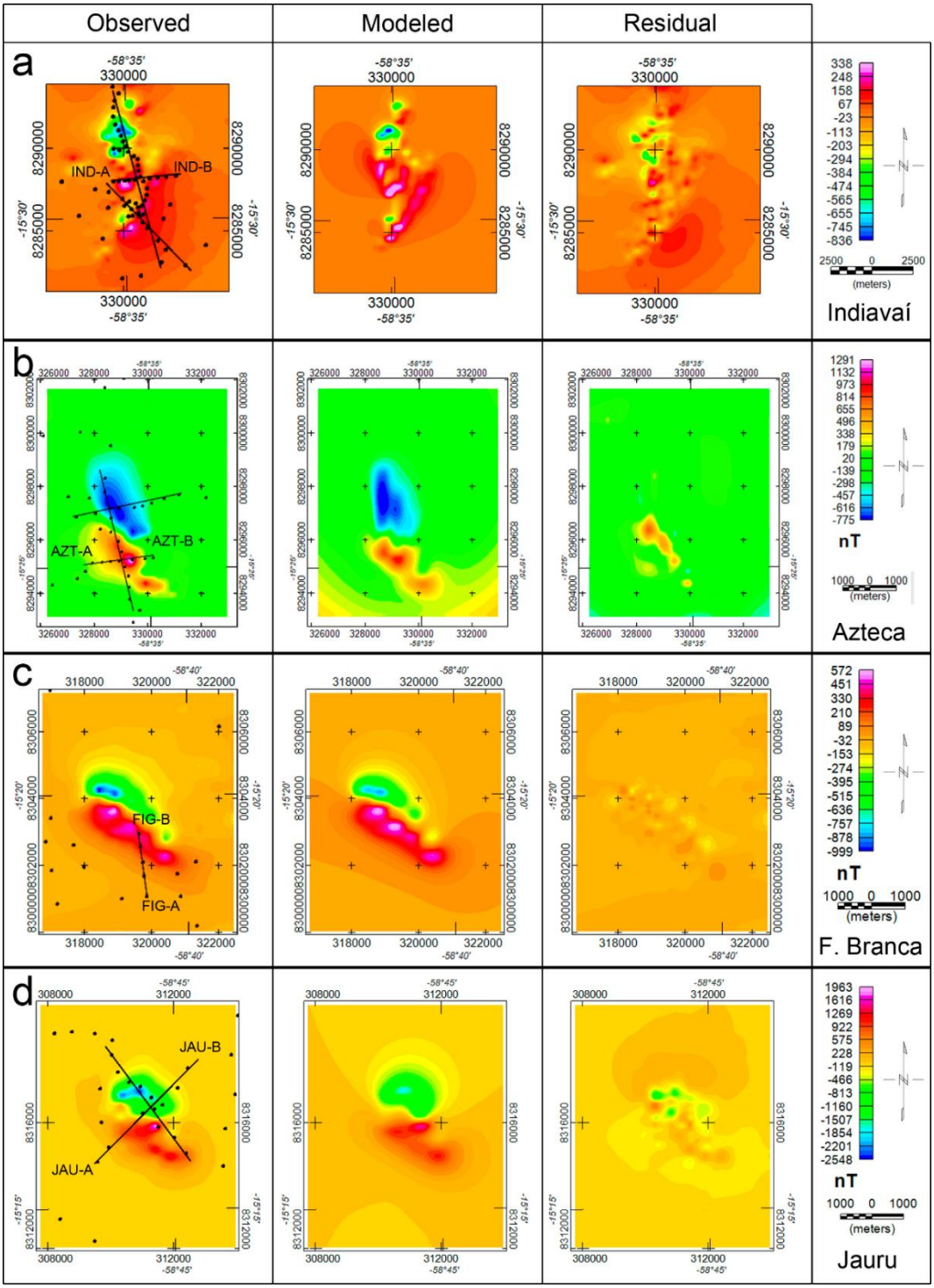

Fig. 10 – Original, modelled and residual magnetic fields of the bodies of Figueira Branca Suite: (a) Indiavaí, (b) Azteca, (c) Figueira Branca, and (d) Jauru. The black circles refer to the gravity measurements. The lines indicate the profiles used in the gravity inversion.

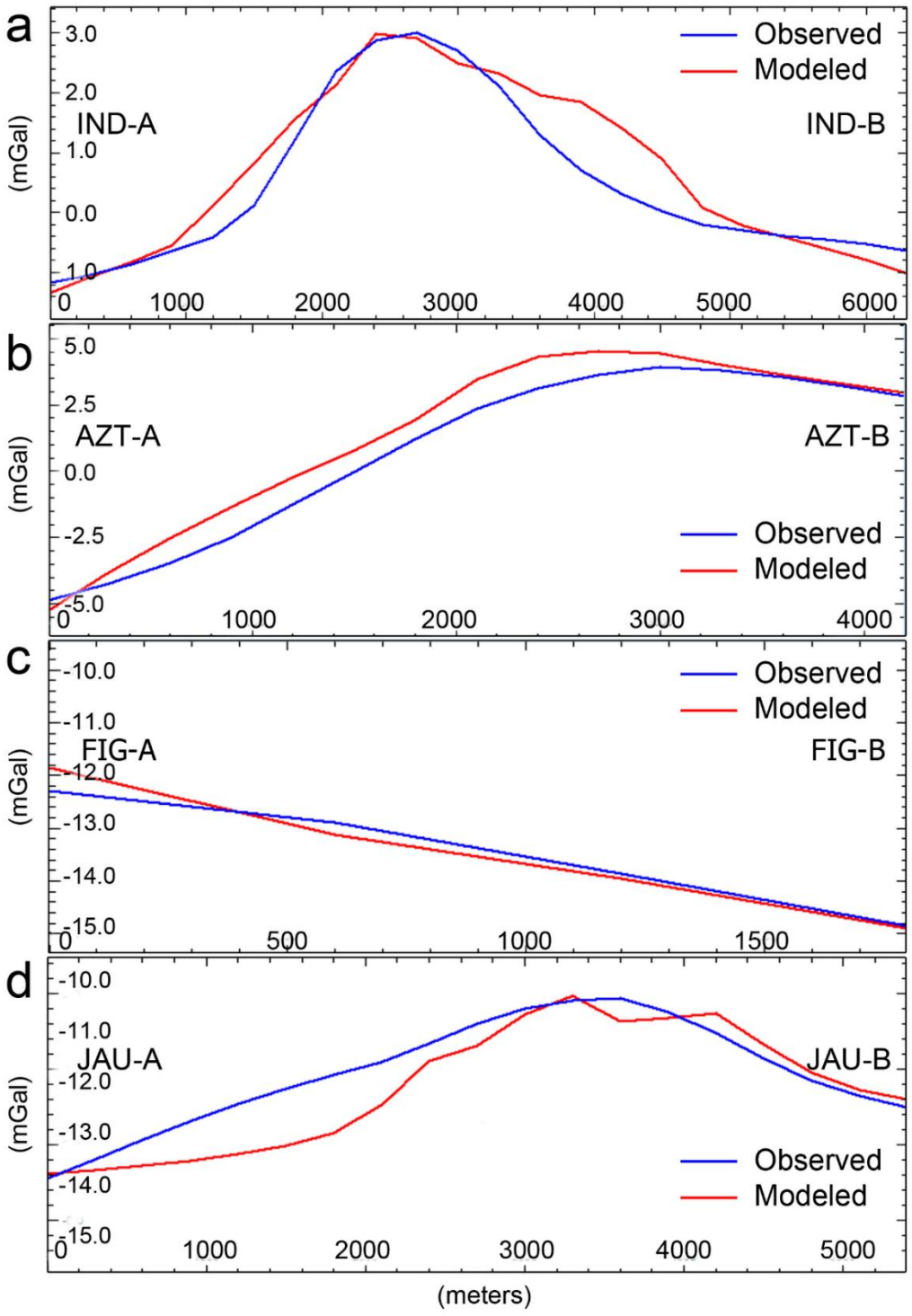

Fig. 11 – Original (blue lines) and modelled (red lines) of the Bouguer anomaly profiles: (a) IND-A to IND-B of the Indiavaí body, (b) AZT-A to AZT-B of the Azteca body, (c) FIG-A to FIG-B of the Figueira Branca body, and (d) JAU-A to JAU-B of the Jauru body.

The modelled bodies display an overall northwest-southeast trend, varying from 6 to 10 km in this direction, whereas their sizes in the northeast-southwest direction varied from 3 to 5

km (Fig. 12). The shallower horizons of the bodies were kept in the surface, constrained by the location the outcrops found in the field, and the vertical extensions ranged from approximately 330 to 835 m. The vertical extension and, by consequence, the depth of the bottom of the bodies are mostly speculative, as the ambiguity inherent to potential field methods does not allow a precise estimation of these features, even considering the knowledge about the magnetic susceptibility, remanent magnetization, and the location of outcrops.

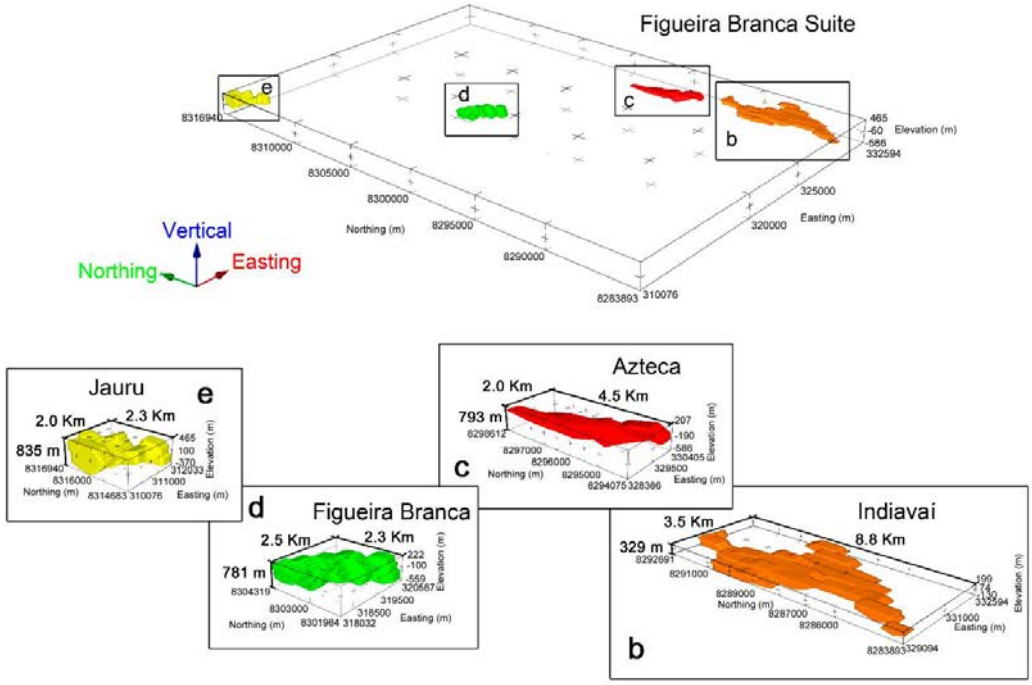

Fig. 12 – Joint magnetic and gravity models of the Figueira Branca Suite. In detail, (a) Indiavaí, (b) Azteca, (c) Figueira Branca and (d) Jauru models.

The magnetization, magnetic susceptibility and density obtained in each model of the Figueira Branca Suite (Fig. 10) agree with the context of gabbroic rocks intruded in a meta-volcanosedimentary environment described by geochemical (this work) and geological observations (D'Agrella-Filho et al., 2012; Teixeira et al., 2011). All cases presented similar values for magnetic susceptibility (Table 3), leaving the cause of the difference in the amplitude of the anomalies to the remanent magnetization. The shapes and depth extents can be associated with sills, as suggested by Teixeira et al. (2011). The layers of different lithologies could not be discriminated through the geophysical methods.

5. *Conclusions*

The Figueira Branca Suite is a layered mafic-ultramafic complex, dated at 1425 Ma, intruded into the Alto Jauru meta-volcanosedimentary group and adjacent to granites from the Santa Helena Orogen. Using magnetic field and gamma-ray geophysical data, we delineated the extent of the suite. Apart from the Indiavaí, Azteca, Figueira Branca and Jauru bodies, only two mafic intrusions in the northwest of the Jauru Terrane showed magnetic and gamma-ray signatures that could be related with the suite, however these two intrusions were recognized as the Morro do Leme and Morro do Sem-Boné complexes, part of the 1349 Ma Cacoal Suite. No other geophysical signatures similar to the four intrusions of the Figueira Branca Suite were found in the Jauru Terrane.

Thin sections of the Figueira Branca Suite indicated a mineralogy dominated by plagioclase, olivine and variable amounts of intergrown pyroxene (0 to 30%). This mineralogy indicates gabbroic rocks, as it was shown in the TAS. Magnetite is likely opaque minerals phase and is present in all samples. The increase in the amount of pyroxene among the samples from one intrusion to another in the Figueira Branca Suite suggests a fractionation in the parental magma. REE analyses normalized to chondrites showed a trend of major enrichment of LREE over HREE elements. The change in the slope of the REE normalized to chondrites indicates an increase in the amount of melt in the parental magma. These two changes suggest that the extraction of magma generated the bodies of the Figueira Branca Suite in the sequence: Indiavaí, Figueira Branca, Azteca and Jauru.

Magnetic and gravity fields were used to compose 3D models constrained by magnetic susceptibility (average of 0.06) and density (average of 2.93 g/cm^3) measurements. This data combined with new field investigation and geochemical data indicate sill-like shapes extending 8 km on average in the northwest direction. The calculated remanent magnetizations are similar to the direction suggested by previously published paleomagnetic data of the Indiavaí gabbro.

Trace element concentrations suggested that the parental magma of the Figueira Branca Suite is associated with metasomatic processes of subduction zones. The magma was characterized by hydrous melts, typical from supra-subduction environments. The northwest alignment of the bodies, indicated by geological observation and geophysical modelling, is perpendicular

to the direction of accretion of the terranes in southwest Amazon Craton and parallel to regional shear zones. The suite is located to east-northeast of the orogen and paleo-subduction zone that generated the Santa Helena orogen, marked by the Piratininga and Caramujo shear zones (Fig. 1).

Previously published isotope data show a juvenile mantle source for the Figueira Branca Suite. The integration of these data with those presented in this paper indicate that the magmatism that generated the Figueira Branca Suite during a phase of extension of the Jauru Terrane. This event occurred during the late stages of emplacement of the Santa Helena orogeny (1425 Ma) and was interpreted as a magmatism in a back-arc setting.

6. *Acknowledgements*

We would like to thank Vanessa B. Ribeiro for the comments, and the Brazilian Geological Service for the data. This work was done with the support of the CNPq, National Council for Technological and Scientific Development – Brazil.

7. *References*

Bettencourt, J.S., Leite Jr, W.B., Ruiz, A.S., Matos, R., Payolla, B.L., Tosdal, R.M., 2010. The Rondonian-San Ignacio Province in the SW Amazonian Craton: An overview. Journal of South American Earth Sciences 29, 28-46.

Cordani, R., Shukowsky, W., 2009. Virtual Pole from Magnetic Anomaly (VPMA): A procedure to estimate the age of a rock from its magnetic anomaly only. J Appl Geophys 69, 96-102.

Cordani, U.G., Fraga, L.M., Reis, N., Tassinari, C.C.G., Brito-Neves, B.B., 2010. On the origin and tectonic significance of the intra-plate events of Grenvillian-type age in South America: A discussion. Journal of South American Earth Sciences 29, 143-159.

Corrêa da Costa, P.C., Girardi, V.A.V., Matos, J.B.d., Ruiz, A.S., 2009. Geocronologia Rb-Sr e características geoquímicas dos diques máficos da região de Nova Lacerda e Conquista D'Oeste (MT), porção sudoeste do Craton Amazônico [Rb-Sr geochronology and

496 geochemical characteristics of mafic Dykes in the Nova Lacerda and Conquista D'Oeste
497 region, Mato Grosso, SW Amazonian Craton]. Geologia USP: Série Científica 9, 17.

498 D'Agrella-Filho, M.S., Trindade, R.I.F., Elming, S.A., Teixeira, W., Yokoyama, E., Tohver,
499 E., Geraldes, M.C., Pacca, I.I.G., Barros, M.A.S., Ruiz, A.S., 2012. The 1420 Ma Indiavai
500 Mafic Intrusion (SW Amazonian Craton): Paleomagnetic results and implications for the
501 Columbia supercontinent. Gondwana Res 22, 956-973.

502 Dickson, B.L., Scott, K.M., 1997. Interpretation of aerial gamma-ray surveys – adding the
503 geochemical factors. AGSO Journal of Australia Geology and Geophysics 17, 13.

504 Fedi, M., Florio, G., Rapolla, A., 1994. A Method to Estimate the Total Magnetization
505 Direction from a Distortion Analysis of Magnetic-Anomalies. Geophys Prospect 42, 261-274.

506 Foss, C., 2006. Evaluation of strategies to manage remanent magnetization effects in
507 magnetic field inversion, 76th Annual SEG International Meeting. SEG, New Orleans, p. 4.

508 Geraldes, M.C., Van Schmus, W.R., Condie, K.C., Bell, S., Teixeira, W., Babinski, M., 2001.
509 Proterozoic geologic evolution of the SW part of the Amazonian Craton in Mato Grosso
510 state, Brazil. Precambrian Res 111, 91-128.

511 Girardi, V.A.V., da Costa, P.C.C., Teixeira, W., 2012. Petrology and Sr-Nd characteristics of
512 the Nova Lacerda dike swarm, SW Amazonian Craton: new insights regarding its
513 subcontinental mantle source and Mesoproterozoic geodynamics. Int Geol Rev 54, 165-182.

514 Kepezhinskas, P., McDermott, F., Defant, M.J., Hochstaedter, A., Drummond, M.S.,
515 Hawkesworth, C.J., Koloskov, A., Maury, R.C., Bellon, H., 1997. Trace element and Sr-Nd-
516 Pb isotopic constraints on a three-component model of Kamchatka arc petrogenesis. Geochim
517 Cosmochim Ac 61, 577-600.

518 Louro, V.H.A., Mantovani, M.S.M., Ribeiro, V.B., 2014. Magnetic field analysis of Morro
519 do Leme nickel deposit. Geophysics 79, K1-K9.

520 Matos, J.B.d., Silva, C.H.d., Costa, A.C.D.d., Ruiz, A.S., Souza, M.Z.A.d., Batata, M.E.F.,
521 Corrêa da Costa, P.C., Paz, J.D.d.S., 2009. Geologia e Recursos Minerais da Folha Jauru
522 (SD.21-Y-C-III), Programa Geologia do Brasil, Cuiabá, p. 134.

523 Mcdonough, W.F., Sun, S.S., 1995. The Composition of the Earth. Chem Geol 120, 223-253.

Menezes, R.G., 1993. Pontes e Lacerda. Folha SD. 21-Y-c-n, Programa Levantamentos Geológicos Básicos do Brasil - PLGB. CPRM - Serviço Geológico do Brasil.

Middlemost, E.A.K., 1994. Naming Materials in the Magma Igneous Rock System. Earth-Sci Rev 37, 215-224.

Nunes, N.S.d.V., 2000a. Geologia e resultados prospectivos da área de Figueira Branca/Indiavaí, Mato Grosso, Série Metais do Grupo da Platina e Associados, 24 ed. CPRM - Serviço Geológico do Brasil.

Nunes, N.S.d.V., 2000b. Geologia e resultados prospectivos das áreas Morro do Leme e Morro Sem Boné/Mato Grosso, Série Metais do Grupo da Platina e Associados, CPRM - Serviço Geológico do Brasil ed. CPRM - Serviço Geológico do Brasil, Goiânia, p. 61.

Quadros, N.L.E.S., Rizzotto, G.J., 2007. Geologia e recursos minerais do Estado de Rondônia: Sistema de Informações Geográficas – SIG: Texto Explicativo do Mapa Geológico e de Recursos Minerais do Estado de Rondônia., Programa Geologia do Brasil. CPRM, Porto Velho, p. 153 p.

Rizzotto, G.J., Santos, J.O.S., Hartmann, L.A., Tohver, E., Pimentel, M.M., McNaughton, N.J., 2013. The Mesoproterozoic Guapore suture in the SW Amazonian Craton: Geotectonic implications based on field geology, zircon geochronology and Nd-Sr isotope geochemistry. Journal of South American Earth Sciences 48, 271-295.

Roest, W.R., Verhoef, J., Pilkington, M., 1992. Magnetic Interpretation Using the 3-D Analytic Signal. Geophysics 57, 116-125.

Ruiz, A.S., 2005. Evolução Geológica do Sudoeste do Cráton Amazônico Região Limítrofe Brasil-Bolívia-Mato Grosso, Departamento de Geociências. UNESP - Rio Claro, Rio Claro, p. 299.

Saes, G.S., Leite, J.A.S., Weska, R.K., 1984. Geologia da Folha Jauru (SD.21.Y.C.III): uma síntese de conhecimentos, 33rd Congresso Brasileiro de Geologia. Sociedade Brasileira de Geologia, Rio de Janeiro.

Shervais, J.W., 1982. Ti-V Plots and the Petrogenesis of Modern and Ophiolitic Lavas. Earth Planet Sc Lett 59, 101-118.

552 Souza, M.Z.A.d., Batata, M.E.F., Ruiz, A.S., Lima, G.A.d., Matos, J.B.d., Paz, J.D.d.S.,
553 Costa, A.C.D.d., Silva, C.H.d., Corrêa da Costa, P.C., 2009. Geologia e Recursos Minerais da
554 Folha Rio Branco (SD-21-Y-D-1), Programa Geologia do Brasil, Cuiabá, p. 178.

555 Sun, S.-s., McDonough, W.F., 1989. Chemical and isotopic systematics of oceanic basalts:
556 implications for mantle composition and processes. Geological Society, London, Special
557 Publications 42, 313-345.

558 Tassinari, C.C.G., Bettencourt, J.S., Geraldes, M.C., Macambira, M.J.B., Lafon, J.M., 2000.
559 The Amazonian Craton, in: Cordani, U.G., Milani, E.J., Thomaz Filho, A., Campos, D.A.
560 (Eds.), 31st International Geological Congress. Sociedade Brasileira de Geologia, Rio de
561 Janeiro, pp. 41-95.

562 Tassinari, C.C.G., Macambira, M.J.B., 1999. Geochronological provinces of the Amazonian
563 Craton. Episodes 22, 174-182.

564 Teixeira, W., Ernst, R.E., Hamilton, M.A., Lima, G., Ruiz, A.S., Geraldes, M.C., 2016.
565 Widespread ca. 1.4 Ga intraplate magmatism and tectonics in a growing Amazonia. Gff 138,
566 241-254.

567 Teixeira, W., Geraldes, M.C., D'Agrella, M.S., Santos, J.O.S., Barros, M.A.S., Ruiz, A.S., da
568 Costa, P.C.C., 2011. Mesoproterozoic juvenile mafic-ultramafic magmatism in the SW
569 Amazonian Craton (Rio Negro-Juruena province): SHRIMP U-Pb geochronology and Nd-Sr
570 constraints of the Figueira Branca Suite. Journal of South American Earth Sciences 32, 309-
571 323.

572 Teixeira, W., Geraldes, M.C., Matos, R., Ruiz, A.S., Saes, G., Vargas-Mattos, G., 2010. A
573 review of the tectonic evolution of the Sunsas belt, SW Amazonian Craton. Journal of South
574 American Earth Sciences 29, 47-60.

575 Vermeesch, P., 2006. Tectonic discrimination diagrams revisited. Geochemistry, Geophysics,
576 Geosystems 7, n/a-n/a.

577 Wang, H., Wu, Y.B., Qin, Z.W., Zhu, L.Q., Liu, Q., Liu, X.C., Gao, S., Wijbrans, J.R., Zhou,
578 L., Gong, H.J., Yuan, H.L., 2013. Age and geochemistry of Silurian gabbroic rocks in the
579 Tongbai orogen, central China: Implications for the geodynamic evolution of the North
580 Qinling arc-back-arc system. Lithos 179, 1-15.

581 Zheng, Y.F., 2012. Metamorphic chemical geodynamics in continental subduction zones.
582 Chem Geol 328, 5-48.

4. Manuscript 3: Magnetic Amazon: where was the Amazon Craton in Nuna?

So far, the Figueira Branca suite was evaluated in scales from microscopic to hundreds of kilometres. In chapter 3, the Figueira Branca suite and the Jauru Terrane in the southwest of the Amazon Craton were assessed with geophysical and geochemical methodologies. This manuscript will increase the area of study once more to continental scales.

A back-arc extension in the later stages of the Santa Helena Orogen was responsible for the intrusion of the Figueira Branca Suite. From a broader perspective, during the 1.6 to 1.4 Ga period, the Amazon Craton had passed for most of its accretionary history, and would still face the accretion of its youngest provinces, the Rondonian-San Ignácio and Sunsás.

The Paleo- to Mesoproterozoic period was marked by the supercontinent Nuna. A variety of models proposed reconstructions for the supercontinent, with different constituent fragments and geometries. The Amazon Craton has been shown attached and separated from the Nuna's major landmass, and the central objective of this chapter is to investigate position of the craton from 1.6 to 1.4 Ga. To achieve it, magnetic field data was used to analyse three reconstructions of Nuna: (1) Mertanen and Pesonen (2012), which is based on paleomagnetic data; (2) Pisarevsky et al. (2014), based on paleomagnetic and geological constraints; and (3) Pehrsson et al. (2015) who integrated paleomagnetic and geological data with patterns and features of ore deposit distribution.

The dataset used to evaluate the reconstructions was the global magnetic anomaly map, EMAG2 (Maus et al., 2009). It was used to map the Amazon and other cratons suggested to be connected from 1.6 to 1.4 Ga: West African, Baltic and the North China cratons. Magnetic field regimes and lineaments were used to evaluate coeval blocks of different cratons. By recognizing the supercontinent reconstruction model that the magnetic field best supported, it

was possible to suggest the condition and location of the Amazon Craton during the intrusion of the Figueira Branca Suite.

Manuscript Details

Manuscript number	PRECAM_2017_82
Title	Magnetic Amazon: where was the Amazon Craton in Nuna?
Article type	Research Paper

Abstract

A variety of reconstructions have been proposed for the Paleo- to Mesoproterozoic supercontinent Nuna. Most involve the juxtaposition of Laurentia and Baltica with Siberia occupying an adjacent or nearby position. But the disposition of other cratonic blocks around these core elements, or whether they were even part of Nuna, is unresolved. We use magnetic field data from the global magnetic anomaly map, EMAG2, from the Amazon, Baltic, West African and North China cratons to observe potential continuity of magnetic lineaments and regimes in domains of similar ages within these cratons. On this basis, a permissible early Mesoproterozoic configuration of these cratonic fragments involves southwest Baltica (Sarmatia) abutting the northern portion of the Amazon Craton (Maroni-Itacaiúnas), whereas the western or the southern border of West Africa would be close to, or connected with, the northeast side of the Amazon Craton. This data is consistent with those models that locate the Amazon Craton at the southern end of the main Nuna landmass.

Keywords	Amazon Craton; Nuna; Mesoproterozoic; Magnetic Field; EMAG2.
Corresponding Author	Vinicius Louro
Order of Authors	Vinicius Louro, Marta Mantovani, Peter A. Cawood, VANESSA RIBEIRO
Suggested reviewers	Johanna Salminen, Sally Pehrsson, Joseph Meert, David Evans, M. Santosh

Submission Files Included in this PDF

File Name [File Type]

Louro et al - 2017 - Magnetic Amazon - Cover Letter.docx [Cover Letter]

Louro et al - 2017 - Magnetic Amazon.docx [Manuscript File]

Fig 1 - Nuna Theories.tif [Figure]

Fig 2 - Magnetic regimes.tif [Figure]

Fig 3 - Amazon Craton - Balburgh et al - 2009.tif [Figure]

Fig 4 - West Africa Craton - Youbi et al - 2013.tif [Figure]

Fig 5 - Baltica Craton - Bogdanova et al - 2007.tif [Figure]

Fig 6 - North China Craton - Wu et al - 2013.tif [Figure]

Fig 7 - Amazon Craton - Mag.tif [Figure]

Fig 8 - West African Craton - Mag.tif [Figure]

Fig 9 - Baltica Craton - Mag.tif [Figure]

Fig 10 - North China Craton - Mag.tif [Figure]

Fig 11 - Nuna - Mertanen and Pesonen - 2012.tif [Figure]

Fig 12 - Mertanen and Pesonen - Terranes.tif [Figure]

Fig 13 - Columbia - Pisarevsky - 2014.tif [Figure]

Fig 14 - Pisarevsky - Terranes.tif [Figure]

Fig 15 - Columbia - Pehrsson - 2014.tif [Figure]

Fig 16 - Pehrsson - Terranes.tif [Figure]

Louro et al - 2017 - Magnetic Amazon - Table 1.docx [Table]

Highlights.docx [Highlights]

To view all the submission files, including those not included in the PDF, click on the manuscript title on your EVISE Homepage, then click 'Download zip file'.

Magnetic Amazon: where was the Amazon Craton in Nuna?

Vinicius H. A. Louro[1,2], Peter A. Cawood[2,3], Marta S. M. Mantovani[1], Vanessa B. Ribeiro[1,4]

[1] Instituto de Astronomia, Geofísica e Ciências Atmosféricas, Universidade de São Paulo, São Paulo, Brazil.

[2] Department of Earth and Environmental Sciences, University of St. Andrews, St. Andrews, UK.

[3] School of Earth, Atmosphere & Environment, Monash University, Melbourne, VIC 3800, Australia

[4] Universidade Federal de Pernambuco – UFPE, Recife, Pernambuco, Brazil.

E-mails: vilouro@usp.br, peter.cawood@monash.edu, msmmanto@usp.br, van.biondo@gmail.com

Corresponding author: Vinicius H. A. Louro.

E-mail: vilouro@usp.br

Present Address: Rua do Matão, 1226, Sala A-204, Laboratório de Geofísica da Litosfera – GEOLIT, Instituto de Astronomia, Geofísica e Ciências Atmosféricas, Universidade de São Paulo, Cidade Universitária, São Paulo, Brazil. CEP: 05508-090

Phone: +55 (11) 99985 1501

Date of Submission: 05 February 2017

Abstract

A variety of reconstructions have been proposed for the Paleo- to Mesoproterozoic supercontinent Nuna. Most involve the juxtaposition of Laurentia and Baltica with Siberia occupying an adjacent or nearby position. But the disposition of other cratonic blocks around these core elements, or whether they were even part of Nuna, is unresolved. We use magnetic field data from the global magnetic anomaly map, EMAG2, from the Amazon, Baltic, West African and North China cratons to observe potential continuity of magnetic lineaments and regimes in domains of similar ages within these cratons. On this basis, a permissible early Mesoproterozoic configuration of these cratonic fragments involves southwest Baltica (Sarmatia) abutting the northern portion of the Amazon Craton (Maroni-Itacaiúnas), whereas the western or the southern border of West Africa would be close to, or connected with, the northeast side of the Amazon Craton. This data is consistent with those models that locate the Amazon Craton at the southern end of the main Nuna landmass.

Keywords

Amazon Craton, Nuna, Mesoproterozoic, Magnetic Field, EMAG2.

1. Introduction

The location and composition of the Paleo- to Mesoproterozoic supercontinent Nuna, also known as Columbia and Hudsonland, and its constituent fragments is much debated and a variety of models, some of which entail mutually exclusive configurations, have been proposed (Evans and Mitchell, 2011; Johansson, 2009; Pisarevsky et al., 2014; Rogers and Santosh, 2002; Williams et al., 1991; Zhao et al., 2002; Zhao et al., 2004; Zhao et al., 2001). Understanding the processes of supercontinent amalgamation and breakup, as well as their paleogeographic configuration, provides valuable insights into the evolution of the Earth, including the role of Large Igneous Provinces (LIP) (Youbi et al., 2013), their relationship to patterns of ore deposits (Cawood and Hawkesworth, 2015; Pehrsson et al., 2015), and their potential impact on the Earth's surficial environments, including atmosphere and ocean composition and the biosphere (e.g., Cawood and Hawkesworth, 2015, and references therein).

Historically, supercontinent reconstructions are based on the integration of one or more datasets involving stratigraphic and tectonic correlations, geochemical and isotopic compositions, and paleomagnetic data. In this paper, we evaluate the position of the Amazon Craton in the Nuna supercontinent using magnetic field data and, in particular, we assess a number of recent reconstructions that highlight the range of Nuna configurations and the datasets used to justify those configurations, including: (1) Mertanen and Pesonen (2012), which is based on paleomagnetic data; (2) Pisarevsky et al. (2014), based on paleomagnetic and geological constraints; and (3) Pehrsson et al. (2015) who integrated paleomagnetic and geological data with patterns and features of ore deposit distribution (Fig. 1).

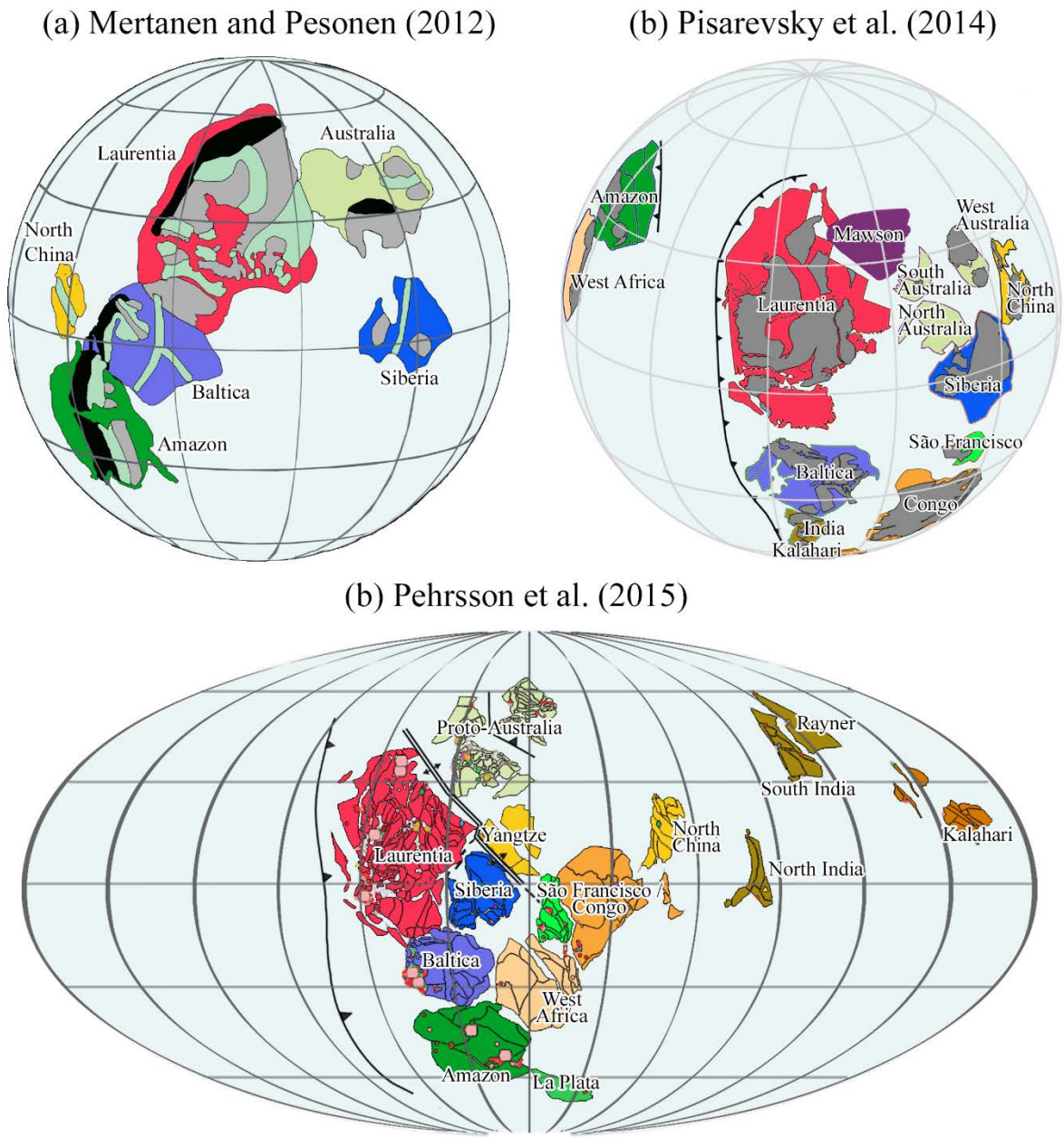

78

79 Fig. 1 – Reconstructions of Nuna proposed by (a) Mertanen and Pesonen (2012), (b)
80 Pisarevsky et al. (2014), and (c) Pehrsson et al. (2015).

81

82 Our assessment is based on a combination of Total Magnetic Field, the Amplitude of the
83 Analytic Signal 3D (Roest et al., 1992), and Tilt data (Verduzco et al., 2004) of the Amazon
84 and potential adjacent cratons, to compare magnetic signature, which along with geologic and
85 age data of these cratons enables us to revaluate proposed Nuna reconstructions. Unfortunately,

paleopole data for the Amazon Craton for the relevant period of Nuna assembly is limited: the 1420 Ma Indiavaí (D'Agrella-Filho et al., 2012) and Nova Guarita intrusives (Bispo-Santos et al., 2012), and the 1790 Ma Colider (Bispo-Santos et al., 2008) and Avanavero intrusives (Reis et al., 2013). The small number of Proterozoic reference poles in the Amazon Craton, as well as West Africa (Pisarevsky et al., 2014), in part reflects the vast area of the Amazon forest with limited access and poor exposure, as well as areas of civilian unrest, or of military and strategic value, and thus complicates the reconstruction of the Amazon Craton in Nuna. In this paper, we demonstrate that remotely accessed data, such as magnetic field data, can provide additional information to constrain the relationship between blocks in Nuna. In particular, we use magnetic field data and its products to evaluate field regimes and magnetic lineaments within and between cratons. Magnetic field regimes are defined by the concentration of magnetic anomalies within a designated region. The regimes can be interpreted as calm, intermediate or agitated depending on the frequency pattern of the magnetic anomalies (Fig. 2). Magnetic lineaments are normally expressions of contacts, faults, boundaries between terranes, and folds, where secondary magnetite is created through the insertion of oxygen in a Fe-bearing environment (Grant, 1985b; Rotherham, 1997).

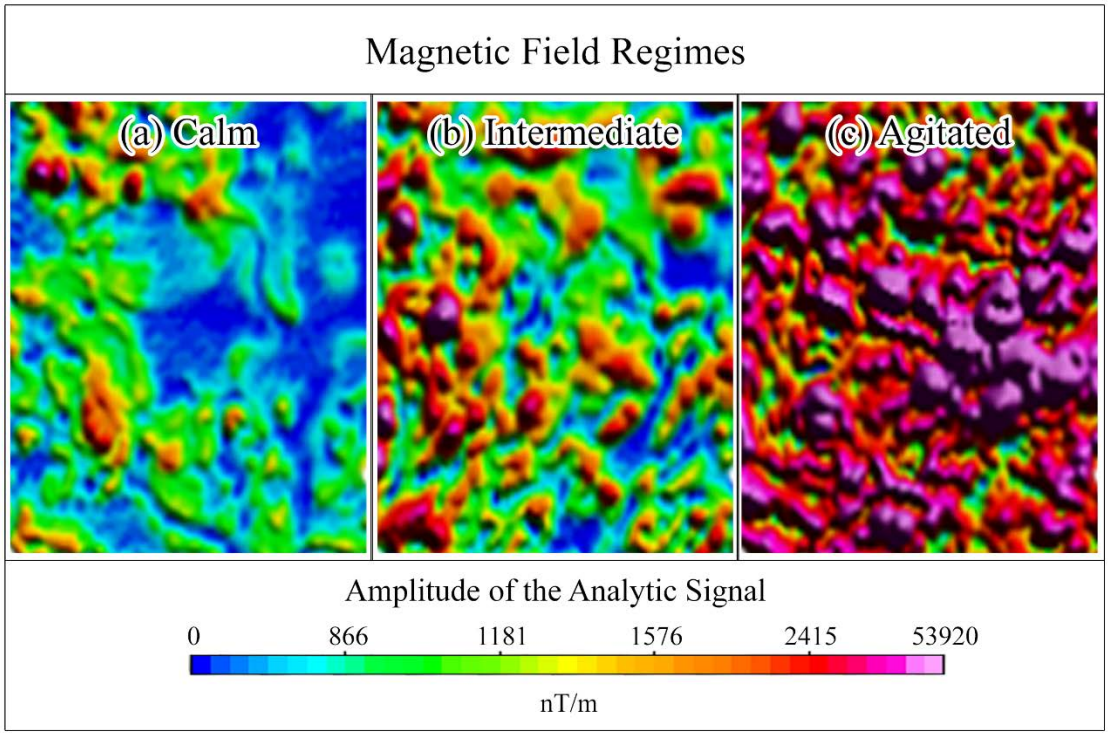

Fig. 2 – Magnetic field regimes using the Amplitude of the Analytic Signal: (a) calm, (b) intermediate, and (c) agitated.

2. Geology of the Cratons

The evaluation of the role of Amazonia in Nuna, or indeed whether it was even part of Nuna, requires an outline of available geological constrains. Our focus is the Amazon Craton and most published models suggest that it is linked with one or more of West African, Baltic and/or the North China cratons. Outlined below are the key geological features of these blocks.

2.1. Amazon Craton

Tassinari and Macambira (1999) and Teixeira et al. (2010) divide the Amazon craton into six structural and geochronological provinces: Central Amazon (> 2.6 Ga), Maroni-Itacaiúnas (2.25 to 2.10 Ga), Ventuari-Tapajós (1.98 to 1.81 Ga), Rio Negro-Juruena (1.79 to 1.52 Ga), Rondonian-San Ignácio (1.55 to 1.30 Ga) and Sunsás (1.28 to 0.97 Ga) (Fig. 3). The stable Archean nuclei of the Central Amazon is a granite-greenstone terrain. It was not affected by the 2.2 Ga to 1.9 Ga Trans-Amazonian Orogeny (Hurley et al., 1967), however Paleoproterozoic magmatic and sedimentary events are recorded across this cratonic core.

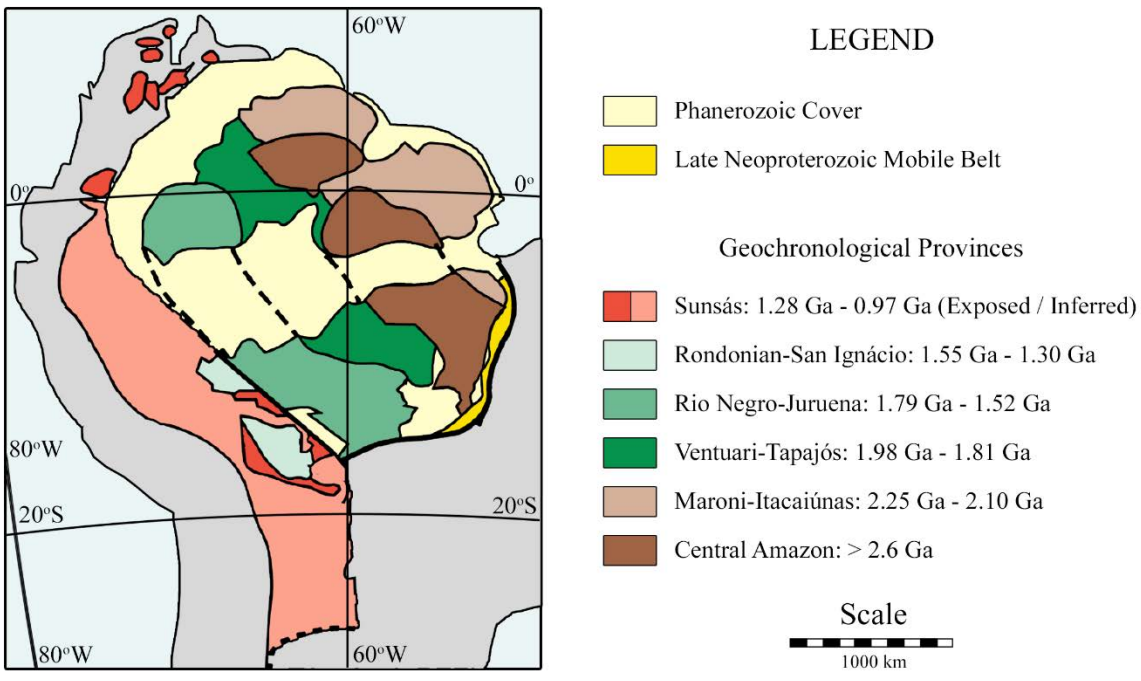

Fig. 3 – Geochronological provinces of the Amazon Craton (Bahlburg et al., 2009).

The Paleoproterozoic Maroni-Itacaiúnas Province is located to the northeast of the Central Amazon and can be traced for 1500 km (Fig. 3). It is characterized by greenstone belts and associated calc-alkaline granitoids, with large metavolcanic-sendimentary sequences metamorphosed from greenschist to amphibolite facies (Tassinari and Macambira, 1999). To the southwest of the Central Amazon, lies the northwest-southeast elongated Ventuari-Tapajós province, composed of calc-alkaline granitoids with juvenile isotopic signatures (Cordani et al., 2010). Further to the southwest, the Rio Negro-Juruena province of granite gneisses and granitoids of granodioritic and tonalitic compositions forms a 2000 km long and 600 km wide belt aligned northwest-southeast (Fig. 3).

The Rondonian-San Ignácio and Sunsás are the largest provinces of the Amazon Craton (Fig. 3). The 1.55 to 1.30 Ga Rondonian-San Ignácio has granite-gneiss-migmatitic terranes metamorphosed to amphibolite or granulite facies composing its basement (Tassinari and Macambira, 1999). Cordani and Teixeira (2007) associate the formation of the Rondonian-San Ignácio province to the amalgamation of intra-oceanic magmatic arcs and accretionary prisms and ultimately their collision to the southwest with the Rio Negro-Juruena province. The Sunsás orogenic belt is the youngest province of the Amazon Craton. It is the expression of the collision between Amazonia and Laurentia, during the assembly of the Rodinia (Cawood and Pisarevsky, 2017; Sadowski and Bettencourt, 1996; Tohver et al., 2006). The Sunsás province is characterized by metamorphosed volcano-plutonic-sedimentary sequences intruded by Neoproterozoic granitic suites (Boger et al., 2005).

2.2. West African Craton

The West African Craton, northwest Africa (Fig. 4), has been stable since 2 Ga (Youbi et al., 2013). It consists of the Archean Reguibat and Man shields to the north and south, respectively, large Paleoproterozoic domains separated by cratonic sedimentary basins, and at the northern end, the Anti Atlas belt. The Man shield is composed by TTG-type banded gneiss, older than 3.0 Ga (Beckinsale et al., 1980), overlain by greenstone belt lithologies intruded by granites. The Reguibat Shield contain Archean and Paleoproterozoic migmatites interlayered with mafic gneisses, greenstone belts, and voluminous tonalitic or granodioritic plutons (Key et al., 2008). Between the shields, in the central portion of the West African Craton, the late Proterozoic to

Paleozoic Taoudeni basin, and to the north of the Reguibat Shield, the Paleozoic Tindouf basin, overlie basement (Guerrak, 1989; Windley, 1987).

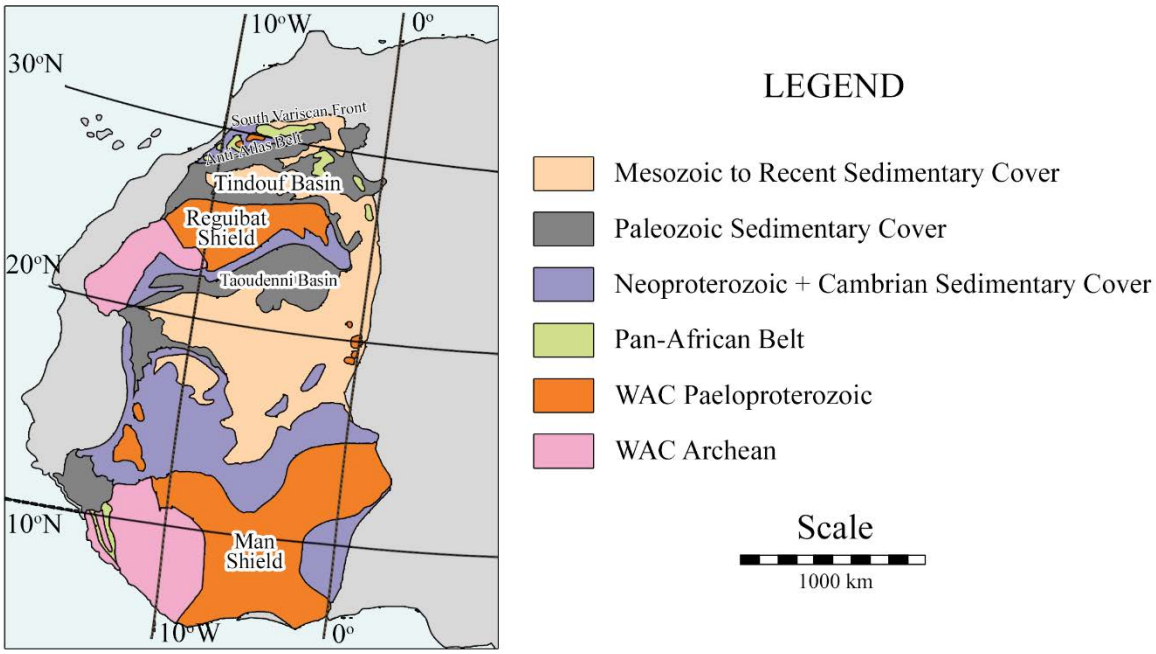

Fig. 4 – West African Craton (WAC) (Ennih and Liégeois, 2008).

The Anti-Atlas belt is located between the Alpine Atlas chain and the Tindouf basin. It is composed of Proterozoic low- to medium-grade schists and intrusive granitoids, and a thick (ca. 10 km) late Neoproterozoic to Paleozoic sedimentary cover (Soulaimani and Burkhard, 2008). Many orogenic cycles are recognized in the West African Craton, spanning from 3.5 to 1.75 Ga, along with the 750 to 550 Ma Pan African orogenic event (Ennih and Liégeois, 2008). Söderlund et al. (2013), El Bahat et al. (2013), Kouyaté et al. (2013) and Youbi et al. (2013) indicate that the interval from 1.7 to 1.0 Ga was marked by intraplate magmatic events.

2.3. Baltic Craton

Baltica is divisible into the Archean proto-continents of Sarmatia, Volgo-Uralia and Fennoscandia (Fig. 5) that were assembled into Baltica along Paleoproterozoic to Mesoproterozoic orogenic belts (Bogdanova et al., 2008).

The Fennoscandian Shield, northwest Baltica, is surrounded by Paleoproterozoic crust formed between 1.95 and 1.90 Ga, and intruded by the 1850-1650 Ma Transcandinavian Igneous Belt (Bingen et al., 2008). Basement within the shield is cut by Anorthosite-Mangerite-Charnockite-Granite (AMCG) (Emslie et al., 1994) and A-type granitoid suites, dolerite dykes and sills, tholeiitic basalt, mafic metavolcanic rocks, and gabbro-tonalite complexes were emplaced between 1.73 to 1.44 Ga (Bogdanova et al., 2006; Bogdanova et al., 2008). The Central Russian collisional belt connects Fennoscandia and Sarmatia (Fig. 5). It contains blocks of Archean rocks reworked during the Paleoproterozoic.

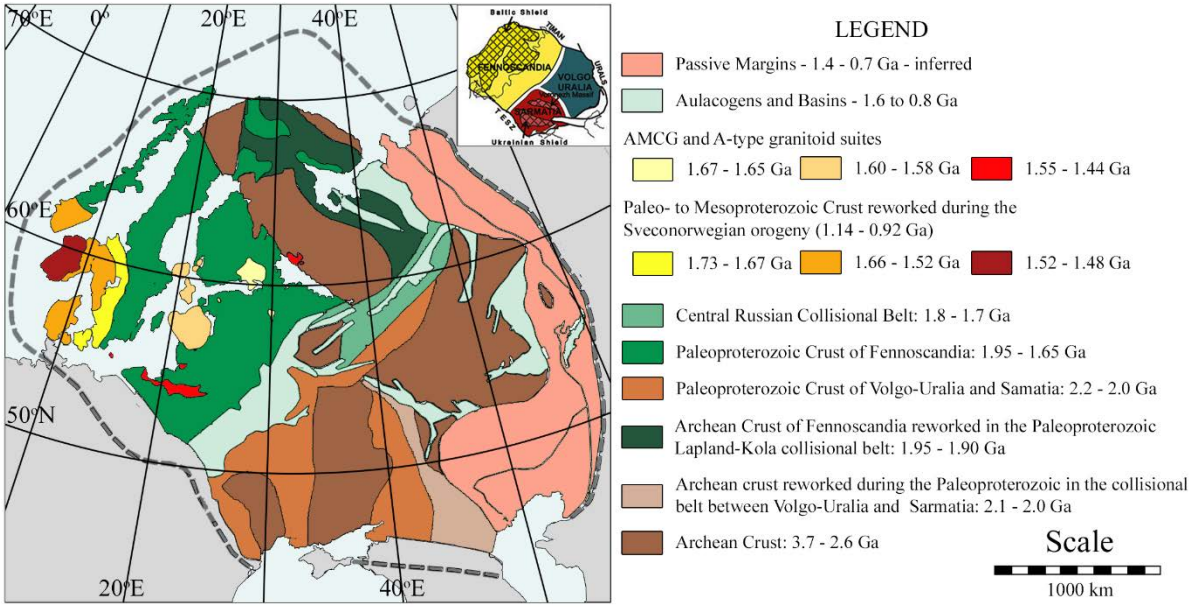

Fig. 5 – Baltic Craton (Bogdanova et al., 2008).

The Volgo-Uralia Shield in eastern Baltica, contains granitic gneiss as old as 3.3 Ga (Bogdanova et al., 2005) and is characterized by 3.0 to 2.7 Ga belts of metasedimentary and metaigneous granulites, and subordinate komatiite-bearing greenstone sequences (Bogdanova et al., 2008). The collisional belt between the Volgo-Uralia and Sarmatia contains turbiditic pelites and greywackes with carbonaceous rocks (Shchipansky et al., 2007). To the north and east of the Volgo-Uralia, lies an infered 1.4 to 0.7 Ga passive margin succession (Bogdanova et al., 2008).

Sarmatia is the result of the amalgamation of 3.7 to 2.6 Ga blocks intercalated by 2.2 to 2.1 Ga Paleoproterozoic belts (Bogdanova et al., 2008). Bogdanova et al. (2006) report north-south

trends, both in the Paleoproterozoic belts and reworked Archean crust, but with an abrupt change to a northeast-southwest orientation at the northeastern limit of the block. This change marks the continental-margin igneous belt formed at 2.0 to 1.95 Ga with the collision of Sarmatia with the Volgo-Uralia.

2.4. North China Craton

The North China Craton consists of four Archean blocks (Yinshan, Ordos, Longgang and Nangrim), amalgamated by younger orogenic belts (Fig. 6) (Zhao and Cawood, 2012). The Yinshan and the Ordos blocks are separated by the 1.95 to 1.92 Ga Khondalite Belt, which together form the Western Block of the North China Craton (Dong et al., 2007; Wu et al., 2013; Zhao and Cawood, 2012). The Longgang and the Nangrim blocks, united by the Jiao-Liao-Ji belt at 1.90 Ga, constitute the Eastern Block of the North China Craton (Wu et al., 2013; Zhao and Cawood, 2012). The Western and Eastern blocks collided at ca. 1.85 Ga, forming the Paleoproterozoic Trans-North China Orogen (Zhao et al., 2012).

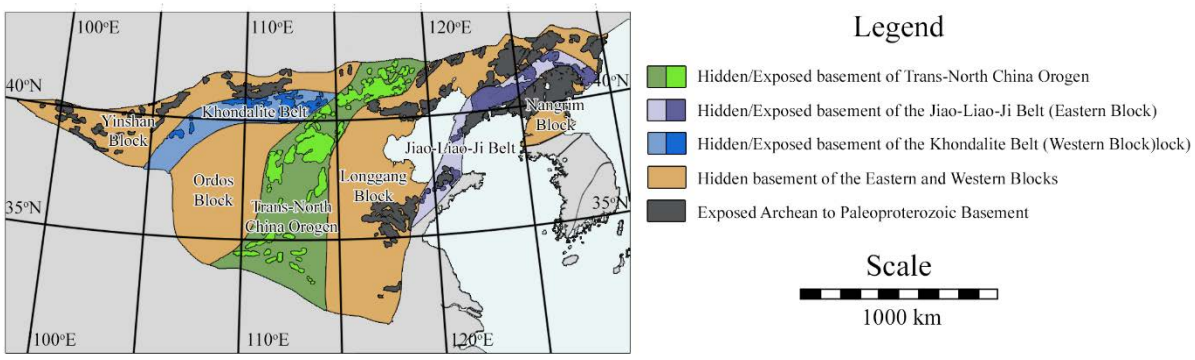

Fig. 6 – North China Craton (Zhao et al., 2004).

The Yinshan Block is composed of Neoarchean tonalite-trondhjemite-granodiorite (TTG) gneisses and minor supracrustal rocks metamorphosed at ca. 2.5 Ga (Wu et al., 2013). The 1.95 to 1.92 Ga Khondalite Belt, separating the Yinshan and the Ordos blocks is dominated by gneisses, paragneisses, calc-silicate rocks and marbles (Zhao and Zhai, 2013). The Ordos Block, to the south of the Khondalite Belt, is largely covered by the Mesozoic to Cenozoic Ordos basin.

In the Eastern Block, the Longgang and the Nangrim blocks consist of 3.8 to 3.0 Ga TTG gneisses, 2.7-2.5 Ga syntectonic granitoids, supracrustal ultramafic (komatiitic) to felsic volcanic rocks and metasedimentary rocks (Zhao et al., 2001). The Jiao-Liao-Ji Belt, separating the Longgang and Nangrim blocks, is characterized by metamorphosed sedimentary-volcanic successions and associated granitic and mafic intrusions (Zhao and Zhai, 2013).

The Trans-North China Orogen extends north-south for approximately 1200 km and is up to 300 km wide (Zhao et al., 2012). It contains late Neoarchean to early Paleoproterozoic (2560 to 2475 Ma) TTG gneisses, granitoids and greenstone belts developed under continental magmatic arc, island arc- or back-arc basin environments (Wilde et al., 2005; Zhao et al., 2012; Zhao and Zhai, 2013).

3. Methodology

3.1. Data

The magnetic field data used here was obtained through the Earth Magnetic Anomaly Grid (EMAG2) (Maus et al., 2009). This compiled and corrected data set incorporates satellite, ship and airborne surveys, of which the last two had been given preference where available. The resolution of the grid is 2 arc min (ca. 3.7 km in the equator), and the altitude normalized to 4 km above the geoid. Wavelengths longer than 330 km were obtained with the latest CHAMP satellite magnetic field model MF6 (http://geomag.org/models/MF6.html, accessed 28/02/2017).

3.2. Magnetic Field Techniques

We analysed the crustal magnetic field data obtained by EMAG2 to evaluate Nuna reconstructions. Three features of the magnetic field were considered to facilitate comparison of continental-scale structures: the magnetic regime (agitated, intermediate, or calm, e.g. Fig. 2), the size of the anomalies, and the orientation of the magnetic lineaments. The resolution

and normalized altitude obtained from the EMAG2 are compatible with the scale of the investigated tectonic features (> 3.7 km).

Geological and tectonic features usually present different amounts of magnetic minerals, resulting in the generation of a magnetic signal, whether inserted in an external (geomagnetic) field or not. Magnetite is a minor accessory mineral present in most rocks, rarely constituting more than 1 % by volume of a rock (Grant, 1985a). The formation of magnetite, primary or secondary, is mainly associated with the supply of oxygen in the system. The most important factors that determine the bulk magnetic properties of a rock are the total iron content, the oxidation state, the initial crystallization environment, the degree of metamorphism, the degree of silica saturation, the grain size of original sediment (in metasedimentary rocks), and the major element chemistry (Grant, 1985a).

The magnetic regimes were evaluated based on the frequency that magnetic anomalies appear in each domain of the cratons. An agitated regime (Fig. 2) is interpreted to represent greater tectonic activity through the entire history of the block, but not necessarily in a single period, while intermediate and calm regimes indicate less active settings, e.g., passive margins undergoing thermally driven subsidence (Olesen et al., 2007). To observe the magnetic regimes, the Total Magnetic Field (TMI) and the Amplitude of the Analytic Signal 3D (AAS) (Roest et al., 1992) were analysed. The TMI shows overall patterns of anomalies, but depends on the geomagnetic (inducing) field at the time of the survey. This dependence is relevant in studies of large areas, in which the magnetic field changes in orientation and intensity, i.e. the present magnetic field in the Amazon Craton varies in inclination from -30° to +30°, declination from -20° to -10°, and intensity from 33012 to 22890 nT, depending on the location, whereas in Baltica, it changes from +68° to +78° in inclination, from -2° to +10° in declination, and from 52952 to 54635 nT in intensity (https://www.ngdc.noaa.gov/geomag-web/#igrfwmm, accessed in 28/02/2017, the magnetic field refers to the International Geomagnetic Reference Field model for same date the data was accessed in the website).

The AAS is given by the expression (Roest et al., 1992):

$$AAS = \sqrt{[(\partial T/\partial x)^2 + (\partial T/\partial y)^2 + (\partial T/\partial z)^2]} \qquad (1)$$

where T refers to the TMI, and x, y, and z directions in Cartesian space. The AAS is one of the most commonly used techniques to evaluate the lateral limits of sources of potential field anomalies.

Linked to the magnetic regime, the size of the anomalies was explored with the AAS (Figs. 7b, 8b, 9b and 10b). This technique, based on directional derivatives of the field, reveals the lateral limits of discrete bodies and geological features. It displays little dependence on the direction of the magnetic field, so the location of the anomaly or the presence of remanent magnetization does not interfere with the results. Coeval domains connected at some point in Earth evolution tend to present structures of similar sizes (Olesen et al., 2007) if no posterior event altered significantly its composition and size. Regional tectonothermal events involving magmatism, deformation and metamorphism can generate strain and thermal energy sufficient to alter the size of the anomalies, whether by distorting the body, by changing and or extinguishing the remanent magnetization, or by opening the system to oxygenated fluids and formation of secondary magnetite. These changes can be observed in large areas that not necessarily are limited to one specific domain.

The assembly of terranes and regional movements inside the cratons are considered by evaluating the size of the anomalies. These events can alter the direction of magnetic lineaments, especially close to the boundary zone, and less significantly in distal regions from the event. The magnetic lineaments were assessed primarily with the Tilt technique (Verduzco et al., 2004), and complemented by AAS. The Tilt technique is given by the relation:

$$TILT = \tan^{-1}\{[\sqrt{(\partial T/\partial z)^2}]/\ \sqrt{[(\partial T/\partial x)^2 + (\partial T/\partial y)^2]}\} \quad (2)$$

where T refers to the TMI, and x, y, and z directions in Cartesian space.

In successful supercontinent reconstructions, coeval stable domains in adjacent cratons, created under similar circumstances, should display parallel to subparallel lineaments, and continuity from one craton to another. Magnetic overprinting can occur after the stabilization of the domain, commonly in cratonization events; for example, a regional thermal overprint occurred in the southwest Amazon Craton at ca. 1.3 Ga (Bettencourt et al., 2010). This kind of event is accompanied by tectonic reactivation, deformation, and magmatism, which are manifested by extensive shear zones, mylonitic belts, rifts and sedimentary basins, and post-tectonic and anorogenic intrusions (Cordani and Teixeira, 2007). The magnetic overprint can change the orientation of the magnetic lineaments to directions that differ from those obtained during the formation of the domain. Such later tectonic events are generally associated with a regional thermal anomaly of sufficient magnitude to unblock the magnetic moments, which vary depending on the mineral and size of the grains. These are large-scale events and were mostly recognized in the cratons used in this work, and are incorporated into our interpretation.

4. Magnetic Signatures

To aid the visualization and interpretation of tectonic provinces and lineaments, the colours of the provinces were normalized to the colours used in the Amazon Craton map according with their respective ages (Fig. 3). The age relations and magnetic regimes are summarized in Table 1.

Table 1 - The age relations and magnetic regimes of the Amazon, Baltic, West African and North China Cratons.

Craton	Terrane	Normalization (AC)	Magnetic Regime
Amazon	Central Amazon	n/a	Agitated, decreasing to the south
Amazon	Maroni-Itacaiúnas	n/a	Agitated
Amazon	Ventuari-Tapajós	n/a	Intermediate
Amazon	Rio Negro-Juruena	n/a	Intermediate, increasing to the south
Amazon	Rondonian-San Ignácio	n/a	Calm to Intermediate
Amazon	Sunsás	n/a	Calm, agitation in the central area
Amazon	Phanerozoic Cover	n/a	Calm to Intermediate
Baltica	Archean Crust	Central Amazon	Intermediate to agitated
Baltica	Archean Crust reworked - Volgo-Uralia/Sarmatia Collision	Maroni-Itacaiúnas	Calm to agitated
Baltica	Paleoproterozoic Crust of Volgo-Sarmatia	Maroni-Itacaiúnas	Intermediate to agitated
Baltica	Archean Crust reworked of Fennoscandia	Ventuari-Tapajós	Calm
Baltica	Paleoproterozoic Crust of Fennoscandia	Rio Negro-Juruena	Intermediate to agitated
Baltica	Central Russian collisional belt	Rio Negro-Juruena	Calm to intermediate
Baltica	1.73 - 1.67 Ga crust reworked during the Sveconorwegian orogeny (1.14 - 0.92 Ga)	Rio Negro-Juruena	Calm
Baltica	1.66 - 1.52 Ga crust reworked during the Sveconorwegian orogeny (1.14 - 0.92 Ga)	Rio Negro-Juruena	Calm to intermediate
Baltica	1.67 - 1.65 Ga AMCG and A-type granitoid suites	Rio Negro-Juruena	Intermediate
Baltica	1.60 - 1.58 Ga AMCG and A-type granitoid suites	Rio Negro-Juruena	Agitated
Baltica	1.52 - 1.48 Ga crust reworked during the Sveconorwegian orogeny (1.14 - 0.92 Ga)	Rondonian-San Ignácio	Calm to intermediate
Baltica	1.55 - 1.44 Ga AMCG and A-type granitoid suites	Rondonian-San Ignácio	Agitated
Baltica	Aulacogens and basins, internal parts of passive margins	Rondonian-San Ignácio	Intermediate to agitated

Baltica	Passive Margins (inferred)	Sunsás	Calm and agitated
West Africa	Archean	Central Amazon	Agitated
West Africa	Paleoproterozoic	Maroni-Itacaiúnas	Calm to agitated
West Africa	Neoproterozoic + Cambrian Sedimentary Cover	Sunsás	Intermediate to agitated
West Africa	Pan-African Belts	Phanerozoic Cover	Intermediate
West Africa	Paleozoic Sedimentary Cover	Phanerozoic Cover	Intermediate
West Africa	Mesozoic to Recent Sedimentary Cover	Phanerozoic Cover	Intermediate to agitated
North China	Archean to Paleoproterozoic basement	Central Amazon	Intermediate
North China	Trans-North China Orogen	Ventuari-Tapajós	Intermediate
North China	Khondalite Belt	Maroni-Itacaiúnas	Calm and agitated
North China	Jiao-Liao Ji Belt	Maroni-Itacaiúnas	Calm to intermediate

4.1. Amazon Craton

The Amazon Craton has a northwest-southeast trend of lithotectonic assemblages (e.g. Fig. 3) that is mimicked by the magnetic field (Fig. 7). The limits of the various provinces recognized within the craton are not clear from the magnetic data set alone, but with the support of geological data, it was possible to associate specific magnetic signatures for each province. The Central Amazon province shows an agitated magnetic domain in the north, with large anomalies up to 100 km wide, and decreasing agitation and anomaly size to the south. The Maroni-Itacaiúnas province has an agitated magnetic domain, with anomalies up to 130 km wide. The Ventuari-Tapajós, Rio Negro-Juruena, Rondonian-San Ignácio, and Sunsás provinces show a progressive decrease in agitation and anomaly size. Further to the southwest, in the Amazon basin, the magnetic signature shows a significant decrease of agitation in all provinces. The areas proximal to the borders of the Amazon basin show a new increase of agitation, but still maintaining the overall trend of a reduction in the size of the anomaly.

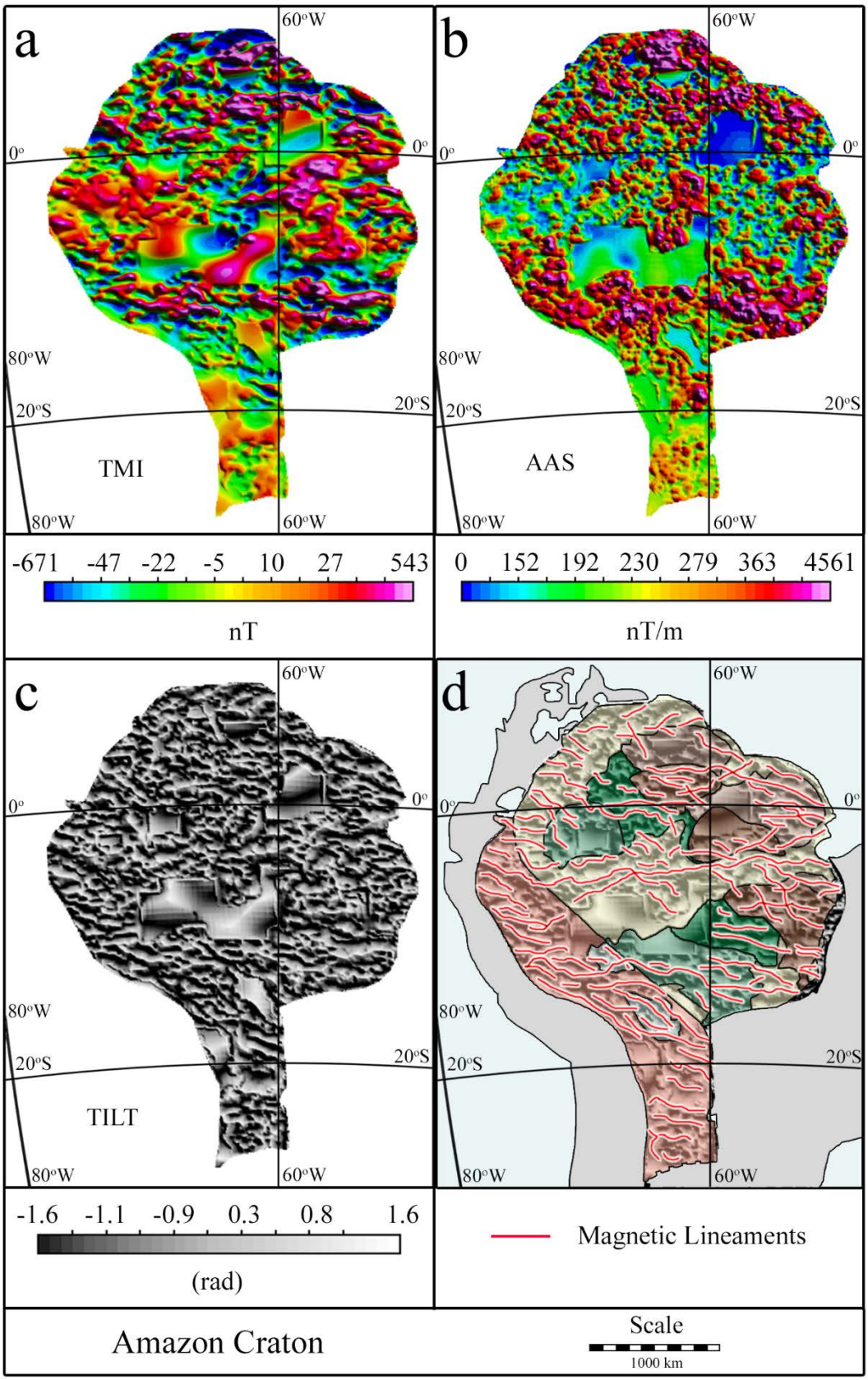

Fig. 7 – Amazon Craton: (a) TMI, (b) AAS, (c) Tilt, and (d) Tilt map overlain by the geological provinces and magnetic lineaments. The colours of the provinces were normalized to the colours used in the Amazon Craton map (Fig. 4) according with their respective ages.

The magnetic lineaments from the Amazon Craton show the overall northwest-southeast trend displayed by the lithotectonic provinces (Fig. 7d). This trend is orthogonal to the northeast-southwest-oriented accretion that occurred around the Central Amazon province since the Paleoproterozoic. The area occupied by the Amazon Basin, central in the map and covered by Phanerozoic cover, shows a significant decrease in the magnetic regime and in the volume of lineaments. A major lineament crosscuts the craton from east to west, starting in the eastern end of the Amazon basin and continuing through the Sunsás Belt to the western border.

4.2. West African Craton

The Archean shield regions of the West African Craton, are equivalent in age to the Central Amazon province, and display an overall agitated regime (Fig. 8). The shields, however, display large areas that lack data. The Paleoproterozoic domains display a calm regime in the south, but agitated in the northern region proximal to the Anti-Atlas belt. In the areas dominated by Neoproterozoic and Cambrian sedimentary cover, the magnetic field has intermediate agitation in the southeast of the West African Craton, but an agitated character in the northeast, proximal to the southern front of Variscan deformation. Like the Archean shields, the Neoproterozoic and Cambrian cover incorporate large areas that lack data.

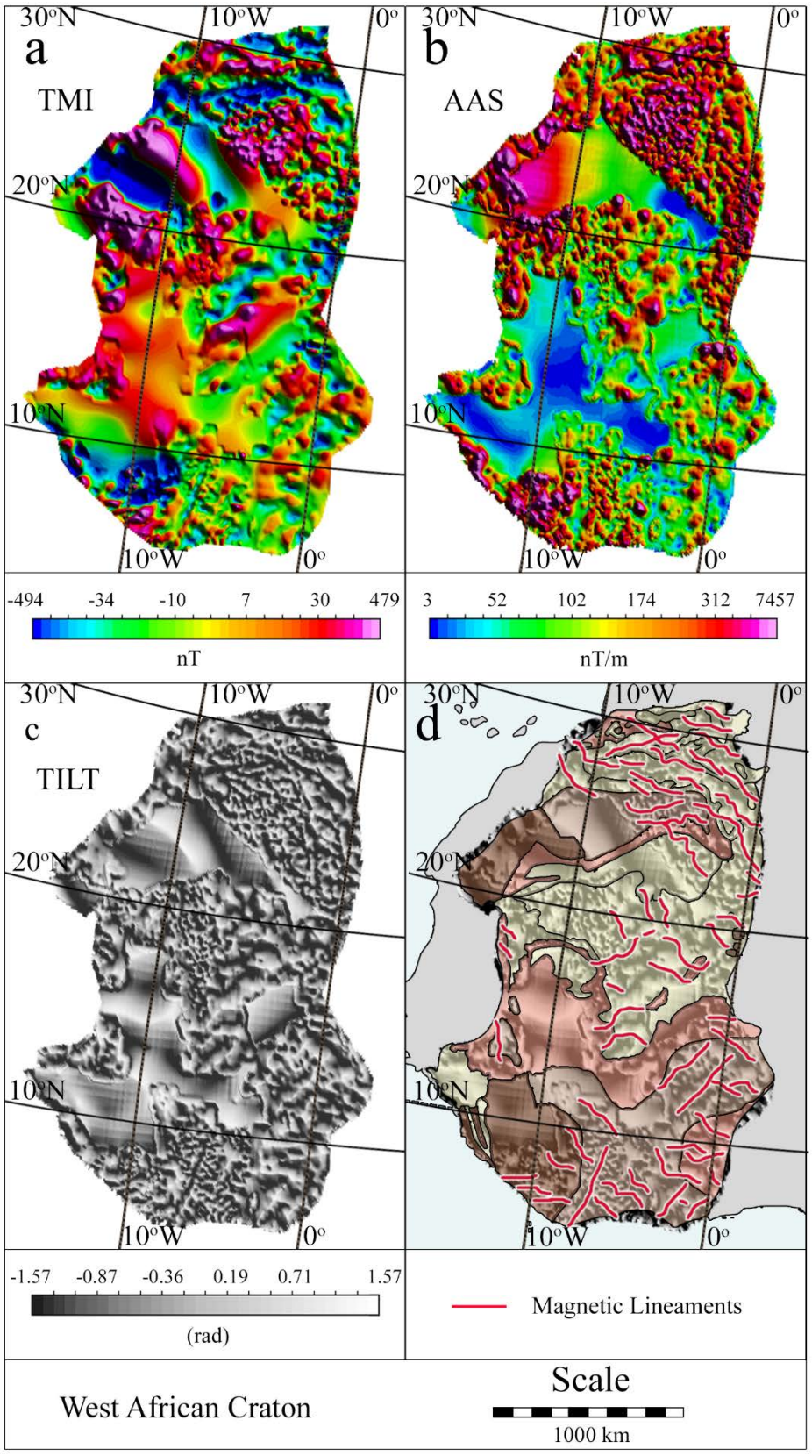

362

363 Fig. 8 – West African Craton: (a) TMI, (b) AAS, (c) Tilt, and (d) Tilt map overlain by the
364 geological provinces and magnetic lineaments. The colours of the provinces were normalized
365 to the colours used in the Amazon Craton map (Fig. 4) according with their respective ages.

366 The relatively small area representing the Pan-African belts within the West African Craton is
367 dominated by a small number of large anomalies up to 100 km wide. The Paleozoic to Recent
368 sedimentary cover, extending over most of the craton, shows intermediate agitation in the
369 magnetic regime. This cover displays a local increase in agitation when proximal to the
370 Southern Front of the Variscan deformation, in the northeast of the craton. Large areas without
371 data compose the sedimentary cover.

372 The north portion of West African Craton has a northwest-southeast trend, parallel to the Anti-
373 Atlas belt and the south Variscan front (Fig. 8d). Orthogonal, northeast-southwest-oriented,
374 lineaments can be seen in the Man Shield in the south of the craton and in the area covered by
375 Mesozoic to recent sediments in the centre of the craton. Significantly large areas in the
376 southwest and northwest West African Craton do not have available magnetic field data,
377 impeding further analysis.

378

379 *4.3. Baltic Craton*

380

381 The Baltic Craton shows an overall calm to intermediate magnetic field in its northern and
382 southern portions. A highly agitated east-west trend crosscuts the craton, occupying the region
383 south of Fennoscandia, the collisional orogens between Fennoscandia and Sarmatia, and
384 between Sarmatia and Volgo-Uralia (Fig. 9). We will refer to this trend as the Central Baltica
385 Magnetic regime. The Archean crust in Baltica shows an intermediate magnetic regime in the
386 central Archean terrane of Fennoscandia and in the Archean domain in southern Sarmatia. In
387 northern Fennoscandia and southwestern Sarmatia, the magnetic regime is agitated. In Volgo-
388 Uralia, the Archean crust presents an agitated regime, especially in its southern area (Central
389 Baltica Magnetic regime). In regions composed of reworked Archean crust, a calm regime
390 dominates the magnetic field, except in areas proximal to the Central Baltica Magnetic regime.

391

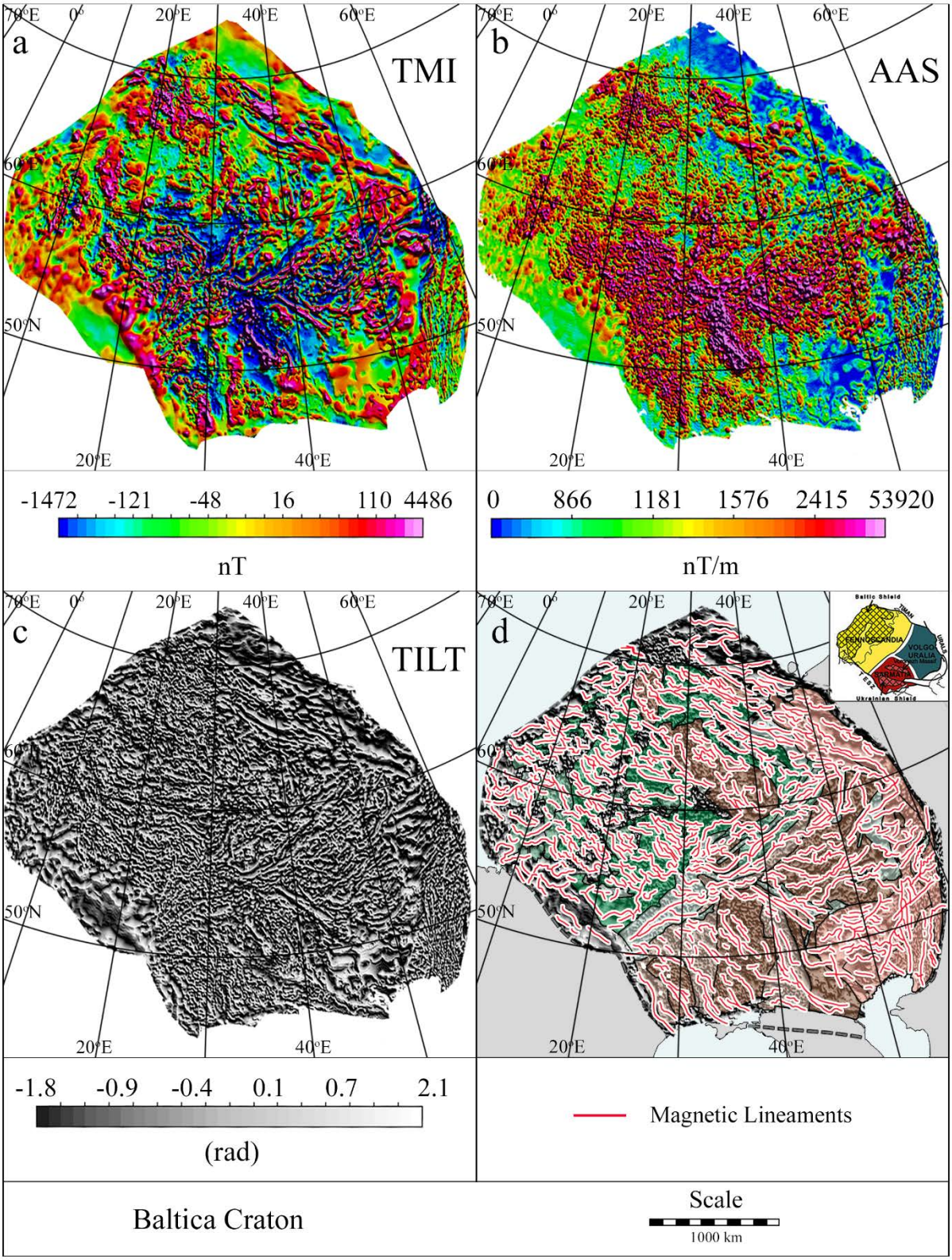

Fig. 9 – Baltic Craton: (a) TMI, (b) AAS, (c) Tilt, and (d) Tilt map overlain by the geological provinces and magnetic lineaments. The colours of the provinces were normalized to the colours used in the Amazon Craton map (Fig. 4) according with their respective ages.

The magnetic field of the Paleoproterozoic crust of Fennoscandia and Volgo-Uralia, shows higher agitation than Archean crust reworked during the same period (Figs. 5 and 9). The late Paleoproterozoic to Mesoproterozoic structures and suites indicate an increasing magnetic setting from calm in the east to agitated in the west, which experienced the late Mesoproterozoic to early Neoproterozoic Sveconorwegian orogeny. In the Central Russian collisional belt, the field remains calm. The mostly inferred passive margins along the northern and eastern borders of the Baltic Craton (Fig. 5) show a predominantly calm regime, with very long wavelength anomalies, typical of this type of tectonic setting (Nemčok, 2016; Parker Jr, 2014). The central area of Baltica, corresponding with the eastern limit of the Central Baltica Magnetic regime, is characterized by a sudden increase in the magnetic regime to agitated.

The Fennoscandia, Sarmatia and Volgo-Uralia domains, and the intervening collisional orogenic belts, are reflected in the distribution and orientation of the magnetic lineaments from the Baltic craton (Fig. 9d). Fennoscandia shows a WNW-ESE trend in lineaments, except near the western limit of the craton with the Sveconorwegian orogen, where the trend varies from east-west to northeast-southwest. An almost orthogonal trend to the Fennoscandian shield occurs in the collisional zone of Fennoscandia and Sarmatia and continues in the northeast-southwest direction through the Central Russia Collisional Belt. The Volgo-Uralia shield displays a similar ENE-WSW orientation. Sarmatia shows an overall northwest-southeast orientation, slightly oblique to that in Fennoscandia. The inferred 1.4 to 0.7 Ga passive margins of Baltic craton do not show a predominant trend of magnetic lineaments.

4.4. North China Craton

The North China Craton is characterized by long wavelength anomalies, and increasing agitation near the limits between the Archean to Paleoproterozoic basement and the orogens and belts (Fig. 10). A northeast-southwest trend is visible in all magnetic fields and derived maps. The Archean to Paleoproterozoic basement presents intermediate to agitated regimes with large magnetic anomalies. The magnetic regimes in the Ordos and Longgang blocks have intermediate frequency, whereas the Yinshan block shows an increased concentration of anomalies. The Nangrim Block, in the Eastern Block, does not have sufficient data to be evaluated.

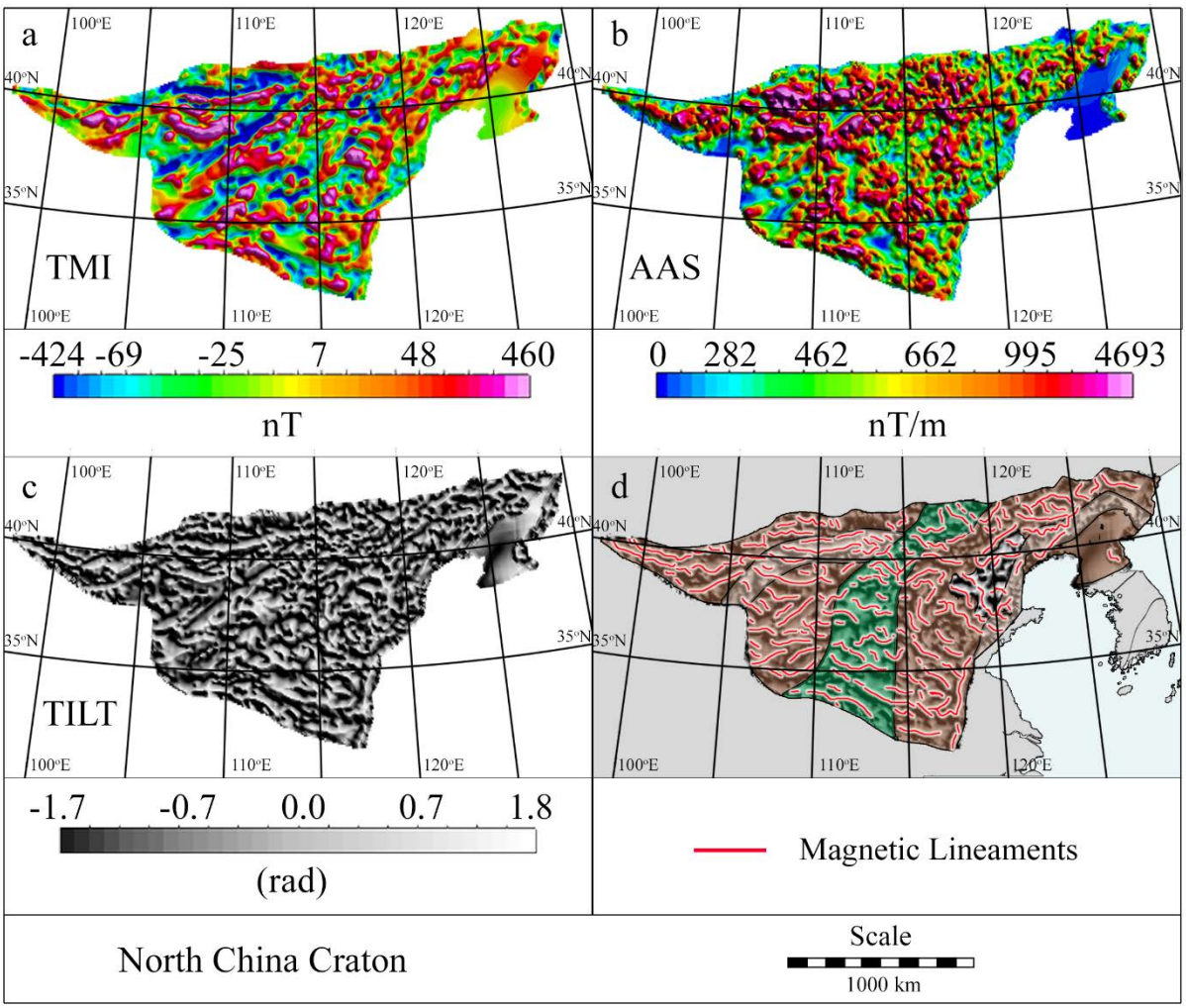

428

429 Fig. 10 – North China Craton: (a) TMI, (b) AAS, (c) Tilt, and (d) Tilt map overlain by the
430 geological provinces and magnetic lineaments. The colours of the provinces were normalized
431 to the colours used in the Amazon Craton map (Fig. 4) according with their respective ages.

432

433 The Trans-North China Orogen displays a similar magnetic regime to that of the Ordos and
434 Longgang blocks, including long wavelengths and intermediate concentration of anomalies.
435 The Khondalite Belt varies from a calm regime in the west, near the border of the craton, to the
436 increasing agglomeration of large anomalies from the centre to the eastern end proximal to the
437 Trans-North China Orogen. The Jiao-Liao-Ji Belt has a calm regime in the south with sparse
438 anomalies from the centre to the northeast area.

439 In the Archean to Paleoproterozoic basement of the North China Craton, the magnetic
440 lineament trends show a northeast-southwest pattern in the Ordos Block (Western Block) and
441 northwest in the Longgang Block (Eastern Block) (Fig. 10d). The northwest portion of the

442 craton, marked by the Yinshan Block and the Khondalite Belt shows a predominant east-west
443 trend. The northwest area, containing the Nangrim Block and the Jiao-Liao-Ji Belt, does not
444 have sufficient data to reveal a major trend.

445

446 **5. Results**

447

448 Based on mapping the magnetic regimes and lineaments for Amazonia, West Africa, Baltica,
449 and North China, Tilt maps were overlain by geological provinces and magnetic lineaments to
450 compare a variety of proposed Nuna reconstructions (Figs. 12, 14 and 16). This enables a visual
451 comparison of the alignment and possible continuity of magnetic lineaments within and
452 between the cratons. The continuity of provinces based on the magnetic field data was
453 compared with respect to available geological and paleomagnetic data to evaluate the Nuna
454 reconstructions of Mertanen and Pesonen (2012), Pisarevsky et al. (2014) and Pehrsson et al.
455 (2015).

456

457 *5.1.Mertanen and Pesonen (2012)*

458

459 Mertanen and Pesonen (2012) used a compilation of Precambrian paleopoles with minimum
460 Q-values of four (Van der Voo, 1990) to propose Nuna reconstructions for 2.45, 1.88, 1.78,
461 1.63, 1.53, 1.26 and 1.04 Ga. The Q-value is a 7-point measure that determines the quality of
462 a paleopole measurement. Their reconstructions show that by 1.53 Ga an assembled Nuna
463 included a continuous landmass formed by Amazonia, Baltica, Laurentia and Australia (Fig.
464 11). Siberia and North China cratons are disconnected from this main landmass reflecting a
465 lack of continuity between their Paleoproterozoic and older orogenic belts with coeval units in
466 their proposed reconstruction. The position of Amazonia with respect to Baltica is based on the
467 inferred continuity of the 1.9 Ga to 1.8 Ga Ventuari-Tapajós Province with the Svecofennian,
468 and the 1.8 Ga to 1.5 Ga Rio Negro-Juruena provinces with the Trans-Scandinavian Igneous
469 Belt. Laurentia is orientated so the 1.8 Ga to 1.5 Ga orogenic belts along its eastern and
470 southwestern margins face an open ocean, thus forming a long lasting accretionary orogen that
471 was only terminated with the Mesoproterozoic Grenville collisional event (Cawood and
472 Pisarevsky, 2017; Hynes and Rivers, 2010; Karlstrom et al., 2000; Zhao et al., 2002).

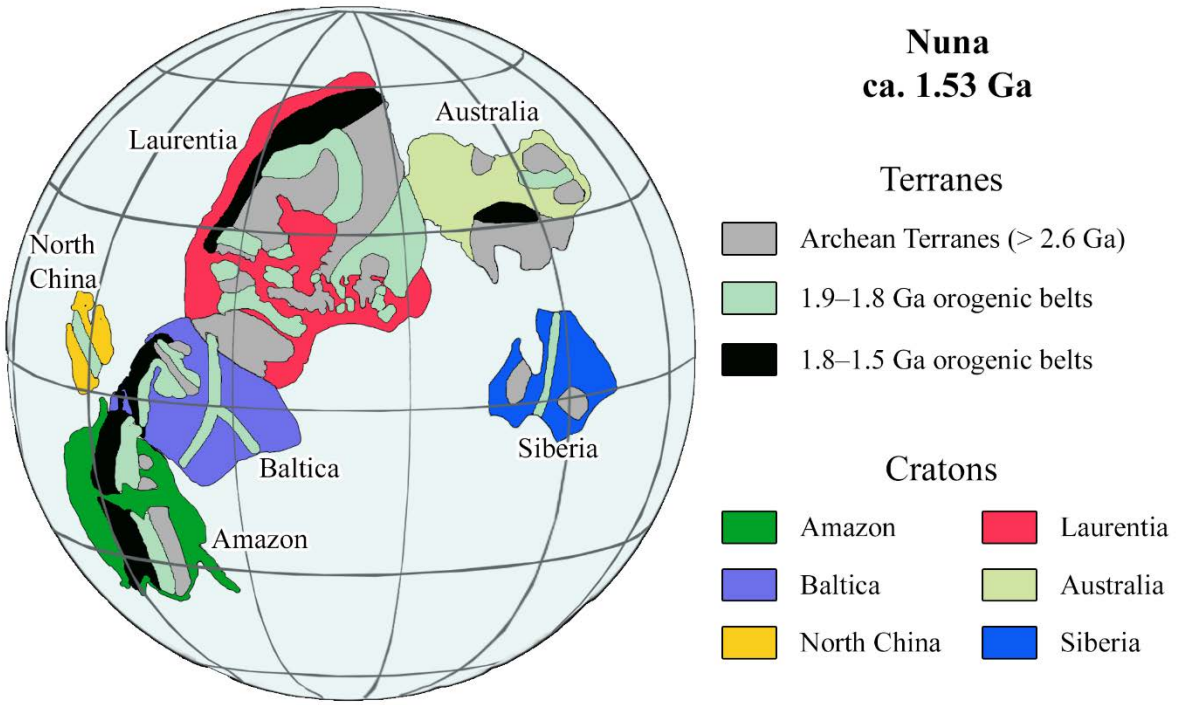

Fig. 11 – Nuna reconstruction at 1.53 Ga.

The Nuna reconstruction proposed by Mertanen and Pesonen (2012) shows Baltica and the North China cratons adjacent to the Amazon Craton (Figs. 11 and 12). The Amazon Craton is rotated approximately 35° clockwise, whereas Baltica is rotated 20° and North China 78° anti-clockwise relative to their present orientation. The magnetic lineaments of the Paleo- to Mesoproterozoic domains from Amazon and Baltica are sub-parallel, displaying a northwest-southeast trend. The Archean Central Amazon and the Archean crust of Sarmatia maintain this alignment and suggest a connection of both cratons. Although the apparent geological and geochronological continuity of the Longgang Block and the Trans-North China Orogen with the Archean and Paleo- to Mesoproterozoic crust of Fennoscandia support their reconstruction, the magnetic lineaments of North China Craton are near orthogonal to those of Fennoscandia (Fig. 12).

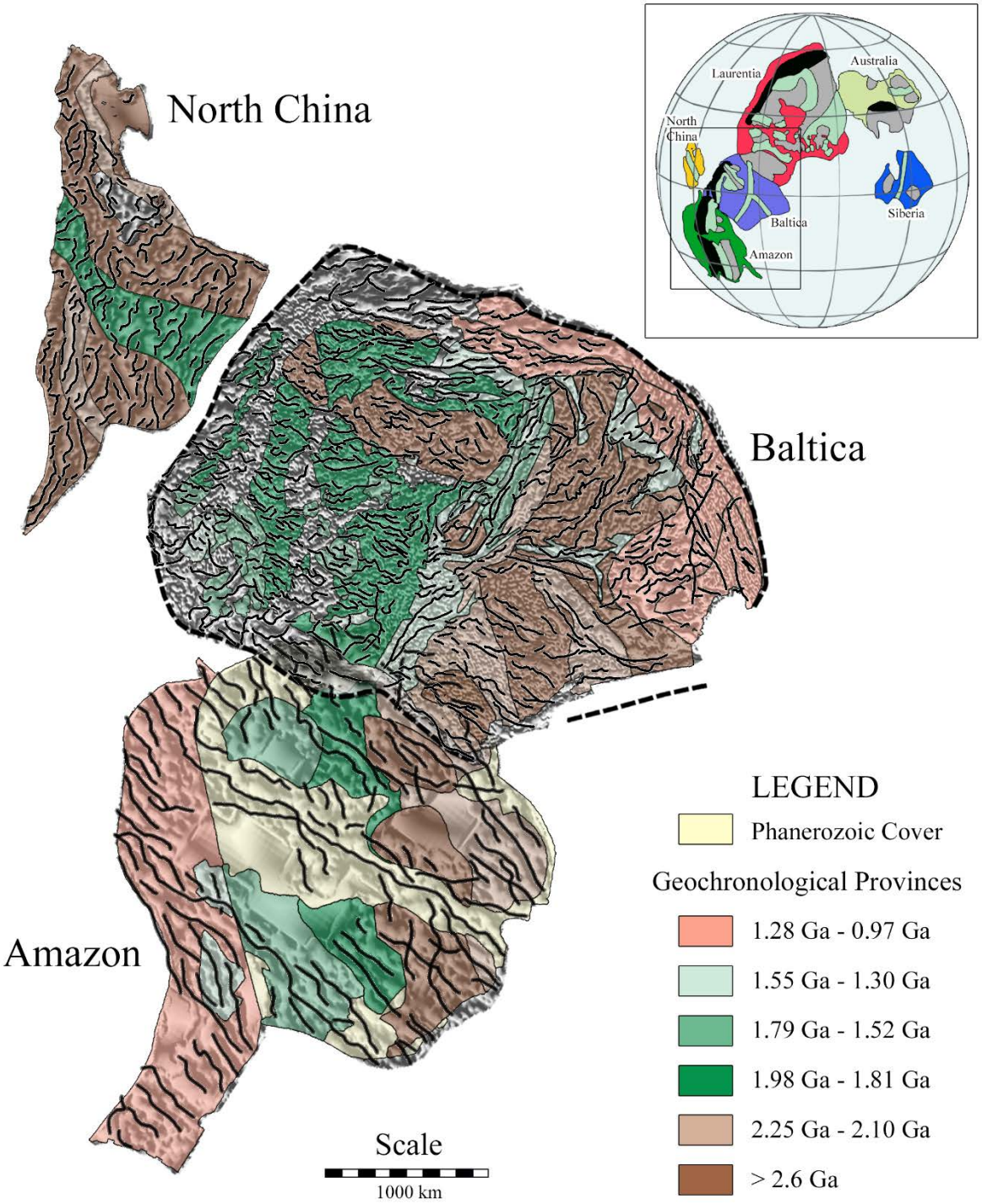

488

489 Fig. 12 – Nuna reconstruction at 1.53 Ga of the Amazon and adjacent cratons, Baltica and
490 North China, according to Mertanen and Pesonen (2012), added by the magnetic lineaments.
491 The colours of the geological units in Baltic and North China cratons were normalized to the
492 colours of provinces of similar age in the Amazon Craton.

493

494 *5.2. Pisarevsky et al. (2014)*

495

496 Pisarevsky et al. (2014) used apparent polar wander paths (APWPs) and coeval paired
497 paleopoles between continents to evaluate possible cratonic connections during the
498 Proterozoic. They propose a model in which two separated landmasses, East and West Nuna,
499 formed a single supercontinent between 1650 and 1580 Ma. Pisarevsky et al. (2014) present
500 the evolution of the Nuna through a series of global paleogeographic reconstructions for 1770,
501 1720, 1650, 1580, 1500, 1470, 1450, 1380 and 1270 Ma. West Nuna was composed by
502 Laurentia, Baltica and possibly India, whereas the East Nuna contained Australia, Mawson
503 (Antarctica), and North China. After ca. 1500 Ma, Siberia and Congo/São Francisco joined
504 Nuna, whereas West African and the Amazon cratons formed a separate continent from Nuna
505 (Fig. 13).

506

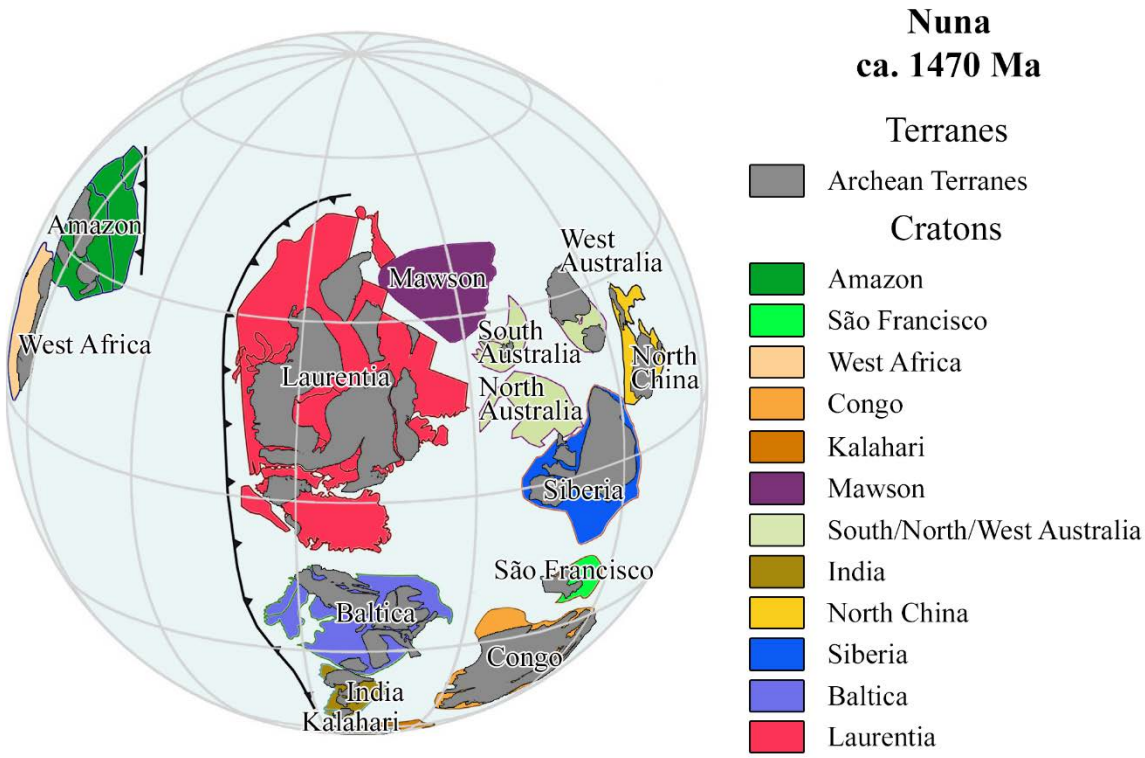

507

508 Fig. 13 – Nuna reconstruction at ca. 1470 Ma.

509

In the Pisarevsky et al. (2014) reconstruction the Amazon and the West African cratons are separate from the Nuna supercontinent. Both cratons lie northwest of the main Nuna landmass with Amazonia rotated 137° and the West Africa 74° anti-clockwise relative to their present orientation. No geological or geochronological continuity between the two cratons is visible in this reconstruction (Fig. 14). The Paleoproterozoic Maroni-Itacaiúnas (1.98 to 1.81 Ga) presents a northeast-southwest trend in the magnetic lineaments subparallel with one of the two trends shown in the Man Shield. None of the remaining domains from the West African Craton display a similar parallelism with coeval provinces in the Amazon Craton.

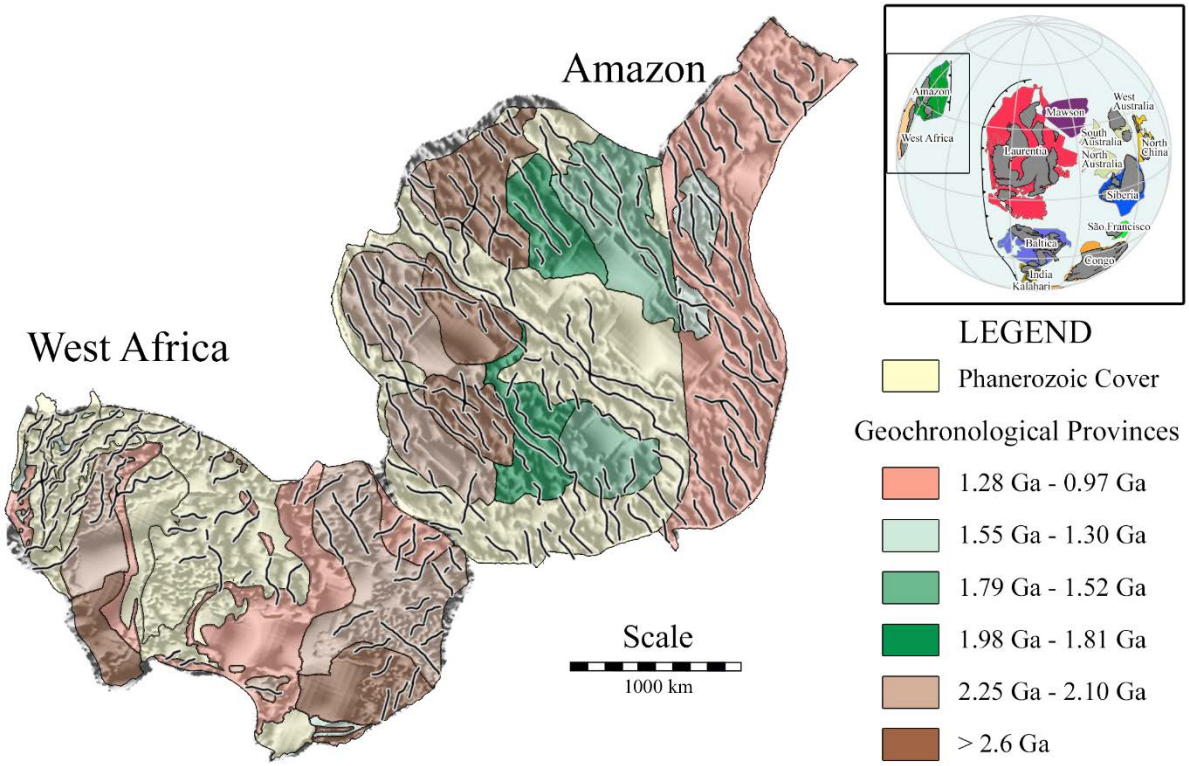

Fig. 14 – 1450 Ga Nuna reconstruction of the Amazon and the adjacent West Africa, added by the magnetic lineaments. The colours of the geological units in the West African Craton were normalized to the colours of provinces of similar age in the Amazon Craton.

5.3. Pehrsson et al. (2015)

The reconstruction proposed by Pehrsson et al. (2015) attempts to integrate data from previous models, including paleomagnetic data, with constraints from ore deposit as the formation and preservation of such deposits is linked to the supercontinent cycle (Cawood and Hawkesworth, 2015). The deposits types were used to test the reconstructions, based on the expected environment and age for each deposit type; i.e. volcanic-hosted massive sulphides in collisional or accretionary settings, sediment-hosted copper deposits in extensional settings, and uranium mineralization in subtropical latitudes.

Pehrsson et al. (2015) show a Nuna reconstruction from 1.6 and 1.4 Ga (Fig. 15), with a main landmass composed of Laurentia, Baltic, Amazon, Rio de la Plata, West African, Siberia and São Francisco/Congo cratons. Proto-Australia (South, North and West Australia) and the Yangtze cratons are located northeast of the main Nuna mass and separated by a zone undergoing regional extension, leading ultimately to ocean formation. North China, North and South India, Rayner and the Kalahari cratons are separate from Nuna.

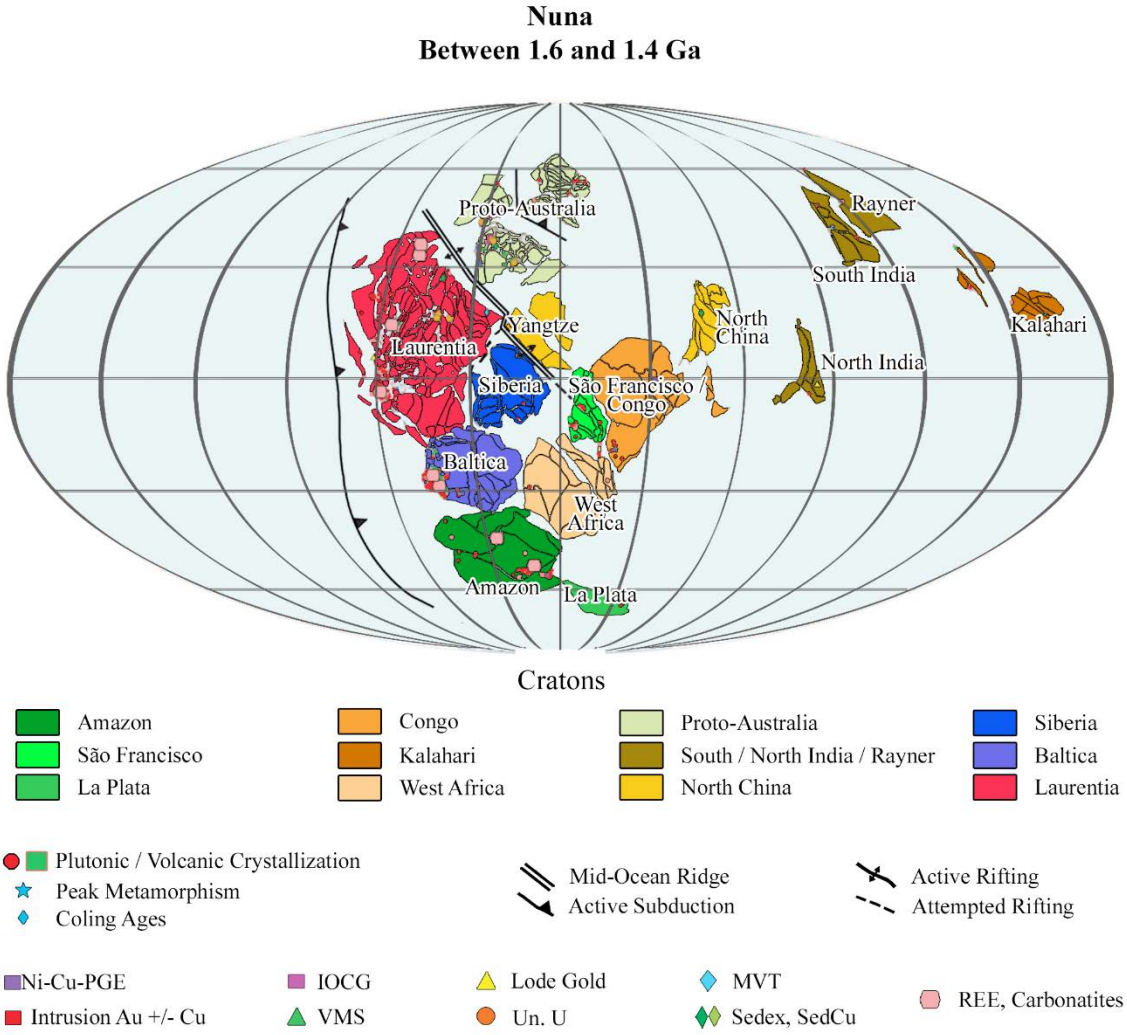

Fig. 15 – Reconstruction of Nuna for the period from 1.6 to 1.45 Ga.

The Pehrsson et al. (2015) reconstruction locates the Amazon Craton in the southern hemisphere, to the south-southeast of Baltica and to the southwest of West Africa (Fig. 16). This reconstruction involves anticlockwise rotation of the Amazon Craton by 20°, Baltica by 51°, and West Africa by 48°. The WNW-ESE-oriented magnetic lineaments of the Ventuari-Tapajós province are subparallel to the lineaments in the Paleo- to Mesoproterozoic crust of Fennoscandia, so are the lineaments in the Maroni-Itacaiúnas and the Paleoproterozoic crust of Sarmatia (Fig. 5). The West African Craton, connected with the present east of the Amazon Craton, displays a similar parallelism between the lineaments of the coeval Man Shield (West Africa), the Maroni-Itacaiúnas province (Amazon) and the Sarmatia Paleoproterozoic crust (Baltica). Lineaments from the south of the Central Amazon province also show a subparallel

555 trend to the lineaments of the Archean domain in the southern part of West Africa. In this last
556 case, however, the parallelism is speculative, given the small number and size of the lineaments
557 in the West Africa due to absence of magnetic field data.

558

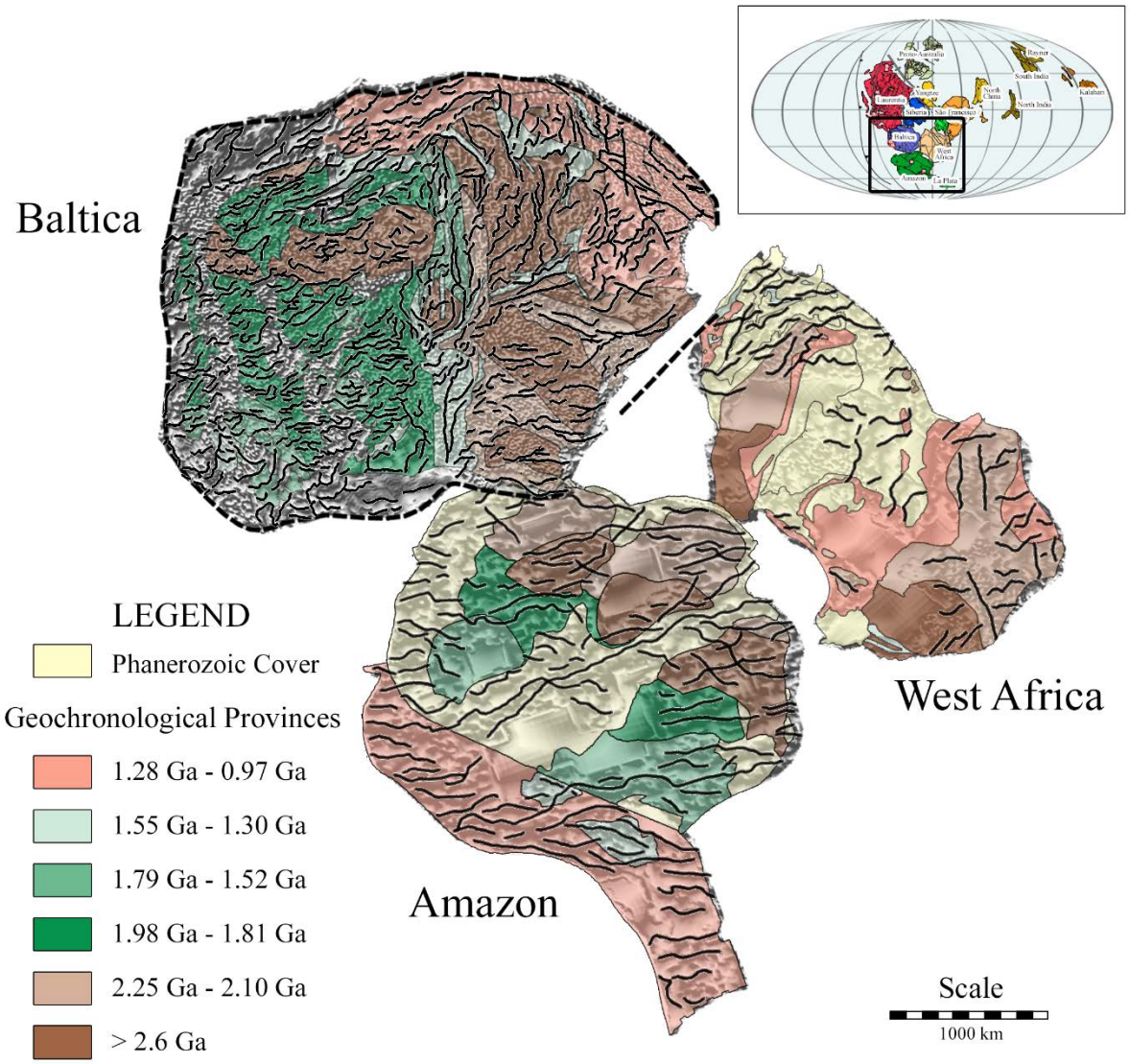

559

560 Fig. 16 – Southern area of Nuna reconstruction for the period of 1.60 to 1.40 Ga, added by
561 the magnetic lineaments. This area presents the Amazon Craton adjacent to Baltica and West
562 Africa. The colours of the geological units in Baltic and West African cratons were
563 normalized to the colours of provinces of similar age in the Amazon Craton.

564

565

6. Discussion

Magnetic anomaly patterns of sources in blocks of different cratons should be different of each other, unless they were together during their formation and/or overprinted during reworking by younger events. The comparison of anomalies for the Amazon, West African, Baltic and North China cratons shows that coeval and possibly related Paleo- to Mesoproterozoic domains in the different cratons have different sizes of anomalies. Thus, the wavelength of anomalies for Amazon and West Africa are predominantly larger than those in Baltica (Figs. 7 to 9; compare the Maroni-Itacaiúnas, Man Shield and the Paleo- to Mesoproterozoic crust of Fennoscandia). Reasons for these differences could include distortion caused by different projections of large landmasses, and the different resolution and amount of data of the compiled magnetic surveys.

In the Mertanen and Pesonen (2012) reconstruction, the approximately coeval Paleo- to Mesoproterozoic provinces in Amazon, Baltic and North China cratons show north-south continuity between the first two cratons, and northwest-southeast with the last two. The Longgang Block of the North China Craton is well aligned with the Archean crust of Fennoscandia, and the Mesoproterozoic terranes (1.79 to 1.52 Ga) of Amazon and Fennoscandia also maintain continuity. The continuity does not, however, extend to the Archean Western Block of North China Craton, which has no counterpart in either Amazon or Baltica. These latter two cratons were still accreting younger provinces until 1.53 Ga, whereas the North China was already stabilized by this time. The lineaments in the 1.98 to 1.81 Ga domains in Amazon and Baltica are well aligned but not with the North China Craton, which are almost orthogonal orientation to those in the other two cratons. The Amazon and Baltica domains show concordant magnetic regimes, which again cannot be extended to those of the North China Craton.

The model of Pisarevsky et al. (2014) is the only one in which the Amazon Craton, along with West Africa, is not included within Nuna in the Mesoproterozoic (Figs. 1 and 14). The relative orientation and juxtaposition of Amazonia and West Africa proposed by Pisarevsky et al. (2014) is not supported by the geological and magnetic data which lack continuity between the two cratons, except perhaps for a small number of lineaments in the Maroni-Itacaiúnas province and Man Shield due to 2.15-2.14 Ga calc-alkaline magmatism in the former (da Rosa-Costa et al., 2006), and the 2.15 Ga Eburnean orogeny in the latter (Abouchami et al., 1990). The Maroni-Itacaiúnas province and the Man Shield, however, show divergent magnetic

598 regimes, the Amazonic domain shows an agitated behaviour, whereas the West African Man
599 Shield presents a calm regime.

600 Pehrsson et al. (2015), like Mertanen and Pesonen (2012), locate Baltica to the north of the
601 Amazon Craton but with a further additional rotation of Baltica to further enhance geological
602 compatibility and continuity of the 1.98 to 1.81 Ga Ventuari-Tapajós province of the Amazon
603 Craton with the coeval terranes of Fennoscandia. This rotation promoted the contact of the 2.25
604 to 2.10 Ga Maroni-Itacaiúnas with the reworked 2.20 to 2.00 Paleoproterozoic crust of
605 Sarmatia. This contact, in the Tilt map (Fig. 14), reveals possible lineament continuity in the
606 extreme north of the Amazonic domain with the Sarmatian crust to the southwest. As discussed
607 with respect to the Mertanen and Pesonen (2012) reconstruction, the connection of Baltica with
608 the Amazon Craton is supported by the magnetic regimes of the coeval domains. The West
609 African Craton, which is significantly rotated from the position proposed by Pisarevsky et al.
610 (2014), allows the alignment of the lineaments from the Central Amazon and the Maroni-
611 Itacaiúnas provinces with the Archean domain and Man Shield, respectively. Evaluating the
612 continuity and parallelism of lineaments between the West Africa and Baltica is impaired by
613 the absence of data in several areas of the West African Craton.

614

615 **7. Conclusions**

616

617 The configuration of the Nuna supercontinent is a matter of ongoing debate as indicated by the
618 diverse distribution of cratonic blocks in the recent reconstructions of Mertanen and Pesonen
619 (2012), Pisarevsky et al. (2014), and Pehrsson et al. (2015). These models, as well as many
620 others (e.g. D'Agrella-Filho et al., 2012; Evans and Mitchell, 2011; Johansson, 2009; Rogers
621 and Santosh, 2002; Zhao et al., 2004), involve a similar configuration for the supercontinents
622 cratonic core juxtaposing northeast Laurentia and northern Baltica, with Siberia occupying an
623 adjacent or nearby position (e.g. Fig. 1). But the configuration of other continental blocks with
624 respect to this core assemblage, and even if these other cratonic fragments were part of Nuna
625 or separate continents, is unresolved. Most attempts to reconstruct Nuna are based on a
626 combination of geologic, geochemical, paleomagnetic, ore deposit data, with variations
627 between models often reflecting differences in the emphasis placed on the different data sets.
628 Thus, in the models evaluated here in, Mertanen and Pesonen (2012) and Pisarevsky et al.
629 (2014) integrated a combination of geological and paleomagnetic data, while Pehrsson et al.

(2015) also used isotopic and ore deposit data. In our evaluation of models of Nuna reconstruction, we incorporated a worldwide compilation of magnetic field data (magnetic field EMAG2). We used this to analyse the magnetic regime of each of the lithotectonic domains recognized in the Amazon, West African, Baltic and North China cratons, as well as the wavelength of the magnetic anomalies, and magnetic lineaments, which we then compare with proposed paleogeographic configurations for these blocks.

Similarities in the geology, age, magnetic regime, and lineaments between Archean to Mesoproterozoic domains of the Amazon and Baltic cratons are consistent with the reconstructions of Mertanen and Pesonen (2012) and Pehrsson et al. (2015). The geological data for the North China Craton shows some similarities to the adjoining Amazonia and Baltic cratons in the configuration proposed by Mertanen and Pesonen (2012), but not in the magnetic field evidence. The connections between the West African and Amazon cratons proposed by Pisarevsky et al. (2014) and Pehrsson et al. (2015) are not entirely supported by the magnetic field data. However, juxtaposition of the present western or southern border of the West African Craton with the northeast of the Amazon Craton would align the magnetic features of the two cratons.

Of three Nuna evaluated reconstructions, the model of Pehrsson et al. (2015) agrees best with the magnetic field data. It locates the Amazon Craton towards the southern portion of the Nuna supercontinent, connected to the West African and Baltic cratons, with an open ocean to its west, where continuous accretion would occur until the mid-Neoproterozoic.

8. Acknowledgements

This work was done with the support of the CNPq, National Council for Technological and Scientific Development – Brazil [grant numbers 443355/2014-2, 200473/2015-8,141587/2013-0]; Peter A. Cawood acknowledges support from the Australian Research Council [grant number FL160100168].

9. References

Abouchami, W., Boher, M., Michard, A. and Albarede, F., 1990. A major 2.1 Ga event of mafic magmatism in west Africa: An Early stage of crustal accretion. Journal of Geophysical Research: Solid Earth, 95(B11): 17605-17629.

Bahlburg, H., Vervoort, J.D., Du Frane, S.A., Bock, B., Augustsson, C. and Reimann, C., 2009. Timing of crust formation and recycling in accretionary orogens: Insights learned from the western margin of South America. Earth-Science Reviews, 97(1–4): 215-241.

Beckinsale, R.D., Gale, N.H., Pankhurst, R.J., Macfarlane, A., Crow, M.J., Arthurs, J.W. and Wilkinson, A.F., 1980. Discordant Rb-Sr and Pb-Pb whole rock isochron ages for the Archaean basement of Sierra Leone. Precambrian Research, 13(1): 63-76.

Bettencourt, J.S., Leite Jr, W.B., Ruiz, A.S., Matos, R., Payolla, B.L. and Tosdal, R.M., 2010. The Rondonian-San Ignacio Province in the SW Amazonian Craton: An overview. Journal of South American Earth Sciences, 29(1): 28-46.

Bingen, B., Andersson, J., Soderlund, U. and Moller, C., 2008. The Mesoproterozoic in the Nordic countries. Episodes, 31(1): 29-34.

Bispo-Santos, F., D'Agrella-Filho, M.S., Pacca, I.I.G., Janikian, L., Trindade, R.I.F., Elming, S.-A., Silva, J.A., Barros, M.A.S. and Pinho, F.E.C., 2008. Columbia revisited: Paleomagnetic results from the 1790 Ma colider volcanics (SW Amazonian Craton, Brazil). Precambrian Research, 164(1–2): 40-49.

Bispo-Santos, F., D'Agrella-Filho, M.S., Trindade, R.I.F., Elming, S.-Å., Janikian, L., Vasconcelos, P.M., Perillo, B.M., Pacca, I.I.G., da Silva, J.A. and Barros, M.A.S., 2012. Tectonic implications of the 1419 Ma Nova Guarita mafic intrusives paleomagnetic pole (Amazonian Craton) on the longevity of Nuna. Precambrian Research, 196–197: 1-22.

Bogdanova, S., De Waele, B., Bibikova, E., Postnikov, A. and Popova, L., 2005. Volgo-Uralia: SHRIMP evidence of strong Palaeoproterozoic reworking of the Archaean crust, Supercontinents and Earth Evolution: Fremantle, Western Australia, Geological Society of Australia Inc., Symposium 2005, Abstracts, pp. 118.

Bogdanova, S., Gorbatschev, R., Grad, M., Janik, T., Guterch, A., Kozlovskaya, E., Motuza, G., Skridlaite, G., Starostenko, V., Taran, L., EUROBRIDGE and *, P.W.G., 2006. EUROBRIDGE: new insight into the geodynamic evolution of the East European Craton. Geological Society, London, Memoirs, 32(1): 599-625.

Bogdanova, S.V., Bingen, B., Gorbatschev, R., Kheraskova, T.N., Kozlov, V.I., Puchkov, V.N. and Volozh, Y.A., 2008. The East European Craton (Baltica) before and during the assembly of Rodinia. Precambrian Research, 160(1–2): 23-45.

Boger, S.D., Raetz, M., Giles, D., Etchart, E. and Fanning, C.M., 2005. U–Pb age data from the Sunsas region of Eastern Bolivia, evidence for the allochthonous origin of the Paragua Block. Precambrian Research, 139(3–4): 121-146.

Cawood, P.A. and Hawkesworth, C.J., 2015. Temporal relations between mineral deposits and global tectonic cycles. Geological Society, London, Special Publications, 393(1): 9-21.

Cawood, P.A. and Pisarevsky, S.A., 2017. Laurentia-Baltica-Amazonia relations during Rodinia assembly. Precambrian Research.

Cordani, U.G., Fraga, L.M., Reis, N., Tassinari, C.C.G. and Brito-Neves, B.B., 2010. On the origin and tectonic significance of the intra-plate events of Grenvillian-type age in South America: A discussion. Journal of South American Earth Sciences, 29(1): 143-159.

Cordani, U.G. and Teixeira, W., 2007. Proterozoic accretionary belts in the Amazonian Craton. Geological Society of America Memoirs, 200: 297-320.

D'Agrella-Filho, M.S., Trindade, R.I.F., Elming, S.A., Teixeira, W., Yokoyama, E., Tohver, E., Geraldes, M.C., Pacca, I.I.G., Barros, M.A.S. and Ruiz, A.S., 2012. The 1420 Ma Indiavai Mafic Intrusion (SW Amazonian Craton): Paleomagnetic results and implications for the Columbia supercontinent. Gondwana Research, 22(3-4): 956-973.

da Rosa-Costa, L.T., Lafon, J.M. and Delor, C., 2006. Zircon geochronology and Sm–Nd isotopic study: Further constraints for the Archean and Paleoproterozoic geodynamical evolution of the southeastern Guiana Shield, north of Amazonian Craton, Brazil. Gondwana Research, 10(3–4): 277-300.

Dong, C., Liu, D., Li, J., Wang, Y., Zhou, H., Li, C., Yang, Y. and Xie, L., 2007. Palaeoproterozoic Khondalite Belt in the western North China Craton: New evidence from SHRIMP dating and Hf isotope composition of zircons from metamorphic rocks in the Bayan Ul-Helan Mountains area. Chinese Science Bulletin, 52(21): 2984-2994.

El Bahat, A., Ikenne, M., Söderlund, U., Cousens, B., Youbi, N., Ernst, R., Soulaimani, A., El Janati, M.h. and Hafid, A., 2013. U–Pb baddeleyite ages and geochemistry of dolerite dykes in the Bas Drâa Inlier of the Anti-Atlas of Morocco: Newly identified 1380 Ma event in the West African Craton. Lithos, 174: 85-98.

Emslie, R.F., Hamilton, M.A., Th, xe and riault, R.J., 1994. Petrogenesis of a Mid-Proterozoic Anorthosite-Mangerite-Charnockite-Granite (AMCG) Complex: Isotopic and

726 Chemical Evidence from the Nain Plutonic Suite. The Journal of Geology, 102(5): 539-
727 558.
728 Ennih, N. and Liégeois, J.-P., 2008. The boundaries of the West African craton, with special
729 reference to the basement of the Moroccan metacratonic Anti-Atlas belt. Geological
730 Society, London, Special Publications, 297(1): 1-17.
731 Evans, D.A.D. and Mitchell, R.N., 2011. Assembly and breakup of the core of
732 Paleoproterozoic–Mesoproterozoic supercontinent Nuna. Geology, 39(5): 443-446.
733 Grant, F.S., 1985a. Aeromagnetics, geology and ore environments, I. Magnetite in igneous,
734 sedimentary and metamorphic rocks: An overview. Geoexploration, 23(3): 303-333.
735 Grant, F.S., 1985b. Aeromagnetics, geology and ore environments, II. Magnetite and ore
736 environments. Geoexploration, 23(3): 335-362.
737 Guerrak, S., 1989. Time and space distribution of Palaeozoic oolitic ironstones in the Tindouf
738 Basin, Algerian Sahara. Geological Society, London, Special Publications, 46(1): 197-
739 212.
740 Hurley, P.M., Rand, J.R., Pinson, W.H., Fairbairn, H.W., de Almeida, F.F.M., Melcher, G.C.,
741 Cordani, U.G., Kawashita, K. and Vandoros, P., 1967. Test of Continental Drift by
742 Comparison of Radiometric Ages. A pre-drift reconstruction shows matching geologic
743 age provinces in West Africa and Northern Brazil, 157(3788): 495-500.
744 Hynes, A. and Rivers, T., 2010. Protracted continental collision — evidence from the Grenville
745 OrogenThis article is one of a series of papers published in this Special Issue on the
746 theme Lithoprobe — parameters, processes, and the evolution of a continent. Canadian
747 Journal of Earth Sciences, 47(5): 591-620.
748 Johansson, Å., 2009. Baltica, Amazonia and the SAMBA connection—1000 million years of
749 neighbourhood during the Proterozoic? Precambrian Research, 175(1–4): 221-234.
750 Karlstrom, K.E., Bowring, S.A., Dehler, C.M., Knoll, A.H., Porter, S.M., Marais, D.J.D., Weil,
751 A.B., Sharp, Z.D., Geissman, J.W., Elrick, M.B., Timmons, J.M., Crossey, L.J. and
752 Davidek, K.L., 2000. Chuar Group of the Grand Canyon: Record of breakup of Rodinia,
753 associated change in the global carbon cycle, and ecosystem expansion by 740 Ma.
754 Geology, 28(7): 619-622.
755 Key, R.M., Loughlin, S.C., Gillespie, M., Del Rio, M., Horstwood, M.S.A., Crowley, Q.G.,
756 Darbyshire, D.P.F., Pitfield, P.E.J. and Henney, P.J., 2008. Two Mesoarchaean terranes
757 in the Reguibat shield of NW Mauritania. Geological Society, London, Special
758 Publications, 297(1): 33-52.

759 Kouyaté, D., Söderlund, U., Youbi, N., Ernst, R., Hafid, A., Ikenne, M., Soulaimani, A.,
760 Bertrand, H., El Janati, M.h. and R'Kha Chaham, K., 2013. U–Pb baddeleyite and
761 zircon ages of 2040 Ma, 1650 Ma and 885 Ma on dolerites in the West African Craton
762 (Anti-Atlas inliers): Possible links to break-up of Precambrian supercontinents. Lithos,
763 174: 71-84.
764 Maus, S., Barckhausen, U., Berkenbosch, H., Bournas, N., Brozena, J., Childers, V., Dostaler,
765 F., Fairhead, J.D., Finn, C., von Frese, R.R.B., Gaina, C., Golynsky, S., Kucks, R.,
766 Lühr, H., Milligan, P., Mogren, S., Müller, R.D., Olesen, O., Pilkington, M., Saltus, R.,
767 Schreckenberger, B., Thébault, E. and Caratori Tontini, F., 2009. EMAG2: A 2–arc min
768 resolution Earth Magnetic Anomaly Grid compiled from satellite, airborne, and marine
769 magnetic measurements. Geochemistry, Geophysics, Geosystems, 10(8): 1-12.
770 Mertanen, S. and Pesonen, L.J., 2012. Paleo-Mesoproterozoic Assemblages of Continents:
771 Paleomagnetic Evidence for Near Equatorial Supercontinents. In: I. Haapala (Editor),
772 From the Earth's Core to Outer Space. Springer Berlin Heidelberg, Berlin, Heidelberg,
773 pp. 11-35.
774 Nemčok, M., 2016. Rifts and Passive Margins: Structural Architecture, Thermal Regimes, and
775 Petroleum Systems. Cambridge University Press.
776 Olesen, O., Ebbing, J., Lundin, E., Mauring, E., Skilbrei, J.R., Torsvik, T.H., Hansen, E.K.,
777 Henningsen, T., Midbøe, P. and Sand, M., 2007. An improved tectonic model for the
778 Eocene opening of the Norwegian–Greenland Sea: Use of modern magnetic data.
779 Marine and Petroleum Geology, 24(1): 53-66.
780 Parker Jr, E., 2014. Crustal magnetism, tectonic inheritance, and continental rifting in the
781 southeastern United States. GSA Today, 24(4).
782 Pehrsson, S.J., Eglington, B.M., Evans, D.A.D., Huston, D. and Reddy, S.M., 2015.
783 Metallogeny and its link to orogenic style during the Nuna supercontinent cycle.
784 Geological Society, London, Special Publications, 424.
785 Pisarevsky, S.A., Elming, S.-Å., Pesonen, L.J. and Li, Z.-X., 2014. Mesoproterozoic
786 paleogeography: Supercontinent and beyond. Precambrian Research, 244: 207-225.
787 Reis, N.J., Teixeira, W., Hamilton, M.A., Bispo-Santos, F., Almeida, M.E. and D'Agrella-
788 Filho, M.S., 2013. Avanavero mafic magmatism, a late Paleoproterozoic LIP in the
789 Guiana Shield, Amazonian Craton: U–Pb ID-TIMS baddeleyite, geochemical and
790 paleomagnetic evidence. Lithos, 174: 175-195.
791 Roest, W.R., Verhoef, J. and Pilkington, M., 1992. Magnetic Interpretation Using the 3-D
792 Analytic Signal. Geophysics, 57(1): 116-125.

Rogers, J.J.W. and Santosh, M., 2002. Configuration of Columbia, a Mesoproterozoic Supercontinent. Gondwana Research, 5(1): 5-22.

Rotherham, J.F., 1997. A metasomatic origin for the iron-oxide Au-Cu Starra orebodies, Eastern Fold Belt, Mount Isa Inlier. Mineralium Deposita, 32(3): 205-218.

Sadowski, G.R. and Bettencourt, J.S., 1996. Mesoproterozoic tectonic correlations between eastern Laurentia and the western border of the Amazon Craton. Precambrian Research, 76(3): 213-227.

Shchipansky, A.A., Samsonov, A.V., Petrova, A.Y. and Larionova, Y.O., 2007. Geodynamics of the eastern margin of Sarmatia in the Paleoproterozoic. Geotectonics, 41(1): 38-62.

Söderlund, U., Ibanez-Mejia, M., El Bahat, A., Ernst, R.E., Ikenne, M., Soulaimani, A., Youbi, N., Cousens, B., El Janati, M.h. and Hafid, A., 2013. Reply to Comment on "U–Pb baddeleyite ages and geochemistry of dolerite dykes in the Bas-Drâa inlier of the Anti-Atlas of Morocco: Newly identified 1380 Ma event in the West African Craton" by André Michard and Dominique Gasquet. Lithos, 174: 101-108.

Soulaimani, A. and Burkhard, M., 2008. The Anti-Atlas chain (Morocco): the southern margin of the Variscan belt along the edge of the West African craton. Geological Society, London, Special Publications, 297(1): 433-452.

Tassinari, C.C.G. and Macambira, M.J.B., 1999. Geochronological provinces of the Amazonian Craton. Episodes, 22(3): 174-182.

Teixeira, W., Geraldes, M.C., Matos, R., Ruiz, A.S., Saes, G. and Vargas-Mattos, G., 2010. A review of the tectonic evolution of the Sunsas belt, SW Amazonian Craton. Journal of South American Earth Sciences, 29(1): 47-60.

Tohver, E., Teixeira, W., van der Pluijm, B., Geraldes, M.C., Bettencourt, J.S. and Rizzotto, G., 2006. Restored transect across the exhumed Grenville orogen of Laurentia and Amazonia, with implications for crustal architecture. Geology, 34(8): 669-672.

Van der Voo, R., 1990. The reliability of paleomagnetic data. Tectonophysics, 184(1): 1-9.

Verduzco, B., Fairhead, J.D., Green, C.M. and MacKenzie, C., 2004. New insights into magnetic derivatives for structural mapping. The Leading Edge, 23(2): 116-119.

Wilde, S.A., Cawood, P.A., Wang, K. and Nemchin, A.A., 2005. Granitoid evolution in the Late Archean Wutai Complex, North China Craton. Journal of Asian Earth Sciences, 24(5): 597-613.

Williams, H., Hoffman, P.F., Lewry, J.F., Monger, J.W.H. and Rivers, T., 1991. Anatomy of North America: thematic geologic portrayals of the continent. Tectonophysics, 187(1): 117-134.

827 Windley, B.F., 1987. Geology and mineral resources of West Africa by J.B. Wright et al., Allen
828 & Unwin, 1985. No. of pages: 187. Price: £30.00 (hardback). Geological Journal,
829 22(S1): 211-212.
830 Wu, K.K., Zhao, G., Sun, M., Yin, C., He, Y. and Tam, P.Y., 2013. Metamorphism of the
831 northern Liaoning Complex: Implications for the tectonic evolution of Neoarchean
832 basement of the Eastern Block, North China Craton. Geoscience Frontiers, 4(3): 305-
833 320.
834 Youbi, N., Kouyaté, D., Söderlund, U., Ernst, R.E., Soulaimani, A., Hafid, A., Ikenne, M., El
835 Bahat, A., Bertrand, H., Rkha Chaham, K., Ben Abbou, M., Mortaji, A., El Ghorfi, M.,
836 Zouhair, M. and El Janati, M.h., 2013. The 1750 Ma Magmatic Event of the West
837 African Craton (Anti-Atlas, Morocco). Precambrian Research, 236: 106-123.
838 Zhao, G. and Cawood, P.A., 2012. Precambrian geology of China. Precambrian Research, 222–
839 223: 13-54.
840 Zhao, G., Cawood, P.A., Li, S., Wilde, S.A., Sun, M., Zhang, J., He, Y. and Yin, C., 2012.
841 Amalgamation of the North China Craton: Key issues and discussion. Precambrian
842 Research, 222–223: 55-76.
843 Zhao, G., Cawood, P.A., Wilde, S.A. and Sun, M., 2002. Review of global 2.1–1.8 Ga orogens:
844 implications for a pre-Rodinia supercontinent. Earth-Science Reviews, 59(1–4): 125-
845 162.
846 Zhao, G., Sun, M., Wilde, S.A. and Li, S., 2004. A Paleo-Mesoproterozoic supercontinent:
847 assembly, growth and breakup. Earth-Science Reviews, 67(1–2): 91-123.
848 Zhao, G., Wilde, S.A., Cawood, P.A. and Sun, M., 2001. Archean blocks and their boundaries
849 in the North China Craton: lithological, geochemical, structural and P–T path
850 constraints and tectonic evolution. Precambrian Research, 107(1–2): 45-73.
851 Zhao, G. and Zhai, M., 2013. Lithotectonic elements of Precambrian basement in the North
852 China Craton: Review and tectonic implications. Gondwana Research, 23(4): 1207-
853 1240.

5. Conclusions

A few questions were raised in the introduction of this thesis. The questions argued about how much a single suite can tell about itself and the environment around it, about honest mistakes in during geophysical modelling, and the Earth evolution. Three papers were presented proposing answers for these questions. First, a study considering the effects that using inaccurate constraints have in the outcome of potential field data modelling. Then, the development of a geophysical model from this suite, and a geochemical analysis of the tectonic framework and parental magma that resulted in the intrusion of the Figueira Branca Suite. The third and last part of the thesis consisted on using magnetic field data to evaluate supercontinent reconstruction models.

The Figueira Branca Suite is a 1425 Ma layered mafic-ultramafic complex intruded in the Alto Jauru group, southwest Amazon Craton. This suite has been focus of isotopic and paleomagnetic studies, and was the centre of the three studies that composed this thesis. The suite is composed by four northwest-southeast-oriented bodies: Indiavaí, Azteca, Figueira Branca and Jauru, from southeast to northwest. The environment that surrounds the Figueira Branca Suite consists in the 1.8 Ga Alto Jauru meta-volcanosedimentary group that hosts the suite, the granite-gneiss Santa Helena (to the west) and Água Clara (to the east) suites.

Modelling, in Earth Sciences, is the ultimate effort to represent a part of the Earth that cannot be entirely seen. Geophysics and geochemistry are two of the sciences that most frequently use modelling. This thesis repeatedly used this resource, from testing how a microscopic analysis affects the constraints used in the modelling, to the evaluation of supercontinent reconstruction models with magnetic field data.

Preliminary data showed abnormally low values of density and magnetic susceptibility in hand samples of the Figueira Branca Suite. A preliminary model was developed using these values as constraints. The shape, depth and remanent magnetization from this model, however, did not agree with geological observations and paleomagnetic data. Hand samples did not display clear signs of weathering or evidences that could explain the low properties, so thin sections were extracted to investigate their possible cause. The thin sections displayed intense weathering and serpentinization in some samples. This process justified a deeper investigation on how and how much an inaccurate constraint affect the outcome from modelling. In this case, the density and the magnetic susceptibility were evaluated for gravity (Bouguer anomaly) and magnetic field respectively.

The investigation of the effects of inaccurate constraints was made using a synthetic model and real data from the Indiavaí body, the southernmost intrusion of the Figueira Branca Suite. The investigated cases proved that using inaccurate constraints can produce errors about 50% higher than the correct and shapes significantly different than the reality. The results also showed that in cases that a more thorough analysis in the sources of the constraints, the best solution is to perform the modelling setting the constraints free, instead of fixing inaccurate values and forcing the reduction of the error through the variation of depth and shape of the models.

With a reliable modelling methodology and constraints, it was possible to model the remaining anomalies of the suite. Previous studies of the Figueira Branca Suite suggest that it extended further to the north and northeast of the four cited bodies. However, no other analogue geophysical signature in the Jauru Terrane represented an intrusion of the same geological characteristics of the Figueira Branca Suite bodies.

The geophysical models obtained for the suite intrusive bodies displayed very shallow sill-like shapes extending 8 km on average in the northwest direction. Mineralogy and geochemical data indicated gabbroic rocks with predominance of plagioclase, olivine, and variable amounts of intergrown pyroxene. The increasing presence of pyroxene indicated a fractionation in the parental magma, whereas the change in the slope of the REE normalized to chondrites suggested an increase in the amount of melt. Both datasets together permitted to propose the sequence of magma extraction that generated the bodies of the Figueira Branca Suite was: Indiavaí, Figueira Branca, Azteca and Jauru. Trace elements completed the data, displaying evidences of hydrous melts in the parental magma, typical from supra-subduction environments. This geochemical signature for the parental magma, associated with the tectonic framework where the suite is hosted, was interpreted as a magmatism in the back-arc zone of the Santa Helena Orogen.

The answers for how much a suite can tell about itself and the environment that hosts it, and the larger scale analysis of the Jauru Terrane raised the last question: what about the Earth evolution? Where was the Amazon Craton by the time of the Santa Helena orogeny, and when was the Figueira Branca Suite intrusive event? The supercontinent Nuna position and the cratonic fragments that composed it are a matter of ongoing debate. By consequence, the debate extends to the Amazon Craton. Supercontinent reconstructions varies depending the amount and kind of data used to constraint them (e.g. combination of geologic, geochemical, paleomagnetic, and ore deposit data). Three recent reconstructions Mertanen and Pesonen (2012), Pisarevsky et al. (2014), and Pehrsson et al. (2015) suggest different configurations for the Nuna supercontinent, where Amazonia is adjacent to the West African, Baltic and/or the North China cratons. Using a worldwide compilation of magnetic field data (EMAG2), these reconstructions were analysed based on the magnetic regimes and lineaments of each block, and then the proposed paleogeographic configurations for these blocks.

None of the reconstructions were entirely supported by the magnetic field data, however Pehrsson et al. (2015) reconstruction agrees best with it. This reconstruction locates the Amazon Craton towards the southern portion of the supercontinent, connected in the northeast to the West Africa, and in the north to Baltica cratons. In this reconstruction, the southwest of the Amazon Craton has open ocean to its west, where continuous accretion would occur until the mid-Neoproterozoic, forming the Santa Helena Orogen and, later, the back-arc extension that permitted the intrusion of the Figueira Branca Suite.

6. References

Bettencourt, J. S., Leite Jr, W. B., Ruiz, A. S., Matos, R., Payolla, B. L., & Tosdal, R. M. (2010). The Rondonian-San Ignacio Province in the SW Amazonian Craton: An overview. *Journal of South American Earth Sciences, 29*(1), 28-46. doi:http://dx.doi.org/10.1016/j.jsames.2009.08.006

Maus, S., Barckhausen, U., Berkenbosch, H., Bournas, N., Brozena, J., Childers, V., . . . Caratori Tontini, F. (2009). EMAG2: A 2–arc min resolution Earth Magnetic Anomaly Grid compiled from satellite, airborne, and marine magnetic measurements. *Geochemistry, Geophysics, Geosystems, 10*(8), 1-12. doi:10.1029/2009GC002471

Mertanen, S., & Pesonen, L. J. (2012). Paleo-Mesoproterozoic Assemblages of Continents: Paleomagnetic Evidence for Near Equatorial Supercontinents. In I. Haapala (Ed.), *From the Earth's Core to Outer Space* (pp. 11-35). Berlin, Heidelberg: Springer Berlin Heidelberg.

Pehrsson, S. J., Eglington, B. M., Evans, D. A. D., Huston, D., & Reddy, S. M. (2015). Metallogeny and its link to orogenic style during the Nuna supercontinent cycle. *Geological Society, London, Special Publications, 424*. doi:10.1144/sp424.5

Pisarevsky, S. A., Elming, S.-Å., Pesonen, L. J., & Li, Z.-X. (2014). Mesoproterozoic paleogeography: Supercontinent and beyond. *Precambrian Research, 244*, 207-225. doi:http://dx.doi.org/10.1016/j.precamres.2013.05.014

Tassinari, C. C. G., Bettencourt, J. S., Geraldes, M. C., Macambira, M. J. B., & Lafon, J. M. (2000). *The Amazonian Craton.* Paper presented at the 31st International Geological Congress, Rio de Janeiro.

Tassinari, C. C. G., & Macambira, M. J. B. (1999). Geochronological provinces of the Amazonian Craton. *Episodes, 22*(3), 174-182.

Teixeira, W., Ernst, R. E., Hamilton, M. A., Lima, G., Ruiz, A. S., & Geraldes, M. C. (2016). Widespread ca. 1.4 Ga intraplate magmatism and tectonics in a growing Amazonia. *Gff, 138*(1), 241-254. doi:10.1080/11035897.2015.1042033

Teixeira, W., Geraldes, M. C., D'Agrella, M. S., Santos, J. O. S., Barros, M. A. S., Ruiz, A. S., & da Costa, P. C. C. (2011). Mesoproterozoic juvenile mafic-ultramafic magmatism in the SW Amazonian Craton (Rio Negro-Juruena province): SHRIMP U-Pb geochronology and Nd-Sr constraints of the Figueira Branca Suite. *Journal of South American Earth Sciences, 32*(4), 309-323. doi:10.1016/j.jsames.2011.04.011

Teixeira, W., Geraldes, M. C., Matos, R., Ruiz, A. S., Saes, G., & Vargas-Mattos, G. (2010). A review of the tectonic evolution of the Sunsas belt, SW Amazonian Craton. *Journal of South American Earth Sciences, 29*(1), 47-60. doi:10.1016/j.jsames.2009.09.007